Rabies Glycoprotein-Mediated Uptake Into Epithelial Cells and Compartmentalized Primary Neuronal Culture

RABIES GLYCOPROTEIN-MEDIATED UPTAKE INTO EPITHELIAL CELLS AND COMPARTMENTALIZED PRIMARY NEURONAL CULTURE

A dissertation presented by

SILVIA PICCINOTTI

to

The Division of Medical Sciences

in partial fulfillment of the requirements for the degree of

DOCTOR OF PHILOSOPHY

in the subject of

VIROLOGY

Harvard University

Cambridge, Massachusetts

August 2015

Dissertation Advisor: Sean P. Whelan Silvia Piccinotti

RABIES GLYCOPROTEIN-MEDIATED UPTAKE INTO EPITHELIAL CELLS

AND COMPARTMENTALIZED PRIMARY NEURONAL CULTURE

ABSTRACT

Rabies virus (RABV) subverts host neuronal circuitry to gain access to the brain where it causes generally incurable, lethal encephalitis. The single glycoprotein (G) dictates two defining steps for infection and neuroinvasion: receptor-mediated endocytosis and transport of virus. We generate two recombinant VSV (rVSV) clones that genetically incorporate G (rVSV RABV G) from the fixed RABV strains, SAD B19 and CVS, to study internalization into epithelial cells and compartmentalized primary cultures of peripheral neurons. Through the use of chemical inhibitors and markers for specific endocytic routes, we demonstrate that the predominant RABV entry route in both epithelial and neuronal cells is dynamin- and clathrin- dependent. Viral endocytosis is mediated by actin-dependent, partially coated clathrin pits as evidenced by live high resolution confocal microscopy of envelopment in epithelial cells and transmission electron micrographs in neuronal and non-neuronal cells. Thus, we corroborate the hypothesis that particle size is the sole viral determinant of actin-dependence of coated pits. Through a combination of high resolution microscopy and infectivity-based approaches, we link molecular mechanisms of viral uptake at the single particle level to productive infection. Targeted pharmacological disruption of endosomal acidification at the neurites or cell bodies of peripheral neurons demonstrates that fusion and viral genome release at the cell body, the site of replication, is a prerequisite for infection. This work extends the current understanding of RABV entry by providing a detailed characterization of endocytosis from the plasma membrane to the site of fusion and correlating it with establishment of infection into neuronal populations relevant for pathogenesis *in vivo.*

TABLE OF CONTENTS

LIST OF FIGURES

Introduction

Chapter 1

Chapter 2

Discussion

Appendix

For my family who vicariously lived the PhD through me.

Their unwavering support and encouragement created a lifeline

to face the vagaries of experimental science.

For those engaged in scientific struggle: hang on little tomato(es).

INTRODUCTION

Global impact and clinical manifestations of rabies virus

RABV is the prototypical member of the *Lyssavirus* genus. Although the major causative agent of zoonotic rabies infection worldwide, fourteen rabies-related lyssaviruses are currently known [20]. Several of these also cause fatal rabies-like disease. Rabies and rabies-like viruses claim an estimated 25,000 - 60,000 deaths per annum (95% confidence interval) [22], 40% which are children under the age of fifteen [23]. An additional 10 million are estimated to receive post-exposure prophylaxis. Due to its overwhelming lethality and the lack of broadly effective treatments after emergence of symptoms, an annual expenditure in excess of 6 billion US dollars is spent on prevention and post-exposure prophylaxis [22]. Canine rabies control programs and sweeping wildlife vaccination campaigns in rich, industrialized countries have effectively eliminated rabies in the Europe, North America, Japan, Malaysia and a few Latin American countries (Figure I.1). Unfortunately, the bulk of residual rabies cases are now restricted to impoverished communities in which the cost of post-exposure prophylaxis or preventive vaccination – often borne by affected patients and their families – is prohibitive WHO Expert consultation on rabies, 2015 (TRS982). This has led to rabies being considered a neglected tropical disease by international public health entities such as the World Health Organization [24].

Rabies pathogenesis is strictly neurological. Despite the complex and unpredictable symptomatology of rabies [25], the disease generally manifests as one of two clinical forms termed paralytic or furious. Furious or classic rabies, which affects two thirds of rabies patients, presents with the symptoms most commonly associated with RABV: altered mental state, agitation and hydrophobia [26, 27]. In contrast, paralytic rabies is typified by ascending paralysis from the site of infection and other atypical presentations that complicate diagnosis [26, 28]. Irrespective of the initial presenting symptoms,

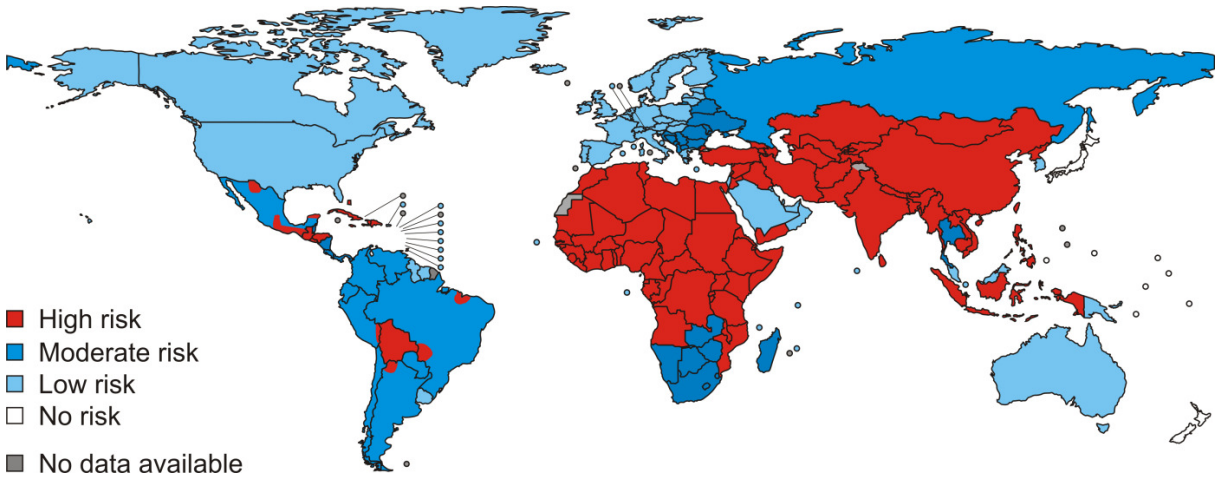

Figure I.1. Global distribution of the risk of contracting rabies.

Colors designate risk levels: high risk is shown in red, moderate and low risk in dark and light blue respectively, and no risk in white. Grey designates areas where data is lacking. Color coding reflects rabies risk rates reported by the World Health Organization in 2013

rabies infection progresses to paralysis, impaired consciousness, coma and finally death [29]. Which specific presentation arises is not currently understood.

At the cellular level, rabies is typically contracted via the bite or scratch of a rabid animal; this exposes host tissues to saliva containing RABV particles. Other reported routes of transmission include inhalation of aerosolized virus [30-33]; contraction via transplant of infected tissues or organs [34, 35]; or contamination of an existing open wound or abrasion with contaminated saliva or tissue [26]. These represent atypical, artificial routes of contagion and can result in non-standard disease progression. At the site of exposure, RABV can undergo a primary amplification in local non-neuronal tissues. Depending on the species of origin, this can occur in the muscle[36] – typical of classic canine rabies – or the cells of the epidermis following infection with bat RABV variants [37, 38]. Neuroinvasion represents the defining step in progression to disease. RABV viruses invade innervating peripheral neurons by internalization at synaptic contacts. Here, both sensory and motor neurons can be infected [26, 39-41]. However, motor neurons are generally accepted as the primary conduit for retrograde transport of RABV to the central

nervous system (CNS) [41]. Infection of these neurons is favored by high affinity association of RABV virions with neuromuscular junctions (NMJ) [42], specialized synapses that interface between muscle fibers and motor neurons. Once the peripheral nervous system (PNS) has been breached, RABV virions retrace synaptic connections from the spinal cord to the brain [41, 43]. Disseminated CNS infection precedes emergence of symptoms resulting in poor prognosis for patients after appearance of early stage symptoms [26].

Following CNS invasion, RABV undergoes a dramatic shift in tissue tropism. Early stages of infection are typified by a uniquely strict neurotropism that excludes infection of non-neuronal CNS cells such as microglia or astrocytes [44]. In contrast, late stage RABV spreads via sensory routes to all major organs [26, 45]. This, in combination with the unpredictable symptomatology and frequency of atypical presentation, accounts for reported cases of accidental RABV contagion from transplantation of contaminated organs [46-48].

A brief overview of the rhabdoviral life cycle

Lyssaviruses belong to the family of negative-strand RNA viruses, Rhabdoviridae, characterized by bullet-shaped enveloped particles (Figure I.2). The rhabdoviral virion incorporates a minimum of five viral proteins which encase the viral genome. The large polymerase (L), nucleocapsid protein (N) and phosphoprotein (P) encapsidate the negative-strand genomic RNA into a tightly ordered helix [49]. Matrix protein (M) then interfaces between the ribonucleoprotein (RNP) and the cytoplasmic tail of the glycoprotein G which studs the plasma membrane-derived viral envelope [50]. Rhabdoviruses encode a single glycoprotein that dictates all steps of entry from association with host receptors at the plasma membrane to pH-dependent fusion within host endosomes. Infection begins by endocytosis of viral particles at the plasma membrane [51, 52]. Endosomes containing incoming virions are transported by

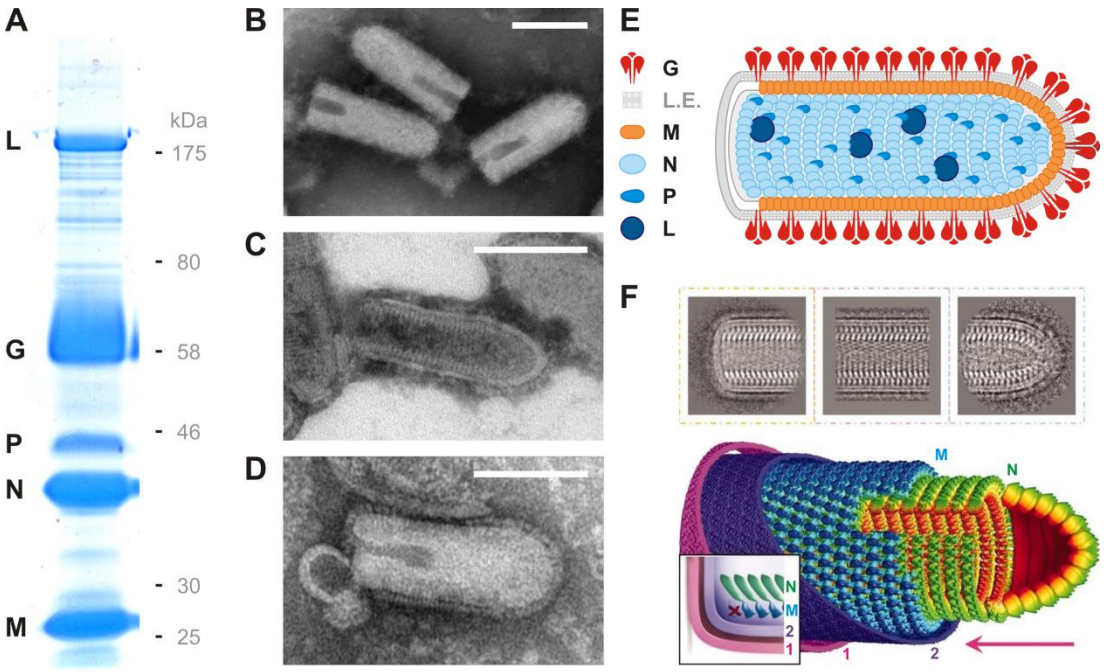

Figure I.2. Rhabdoviral particle structure and morphology.

A. Protein composition of purified VSV virions resolved by SDS-PAGE and stained with SimplyBlue Safe Stain. Viral bands are labeled: large polymerase (L), glycoprotein (G), phosphoprotein (P), nucleoprotrein (N), matrix (M). **B-D.** Transmission electron micrographs of purified virions stained with 1% (wt/vol) phosphotungstic acid (scale bars = 100 nm): B. VSV, C. VSV permeabilized by water wash revealing helical core of the VSV particle, and D. recombinant VSV incorporating RABV G of the CVS strain with clearly visible G spikes. **E.** Simplified schematic of Rhabdovirus particle architecture. Rhabdoviruses are characteristically bullet-shaped. The negative strand RNA genome (not shown) is encapsidated into a tight helix by association with the nucleoprotein (N; pale blue), phosphoprotein (P; blue) and the large polymerase (L; dark blue). Matrix protein (M; orange) forms a reciprocal helix which interfaces with the cytoplasmic tail of the glycoprotein (G; red). Glycoprotein trimers stud the lipid enveloped (L.E.; grey). L and P are shown on the surface of the ribonucleoprotein helix for clarity, this does not necessarily reflect the true positioning of these proteins within the particle. Not depicted in this structure is the core of the particle, which is believed to contain additional matrix protein. **F.** Cryo-EM structure of the VSV particle reproduced from REF. 46. Right: representative two dimensional averages of the virion tip (top), trunk (middle) and base (bottom). Left: Three dimensional model of the viral particle. The tip is a montage model, and the trunk is the Cryo-EM map. The inset illustrates the base region of the particle where an "X" indicates a missing M helical turn below the lowest turn of the N helix. The outer leaflet of the viral membrane (1) is pseudocolored in pink, the inner leaflet (2) in purple, M in blue and N is shown in green. This model excludes a presumed internal core of matrix protein.

microtubule transport from the plasma membrane to the perinuclear region [51, 52]. During transport endosomal acidification leads to conformational changes in G which trigger fusion of the viral membrane with the endosomal membrane and cytoplasmic release of the RNP [52-55]. M dissociates from the RNP and is translocated to the nucleus where it effectuates the shutoff of host gene transcription [56]. In the cytoplasm, L in complex with its cofactor P mediates transcription of viral genes from the N-encapsidated RNA template in a transcription cascade based on gene order. The polymerase complex catalyzes transcription, capping, methylation and polyadenylation of viral mRNAs [57, 58]. This results in the formation of specialized sites of viral transcription and replication which are characterized by high concentrations of the viral proteins L, P and N and significant cytoplasmic mobility [59, 60]. Following several rounds of transcription, L undergoes a functional switch, the regulation of which is not understood, resulting in the initiation of replication. L catalyzes production of the full-length RNA antigenome followed by progeny negative sense genomes from the positive sense template. Progeny genomes encapsidated with N, L and P are then transported to the plasma membrane, where they undergo envelopment and budding by association with M and the cytoplasmic tail of G [61].

The work in this dissertation concerns itself exclusively with the entry events of RABV infection, particularly the process of uptake at the plasma membrane and endosomal transport. Accordingly, subsequent sections will detail the current understanding of three critical events in the process of entry: receptor engagement, internalization at the plasma membrane, and finally endosomal transport.

Rabies receptors

Endocytosis of RABV is receptor-mediated. Accordingly, three putative protein receptors have been described to date: the low affinity neurotrophin receptor, p75TNR [62]; neural cell adhesion

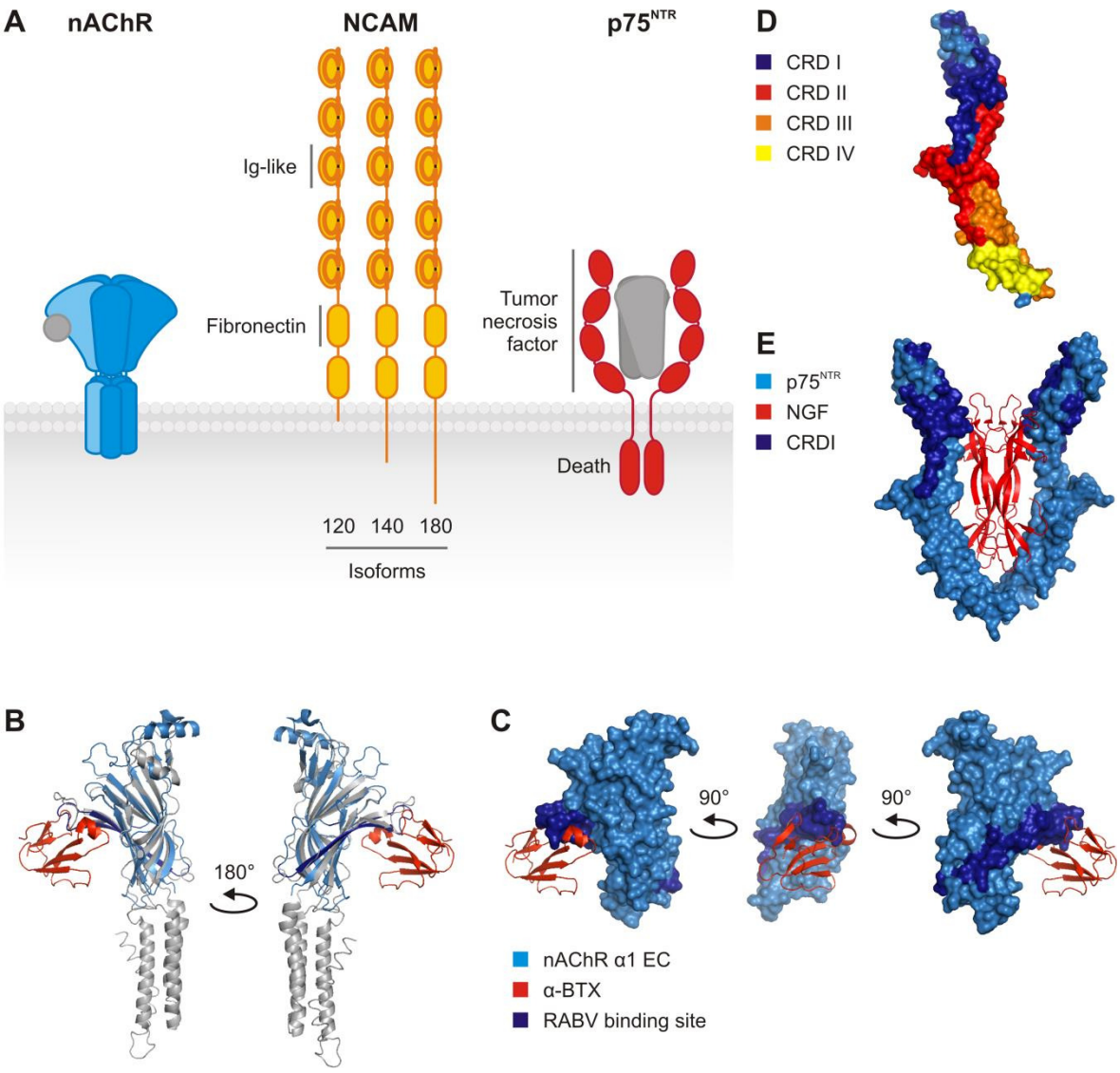

Figure I.3. Putative rabies receptors and known binding sites.

A. Three transmembrane proteins have been identified to serve as receptors or attachment factors for RABV (in order of discovery): the nicotinic acetylcholine receptor (nAChR); neural cell adhesion molecule, NCAM (also known as CD56); and the low affinity neurotrophin receptor, $p75^{NTR}$. RABV virus binds to all three isoforms of NCAM, which differ by the length of the cytoplasmic domain: NCAM-120 lacks a cytoplasmic tail and associates with the membrane by glycosyl phosphatidylinositol-anchoring, whereas NCAM-140 and NCAM-180 are both membrane spanning proteins. **B.** Superimposed crystal structures of the homologous bacterial pentameric ligand gated ion channel of *Erwinia chrysanthemi* (grey; PDB: 2VL0) and the ectodomain of nAChR α1 subunit (light blue) with bound α-bungarotoxin (α-BTX; red; PDB: 2QC1). RABV G binding requires residues 173-204 of the α1 subunit, indicated in dark blue, for nAChR association; these coincide with the beta sandwich binding site of alpha-bungarotoxin. **C.** Surface rendering of the ectodomain (EC)

Figure I.3 (continued) of nAChR α1 subunit (light blue) with bound α-bungarotoxin (α-BTX; red; PDB: 2QC1). RABV binding site shown in dark blue. **D.** Crystal structure of a monomer of $p75^{NTR}$ (PDB: 1SG1) [1]. $p75^{NTR}$ belongs to the tumor necrosis factor receptor (TNFR) superfamily, characterized by four extracellular cysteine-rich domains (CRDs). CRDs I, II, III and IV are pseudocolored blue, red, orange, and yellow, respectively. Additionally, the cytoplasmic tail of $p75^{NTR}$ contains a Death domain. **D.** Crystal structure of dimeric $p75^{NTR}$ in complex with a dimer of neurotrophic factor 3 (NT-3; PDB: 3BUK). The endogenous ligands of $p75^{NTR}$, (NT-3) and nerve growth factor (NGF), both bind $p75^{NTR}$ by nestling in the concavity formed by the dimerization of $p75^{NTR}$ and associating with CRDs III and IV, and the junction between CRD I and II. In contrast, RABV G exclusively binds the first CRD of $p75^{NTR}$. $p75^{NTR}$ is shown in light; NT-3 in red; the binding site of RABV G, CRD I, is shown in dark blue.

molecule (NCAM) [63]; and the nicotinic acetylcholine receptor (nAChR) [64] (Figure I.3A). In addition to these proteinaceous receptors, gangliosides and specific carbohydrate moieties may also play a role in cellular susceptibility to RABV [65, 66]. The existence of multiple putative receptors suggests that receptor usage may vary depending on cell type or stage of disease. However, the functional relevance of any single receptor molecule in rabies entry and pathogenesis remains controversial [67, 68].

The interaction between RABV G and nAChR has been the most extensively studied and characterized. The receptor binding site on G has been mapped, and shares sequence [69] and structural [70] homology with curare-mimetic toxins which also bind nAChR. Extensive evidence from competition experiments [64, 70, 71] and antibody cross-reactivity assays [72, 73] establish unequivocally that RABV G and curare-mimetic toxins share the same binding site on the nAChR α1 subunit [74, 75] (Figure I.3B,C). In contrast, the specific role of nAChR for in vivo infection and neuroinvasion is unclear. RABV antigens are found to concentrate at the NMJ by virtue of the high concentration of nAChR at these synapses [42, 64]. However, these receptors are predominantly located on the postsynaptic membrane[67]. As a result, association with nAChR is likely to underlie internalization and primary viral amplification in muscle tissue rather than neuronal uptake [67]. An indirect contribution to neuroinvasion has also been hypothesized. Here, nAChR may merely facilitate association of virus with receptors on the opposing motor neuron membrane by concentrating viral particles at the target site of neuroinvasion, the NMJ[64,

[67]. This presupposes that endocytosis of nAChR following association with RABV is minimal or inefficient to prevent competition with uptake at the presynaptic membrane. No evidence for such a model exists. Accordingly, nAChR is not considered a major contributor to neuronal infection [67].

Unlike nAChR, $p75^{NTR}$ is expressed on the presynaptic membrane of peripheral neurons [67]. The first cysteine rich domain of $p75^{NTR}$ mediates a high affinity interaction (Kd = 31 pM, cell associated[76]; Kd = 400 nM, soluble $p75^{NTR62}$) with trimeric, soluble RABV G [76, 77] (Figure I.3D, E). Specific residues in G, F318, K330, R333 and H352, mediate association with soluble and membrane-bound $p75^{NTR}$ [62]. Due to the positioning of these sites on RABV G, F318 and H352 may disrupt association with the receptor indirectly by destabilizing prerequisite trimerization of RABV G, whereas K330 and R333 are likely involved directly in $p75^{NTR}$ binding. Importantly, K330 and R333 are also major determinants of RABV virulence and infection in the peripheral nervous system [78]. Exogenous expression of the receptor in resistant cells increases their affinity for soluble G and renders these cell lines susceptible to infection with street RABV isolates [39]. Therefore, as with nAChR, sound biochemical evidence implicates $p75^{NTR}$ as a binding partner for the RABV G ectodomain. However, an equivalently compelling body of evidence challenges the hypothesis that $p75^{NTR}$ serves as a receptor for RABV infection in vitro or in vivo. Although widely disseminated in both sensory and motor neurons during embryogenesis, the expression of $p75^{NTR}$ at the presynaptic membrane of adult NMJ is controversial [67]. Reports of $p75^{NTR}$ expression in adult spinal motor neurons exist [79]; however, detection is variable and studies correlate this localization with neuronal disease states and damage responses which may alter expression levels at the synaptic membranes [80]. Damage responses could arise following a rabid animal bite or abrasion; however, the presence of $p75^{NTR}$ receptors at the site of exposure in vivo remains to be assessed. Expression of $p75^{NTR}$ also does not necessarily correlate with cellular susceptibility to rabies or disease outcome. Only a fraction of $p75^{NTR}$ positive adult murine dorsal root ganglion (DRG) neurons can be infected with fixed

RABV strains in vitro [34]. Furthermore, neuroinvasion and mortality was unaffected in mice lacking the extracellular domains of $p75^{NTR}$ or wild-type mice infected with mutant RABV that lack $p75^{NTR}$ binding [34]. These results suggest that $p75^{NTR}$ may serve merely as a co-factor or attachment factor in RABV uptake [34, 67]. Consistent with this view, soluble $p75^{NTR}$ alone does not neutralize rabies infection in vitro [62].

NCAM, a cell adhesion glycoprotein from the immunoglobulin (Ig) superfamily, is expressed at both the pre- and postsynaptic membranes of adult NMJ [67]. At the plasma membrane, NCAM exists as three isoforms which differ in the membrane anchoring and cytoplasmic tails, but retain the same Ig ectodomain. Unlike $p75^{NTR}$ and nAChR, the role of NCAM in RABV infection has been primarily explored from a virological perspective. Expression of all three isoforms of NCAM confers susceptibility to RABV in resistant cell lines [63, 81]. Inhibition of RABV infection by co-incubation with soluble NCAM, further supports a direct interaction between NCAM and RABV G [63]. In vivo, CNS dissemination of virus following intramuscular inoculation was significantly reduced in NCAM knock-out mice, and correlated with a delay of disease progression and death [63]. However, neuroinvasion from the peripheral inoculation site was not abrogated [63], excluding NCAM as an exclusive determinant of peripheral infection.

Recently, RABV G-dependent cotransport of virions with cognate RABV receptors in neurons of the DRG and spinal cord was demonstrated by live single particle imaging in compartmentalized cultures [8, 36]. In motor neuron preparations, virions undergoing endosomal transport were found to colocalize with nAChR, $p75^{NTR}$ and NCAM [36]. In DRG cells, a distinct entry behavior was observed that correlated with neurotrophin receptor association [8]. RABV particles cotransported with neurotrophin receptor displayed faster more processive axoplasmic transport consistent with a functional role for $p75^{NTR}$ association during RABV entry into sensory neurons. NCAM and nAChR were not evaluated in DRG cultures. These studies provide in vitro evidence that RABV can be internalized concomitantly with each of its putative receptors into peripheral neurons of embryonic origin. How these results translate for in

vivo infection of adult animals remains to be studied. Collectively, the body of research underscores that when and where individual RABV receptors is utilized is still an open question.

Rabies G: Structural and functional considerations

Rhabdoviral glycoproteins belong to a unique class of fusogenic proteins, termed class III, characterized by reversible [82, 83] pH-dependent conformational rearrangements [55, 84]. Two stable conformations of G exist, and these correlate with its functional states. In its native prefusion conformation, at neutral pH, G is trimeric [85] and mediates receptor attachment and association with the cellular membrane. The native state of G retains its fusogenicity, which is triggered upon exposure to an acidic environment. At acidic pH, G adopts an inactive postfusion conformation, which prevents premature fusion of de novo synthesized G during trafficking through the acidic Golgi to the plasma membrane [82, 83]. These two states exist in equilibrium, and transient G intermediates are adopted during rearrangement from the native to the inactive form [86, 87]. The structural changes that occur when G transitions from its prefusion to its postfusion state drive fusion of the viral and host membrane within the endosomal compartment leading to RNP release.

The crystal structures of VSV G at neutral and acidic pH have been solved [54, 55], and sequence analysis and fold prediction of G from other rhabdoviral genera suggests that the structure is conserved [55]. G consists of four domains – lateral (domain I), trimerization (domain II), pleckstrin homology (domain III) and fusion (domain IV)—forming a hairpin structure [54, 55]. Despite major reorientations of the domains of G following transition from the pre- to the post- fusion conformations, only the hinge region and the trimerization domain undergo significant refolding [54]. Restructuring of the hinge region between domains III and IV pivots the fusion domain by 94°, which, in combination with the refolding of the trimerization domain abutting domain II, opens up the hairpin structure. This orients the fusion

domain towards the host endosomal membrane. Fusion loops at the tip of this domain embed into the luminal phospholipid leaflet and form the physical link to the endosomal membrane required for pore formation. Mutation of hydrophobic residues within these loops results in glycoproteins that are non-fusogenic [88]. Finally, refolding of the C-terminal portion of the trimerization domain re-closes the hairpin and brings the transmembrane and fusion domains together. This final restructuring drives pore formation. Because refolding of the trimerization domain coordinates the molecular movements required for fusion, G trimers must dissociate to allow pore formation [54]. Consistent with this view, monomeric intermediate structures of G have been visualized on the viral surface and analyzed biophysically [87].

The structural rearrangements and changes in trimeric state of G during acidification suggest that associations with receptors bound at the plasma membrane will be affected during acidification. Engagement of $p75^{NTR}$ requires a trimeric ligand [76, 77]. Therefore, $p75^{NTR}$ association will likely be abolished as endosomal acidification causes the equilibrium of G conformations to shift towards the post-fusion state. This possibility may explain the observation that $p75^{NTR}$ is not sufficient to mediate susceptibility to RABV [34]: $p75^{NTR}$ cell lines that do not support RABV infection may lack an intracellular receptor required to facilitate fusion. Curiously, studies of the pH dependence of RABV binding to nAChR demonstrate a peak in affinity of G for the receptor at pH 5.5-5.6 which correlates with the pH of fusion for rabies G (pH 5.8) [71]. In contrast, at neutral pH, RABV G affinity for nAChR is 10% of its maximum. Since nAChR is primarily expressed at the postsynaptic membrane, it is unlikely that it serves as an intracellular receptor for RABV. However, the low affinity, high avidity interaction of RABV G with nAChR at the cell surface may explain how nAChR can concentrate RABV and facilitate uptake at the opposing presynaptic membrane rather than sequestering virions to the postsynaptic membrane. It should be noted, nonetheless, that these pH-dependent studies were carried out with the CVS strain of rabies

which bypasses muscle cell infection [89]. Accordingly, the pH dependent affinity for nAChR of G derived from RABV street strains that do infect muscle tissue may differ.

Rabies is a pathogen of the central nervous system; therefore, pathogenicity is strictly dependent on the ability of RABV to invade, replicate and spread within neuronal tissues. RABV G contributes to each of these processes and is, consequently, a major determinant of RABV virulence. Replacement of G of an attenuated strain with that of a pathogenic strain and vice versa confers to the virus a level of pathogenicity that more closely approximates that of the donor virus [90-93]. Five specific amino acids have been further identified to correlate strongly with robust neurotropism and lethality in vivo: A242, D255 and I268 identified by sequence comparison between the Nishigahara and RC-HL strains [94]; and K330 and R333, identified by passage of virus with neutralizing antibodies and comparison of the resultant attenuated strain with its parent strain [78, 95]. Mutation of these residues results in loss of spread of infection in vitro [96] and the CNS in vivo [78, 89, 96]. Interestingly, A242, D255 and I268 are located within the pleckstrin homology domain believed to be involved in receptor binding; similarly, K330 and R333 overlap directly with critical residues for $p75^{NTR}$ binding. Therefore, although differential glycosylation [97, 98], dysregulation of expression levels [99, 100], increased induction of apoptosis [99], and altered interaction with other viral proteins [91] all contribute to G-dependent attenuation of RABV strains, it is apparent that the predominant mechanism by which G modulates rabies virulence is by dictating affinity for and spread between neurons. Therefore, studying the mechanisms by which G mediates uptake and transport of virus within cells may not merely provide us with insights into the biology of RABV, but broaden our understanding of the factors that impact rabies pathogenicity.

Molecular mechanisms of RABV endocytosis at the plasma membrane

The first step in viral endocytosis is invagination and internalization at the plasma membrane. Viruses hijack a variety of endocytic processes to gain the cellular interior: Ebola virus, for example, internalizes within macropinosomes [101, 102], simian virus 40 utilizes caveolae [103], bunyaviruses are endocytosed by clathrin coated pits [104-106], and some viruses such as Lassa and lymphocytic choriomeningitis viruses engage novel endocytic pathways that are yet to be fully characterized [107]. Early studies implicate clathrin-mediated endocytosis as the predominating, conserved mechanism of RABV uptake at the plasma membrane. Incoming rabies virions have been observed within clathrin-coated pits in transmission electron micrographs of infected chick embryo-related cells [108] and hippocampal neurons [109]. However, the existence of multiple rabies receptors and the observation of RABV in intracellular vacuoles in micrographs of hippocampal neurons [109], raises the possibility of differential uptake routes dependent on receptor usage. Consistent with this view, studies of uptake of putative rabies receptors following engagement with endogenous ligands, crosslinking antibodies or toxins indicates that $p75^{NTR}$, NCAM and nAChR internalize by different cellular mechanisms. $p75^{NTR}$ and NCAM internalize via clathrin-mediated endocytosis [28, 110, 111] whereas nAChR uptake into filamentous invaginations from the plasma membrane is clathrin-independent [112, 113]. Furthermore, RABV receptor usage may vary depending on cell type, and RABV uptake has not been assessed in cells that are relevant for neuroinvasion, arguably the most important step in RABV pathogenesis. Transmission electron microscopy, like all fixed microscopic techniques, is limited by its instantaneity. Observation of viral particles within coated pits cannot, therefore, inform about their role in establishment of infection. As a result, further experimentation is needed to determine which endocytic mechanism mediates RABV entry, how these relate to establishment of infection and whether uptake mechanisms differ in cellular populations relevant for disease.

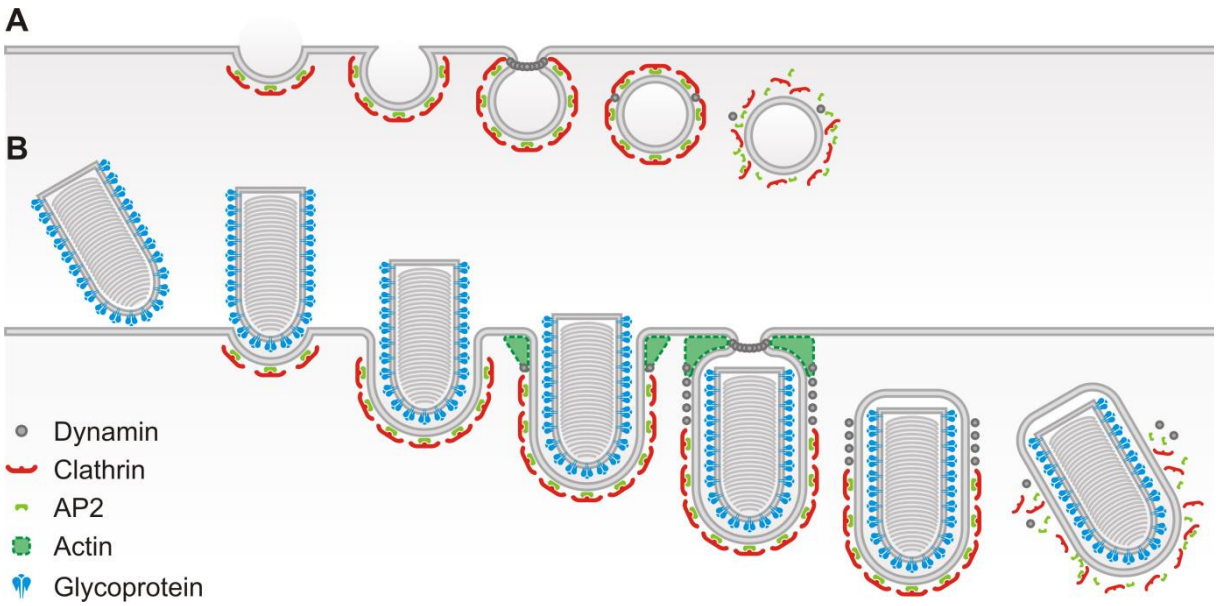

Figure I.4. Model of VSV uptake into actin-dependent, partially coated pits.

A. Simplified schematic of the steps involved in clathrin-mediated endocytosis. Clathrin and its heterotetrameric adaptor complex, assembly polypeptide 2 (AP2), are recruited in a 1:2 stoichiometric complex to the plasma membrane. Accumulation and assembly of clathrin triskelions into a lattice drives invagination and formation of a vesicle at the plasma membrane. Recruitment of dynamin catalyzes scission of the vesicles from the plasma membrane, following which the clathrin-coated pit dissociates and disassembled from the endosome. B. Model of actin-dependent internalization of VSV into partially coated pits. The general mechanism of clathrin-mediated endocytosis proceeds as in A. with some mechanistic differences. Formation of a larger vesicular structure results in greater recruitment of clathrin and its adaptors and a longer duration of the envelopment process. However, at completion of envelopment the clathrin lattice only partially coats the vesicle. To complete the internalization process, actin is recruited to facilitate completion of envelopment and dynamin-dependent scission from the plasma membrane.

In addition, live high resolution microscopy of internalization of the related Rhabdovirus, VSV, whose entry is clathrin-dependent [37, 114, 115], revealed that viral clathrin-coated pits are only partially coated with clathrin triskelions, and require increased actin recruitment to complete envelopment [37] (Figure I.4). The requirement for actin and partial clathrin coating does not represent a novel clathrin-dependent endocytic pathway, but merely accommodation of clathrin-coated pits to the VSV particle whose dimensions exceed the luminal diameter of clathrin-dependent endosomes. Accordingly,

naturally occurring truncated particles of VSV internalize independently of actin within canonical coated pits [116]. These observations galvanized additional research into the actin-dependence of clathrin-coated pits leading to the demonstration that membrane tension dictates actin recruitment [117]. These results underscore the broader relevance of viral entry studies and the opportunity to reveal new cell biology through the study of viral uptake.

Strategies of axoplasmic transport within neurons

To overcome the highly polarized architecture of peripheral neurons, RABV exploits existing cellular mechanisms that relay molecular signals from distal synapses to the somatodendritic compartment. Long range microtubule (MT) networks connect neuronal termini to the perinuclear region and mediate bidirectional axonal transport of a wide array of biologically active molecules and compartments [118, 119]. Among these are proteins [119], mRNAs, organelles and endosomes [119-121]. In neurons, ATP-driven transport along these tracks counteracts the prohibitively restrictive mean-squared displacement inherent in passive cytoplasmic diffusion [122]. Rabies is not unique in subverting existing neuronal circuitry and, by extension, host trafficking systems to evade the blood brain barrier. Several neurotropic pathogens also exploit this route to invade the central nervous system [118, 122] (Table 1). However, viruses differ in both directionality of transport and mode of MT engagement. Alphaherpesviruses, for example, invade sensory neurons and undergo both retrograde and anterograde transport [2]. Depending on the mode of entry, pathogens also differ in the molecular interactions that bridge between the virus and MTs: whereas polio- [3] and adeno- [16] viruses are transported within endosomes which are tethered to MTs via host proteins, alpha herpesviruses [123] interact with cellular motors directly via capsid and tegument proteins.

Table I.1. Viruses and toxins that invade the CNS via the neuronal route. Blood brain barrier (BBB). Neuromuscular juntion (NMJ).

Viral family	Pathogen	Route of neuroinvasion	Pathology	Refs
Herpesviridae	Alphaherpesviruses	Sensory neurons	oral and genital herpes, encephalitis, keratitis	[2]
Picornaviridae	Poliovirus	BBB and NMJs	Paralysis	[3]
	Enterovirus 71	Peripheral nerves	Encephalitis and paralysis	[4]
	Theiler's murine encephalomyelitis virus	Transfer to oligodendrocytes after axonal transport	Inflammation, demyelination and axonal damage	[5, 6]
Rhabdoviridae	Rabies virus	NMJs	Encephalitis	[7, 8]
Paramyxoviridae	Measles virus	BBB and peripheral nerves?	Encephalitis	[9]
Flaviviridae	West Nile virus	BBB and peripheral nerves	Encephalitis and flaccid paralysis	[10, 11]
	St Louis encephalitis virus	Olfactory nerves	Encephalitis and inflammation	[12]
	Tick-borne encephalitis virus	Autonomic nerves		[11]
Bornaviridae	Borna disease virus	Nose and olfactory neuroepithelia	Behavioral changes	[13, 14]
Orthomyxoviridae	Influenza A virus	Peripheral nerves	Encephalitis	[15]
Adenoviridae	Adenovirus	NMJs and ocular infections?	Brain tumours and encephalitis	[16]
Not applicable	Botulinum toxin A	NMJ	Flaccid paralysis	[17, 18, 19]
Not applicable	Tetanus toxin	NMJ	Spastic paralysis	[21]

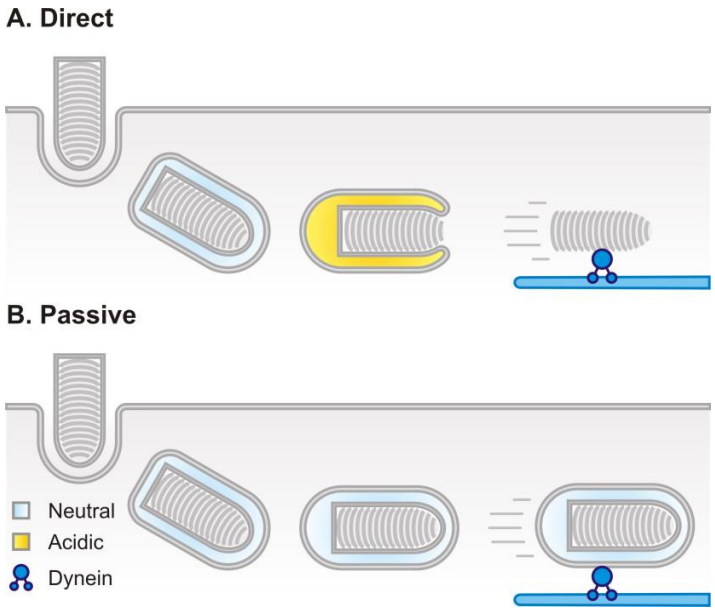

Figure I.5. Model of microtubule engagement for RABV axoplasmic transport.

Two models exist for retrograde transport of rabies virions. **A.** In the direct interaction model, virus is endocytosed at the plasma membrane with endosomes that acidify shortly after uptake. RNP is released and associates with dynein motors on the microtubules directly, likely via the phosphoprotein P which is known to contain a dynein light chain binding motif, LC8. **B.** The passive model, on the other hand, involves endosomal transport prior to acidification. As a result, the virus is a passive passenger, and minus end motors are engaged exclusively via host factors.

The dependence of rabies pathogenesis and spread on axoplasmic flow was first hypothesized by Louis Pasteur in 1884 [124] and proven by prevention of disease progression by severing of ascending fibers in infected animals [125]. It was subsequently demonstrated pharmacologically that microtubule (MT) depolymerizing agents halt infection in vitro [126] and pathogenesis in vivo [124, 127]. MT-dependent RABV transport could proceed by two mechanisms defined by direct MT engagement or passive transport of the virus (Figure I.5). In the direct engagement model, local endosomal acidification at the site of endocytosis results in fusion and RNP release within the neuronal termini. RNPs then engage MT via direct interaction with minus-end motor complexes for transit to the cell body. This scenario dictates that viral core protein(s) as well as G serve as determinants of retrograde transit. The competing model

of passive transport hypothesizes that endocytosed RABV virions remain encased within endosomes throughout long-range travel. In this scenario, endosomal acidification is triggered upon delivery of endosomes to the soma. Here, host proteins are the sole determinants of viral axoplasmic transport following uptake at the plasma membrane. The discovery of a dynein-binding motif in P pointed to the possibility that RABV RNPs directly engage microtubule motors [128, 129]. However, a RABV P mutant lacking dynein association retained its neuroinvasive and pathogenic properties in vivo [130, 131]. This result, combined with the observation that RABV G alone can confer retrograde transport to non-neurotropic viral vectors [36, 132-135], excluded naked RNP transport along MTs as the predominant mechanism of axoplasmic transport [130, 131, 136].

Single particle studies have provided further credence to the RABV endosomal transport model. RABV incorporating fluorescently-tagged transmembrane and RNP proteins translocates intact within axons [7]. Furthermore, receptors recruited at the plasma membrane remain associated with rabies or RABV G-pseudotyped lentiviruses during long-range transport instead of being shed along with the fused viral membrane upon gaining the cellular interior [8, 36]. These reports provide compelling evidence that rabies viruses are transported intact within endosomes. However, no experiment to date has correlated passive transport of RABV with establishment of infection in neuronal cells. The work described in Chapter 2 of this dissertation demonstrates that fusion of virions in the somatodendritic compartment is required for productive rhabdoviral infection in primary neurons of the peripheral nervous system.

Technical advances in the study of rabies virology

The strict neurotropism of RABV results in challenges for its study in vitro. Wild type or “street” isolates from infected animals propagate poorly in tissue culture. The narrow cell tropism of RABV virus

can be overcome by adaptation of rabies isolates to a broader range of cell types. “Fixed” strains are laboratory-adapted derivatives of street isolates that have been serially passaged in tissue culture or research animals to generate viruses with defined pathogenic characteristics. Commonly used fixed strains have been derived from canine, bat and human rabies viruses allowing the study of phenotypic differences in rabies infection resulting from the host species of origin [137]. Despite extensive passaging, these strains display a range of virulence phenotypes [68, 138]. Pathogenic strains retaining near-wild type neuroinvasive traits cause morbidity and death in laboratory animals following peripheral, intramuscular or foot pad, inoculation. These can be used as challenge viruses to assess the effectiveness of rabies vaccines. In contrast, nonpathogenic strains fail to progress to disease or death following intracerebral inoculation and have been used as vaccine strains. Intermediate, attenuated strains may cause disease when inoculated into the CNS, but are defective in propagation from peripheral infection sites to the brain. Lab-adapted viruses can be cultured in a variety of mammalian cells including non-neuronal cell lines and have served as invaluable tools for the study of rabies biology *in vitro*.

In addition to broadened cell tropism, further passaging of pathogenic fixed strains enables generation of derivative substrains with more pronounced attenuation phenotypes. Comparison of these derivative strains with their parental viruses allows study of the viral genetic determinant underlying RABV pathogenicity [90, 91, 94]. The utility of genetic manipulation of virus via passaging has been extended further by the development of reverse genetics systems for non-segmented negative strand RNA viruses [139]. The first complete reverse genetics system was developed for rabies virus [140, 141]; this has been followed by the development of similar systems for several members of the rhabdovirus, paramyxovirus and filovirus families, and for Borna disease virus and nyamavirus [141]. Reverse genetics systems allow de novo synthesis of infectious virus from cloned cDNA, opening up the possibility for deliberate mutation and manipulation of the viral genomic make up. In rhabdovirus virology, it has been

used to artificially codon-reoptimize select viral genes [100]; incorporate fluorescent proteins, either as exogenous genes or as tags onto existing genes, for direct detection and tracking using high resolution imaging techniques; generation of deletion mutants of both entire viral genes or gene elements; and for the production of chimeric recombinant viruses.

Here, we report the use of recombinant vesicular stomatitis viruses (rVSV) incorporating G from vaccine and neuroinvasive RABV (rVSV RABV G) as surrogate viruses for the study of RABV entry. VSV tolerates genetic incorporation of G from foreign enveloped viruses in lieu of its endogenous glycoprotein, and has served as a powerful tool to examine the entry processes of viruses. The robust growth and a broad range of permissive cell types of VSV can extend the tropism of viruses lacking devoted or efficient culture systems facilitating their study in tissue culture [142]. Furthermore, VSV and rVSV clones can be worked with under biosafety level 2 conditions enabling the study of dangerous pathogens, such as Ebola [102, 143, 144] and Lassa[145], outside of the restrictive environment of higher biosafety level labs. They are therefore useful in the study of viruses which lack in vitro culturing systems, grow to low titers, are restricted in common cell culture systems, or lack molecular tools for their study. In the study of RABV entry, rVSV RABV G viruses allow investigation of rabies entry with increased safety, but more importantly allows the determination of the role of G in isolation of other RABV genetic factors. Although limited in their utility for the study of rabies pathogenesis, rVSV RABV G serve as useful tools for the study of entry and neurotransmission.

The study of rabies entry poses challenges for virologists also due to the complexities inherent in studying a predominantly neuronal infectious process. Neurons are highly polarized cells with complicated geometries. Axons extend distances that far exceed the dimensions of the neuronal cell body, and incorporate highly functionally specialized cellular and membrane domains. Synapses, in particular, have unique exo- and endocytic environments as well as local gene expression profiles that

may impact the entry processes of pathogens that gain access to the nervous system by internalization at their membranes. In addition, the broad range of functionally and morphologically distinct neuronal subtypes raises doubts about the generalizability of entry from one neuronal population to another. Therefore, a challenge in rabies biology is the establishment in vitro of physiologically relevant neuronal systems to study the infectious process.

To address the fact that RABV is endocytosed at neuronal termini and undergoes long-range microtubule-dependent transport to the cell body, rabies infection has been studied in neurons cultured in compartmentalized Campenot chambers [146] that allow isolation of somatodendritic complexes from their termini [147]. Here, a Teflon ring with two culturing subdivisions is adhered to a coverslip in which guiding grooves for neuronal outgrowth have been manually scratched into the surface. The Teflon ring is adhered by means of biologically compatible silicone grease sealant. Neurons seeded into one compartment extend processes along the grooves through the grease layer into adjacent, otherwise isolated, compartments. In neuroscience, Campenot chambers have been used for the study of peripheral neuron axon biology and, in particular, axonal transport of nerve growth factors [147-149]. In virology, these devices have been used extensively to study the biological mechanisms of herpesvirus uptake and release [150-152]. Compartmentalized cultures of this sort have further allowed the demonstration of retrograde transport of RABV following entry [146] and the occurrence of anterograde release of progeny virions from primary DRG neurons [153]. Despite the obvious utility of the Campenot system, it is suitable only for the study of select populations of neurons, primarily peripheral neurons. It further suffers from poor reliability and experiment-to-experiment reproducibility of culturing conditions [154]. To overcome some of these limitations, we implemented microfluidic compartmentalized techniques for the culture of neurons.

Microfluidic devices are culturing chambers typically molded from polydimethylsiloxane (PDMS). In the context of compartmentalized neuronal culture, these involve two or more compartments connected by micrometer scale grooves molded directly into the PDMS. Direct incorporation of microgrooves in the culturing device eliminates the need for scratches on the coverslip surface as axonal growth guides and enables precise manipulation of the geometry of these device features. In particular, in-house customization allows the experimenter to define groove length extending the technology of compartmentalized culture to neuronal populations with shorter processes. Indeed, microfluidic techniques were adopted by neuroscientists for the study of CNS neurons that cannot be cultured in standard Teflon chambers [147, 154]. Devices are manufactured by photolithography and replicate molding. Photolithographic techniques are used to generate a relief mold of the desired culturing platform out of UV-reactive epoxy-based photoresist. Exposure to UV through a transparency allows patterned application of the photoresist onto a silicon substrate. PDMS devices can then be cast reproducibly against the master mold allowing consistent reproduction of identical culturing devices. The surface chemistry of PDMS allows these to be subsequently adhered to a variety of substrates, including glass and plastic. This is accomplished by irreversible plasma bonding or reversibly by chemical treatment of the PDMS and acceptor surfaces. Importantly, it eliminates the need for and technical challenge inherent to device adherence via silicone sealant. Accordingly, these culturing platforms provide an ideal system to model rabies entry from the neuronal termini to the cell body in a variety of neuronal cell types.

The advent of these techniques and their recent commercialization has spurred a recent flurry of publications studying anterograde and retrograde viral axoplasmic transport [8, 36, 136]. We also adopt a customized microfluidic device [155, 156] to characterize the endocytic mechanism underlying rabies uptake at the termini of neurons of the dorsal root ganglion and spinal cord. Beyond compartmentalization,

microfluidics represent a significant advance over traditional Campenot chambers because they provide the experimenter with the ability to autonomously tailor device design to address a specific research question. Fully customizable device geometries have rendered feasible the exquisite chemotemporal control of cellular environments at the micron scale. These advances in neuronal culture paired with reverse genetic techniques uniquely position us to approach fundamental questions about rabies infection in relevant neuronal populations in vitro.

Viral entry is not merely the process of translocation across the cellular membrane. It is the collection of events coordinating delivery of pathogenic genetic material from the extracellular environment to a specific intracellular site of replication. Rabies virus (RABV) invades the central nervous system (CNS) by retracing peripheral neuronal circuitry from the site of inoculation, through the spinal cord to the brain. This neuroinvasive route requires that virions traverse the most extreme of cellular morphologies: in excess of a meter of cytoplasm can separate spinal cord synapses, the sites of RABV uptake, from their somatodendritic compartments where viral replication occurs. To accomplish this logistical feat, RABV subverts existing cellular infrastructure that relays molecules and organelles at the neuronal termini back to the soma. The work in this dissertation uses a recombinant vesicular stomatits virus (rVSV) incorporating RABV G to characterize the mechanism of RABV internalization at the cell surface of epithelial cells and primary peripheral neurons. The combination of studies in epithelial and primary cell culture has allowed us to investigate kinetic aspects of RABV entry via clathrin-mediated endocytosis (CME) as well as the primary mode of cellular internalization, and relate these to infection in cell populations that are important for viral pathogenesis.

CHAPTER 1:

UPTAKE OF RABIES VIRUS INTO EPITHELIAL CELLS

BY CLATHRIN-MEDIATED ENDOCYTOSIS DEPENDS UPON ACTIN

Silvia Piccinotti[1,3], Thomas Kirchhausen[2,3,4], and Sean P. Whelan[1,3]

Departments of Microbiology and Immunobiology[1], and Cell Biology ,[2]
Program in Virology[3], Harvard Medical School, Boston, Massachusetts, USA
Program in Cellular and Molecular Medicine[4], Boston Children's Hospital, Boston, Massachusetts, USA

Data within this chapter is published and a reprint of the article is provided with the archived copy of the dissertation.

The published manuscript may also be accessed as follows:

Journal of Virology, November 2013;87(21):11637-47 doi: 10.1128/JVI.01648-13

http://jvi.asm.org.ezp-prod1.hul.harvard.edu/content/87/21/11637.long

N.B. In this manuscript the abbreviation rVSV RABV G denotes the rVSV SAD B19 G strain. Elsewhere in this dissertation rVSV RABV G signifies any rVSV incorporating RABV G.

ABSTRACT

Rabies virus (RABV) causes a fatal zoonotic encephalitis. Disease symptoms require replication and spread of the virus within neuronal cells; however, in infected animals as well as in cell culture the virus replicates in a broad range of cell types. Here we use a single-cycle RABV and a recombinant vesicular stomatitis virus (rVSV) in which the glycoprotein (G) was replaced with that of RABV (rVSV RABV G) to examine RABV uptake into the African green monkey kidney cell line BS-C-1. Combining biochemical studies and real-time spinning-disk confocal fluorescence microscopy, we show that the predominant entry pathway of RABV particles into BS-C-1 cells is clathrin dependent. Viral particles enter cells in pits with elongated structures and incomplete clathrin coats which depend upon actin to complete the internalization process. By measuring the time of internalization and the abundance of the clathrin adaptor protein AP2, we further show that the pits that internalize RABV particles are similar to those that internalize VSV particles. Pharmacological perturbations of dynamin or of actin polymerization inhibit productive infection, linking our observations on particle uptake with viral infectivity. This work extends to RABV particles the finding that clathrin-mediated endocytosis of rhabdoviruses proceeds through incompletely coated pits which depend upon actin.

INTRODUCTION

Rabies virus (RABV) is the prototypical member of the zoonotic lyssavirus genus responsible for fatal encephalitis in animals and humans. A single-stranded negative-sense RNA virus, RABV encases its RNA genome in a bullet-shaped, enveloped particle that incorporates a single surface glycoprotein (G). RABV G mediates all internalization steps from cell binding to membrane fusion. In addition, G is a major determinant of RABV neurotropism [157]. Conjugation or pseudotyping with the ectodomain of pathogenic RABV G or peptides derived from receptor-binding regions allows retargeting of biologically active molecules to the central nervous system (CNS) for drug delivery or as neurotracers [133, 134]. Since a large part of RABV pathogenesis is reliant on the virus garnering access to neurons and the CNS, G is also a determining factor in RABV virulence. The pathogenicity of attenuated strains can be effectively increased by replacing the glycoprotein with one from a neurotropic, virulent strain [93].

Like other rhabdoviruses, RABV gains access to the cellular interior by endocytosis and subsequent low pH-dependent fusion [53, 158, 159]. Electron micrographs of viral particles in vesicles with electron-dense coats suggest that clathrin-coated pits mediate the uptake of RABV in both neuronal and nonneuronal cells [108, 160]. However, static images cannot inform on the fate of such particles or the relevance of these interactions for subsequent infection. High-resolution live-imaging techniques permit tracking of viral uptake into coated pits [37, 114, 116, 161-163]. Fluorescence tagging of coated-pit components and quantitative analysis methods have revealed differences for the pits engaging fluorescently tagged viral particles [37, 116]. In particular, vesicular stomatitis virus (VSV) particles are internalized through partially coated clathrin pits that require actin for the completion of envelopment [37]. The morphology of the particle is a key determinant of actin dependence, since a truncated, defective interfering particle of VSV, DI-T, does not require actin polymerization [116]. This observation also extends to other viruses with

dimensions compatible with canonical coated pits, as clathrin-dependent uptake of the 60-nm-diameter parvovirus is also actin independent [116, 161].

In the present study, we employed biochemical and high-resolution imaging approaches to study RABV internalization. For this purpose, we used a recombinant VSV (rVSV) expressing RABV G (rVSV RABV G) that mimics the morphology of authentic RABV and allows experimentation at biosafety level 2. To establish rVSV RABV G as a surrogate virus, we compared its entry behavior with that of a "single-cycle" version of RABV which lacks a copy of the G gene and is amplified in cells that express RABV G (rRABV ΔG). We show that, like that of VSV, the predominant internalization route of RABV into BS-C-1 cells is through pits that are partially coated with clathrin and depend upon actin for internalization. The kinetics of internalization of RABV particles are also indistinguishable from those of VSV in the time between particle attachment to cells and association of the particles with the clathrin machinery and in the time of clathrin-dependent uptake.

MATERIALS AND METHODS

Cells and viruses. African green monkey kidney BS-C-1 cells (ATCC CCL-26; American Type Culture Collection, Manassas, VA), either the wild type or a line stably expressing the σ2 subunit of AP2 fused to enhanced green fluorescent protein (eGFP) (AP2-eGFP) [164], were maintained at 37°C and 5% CO2 in Dulbecco's modified Eagle medium (DMEM; Invitrogen, Carlsbad, CA) supplemented with 10% fetal bovine serum (FBS; Tissue Culture Biologicals, Tulare, CA). Recombinant G deletion RABV strain SAD L16 expressing eGFP (rRABV ΔG) was a kind gift of E. M. Callaway [165]. rRABV ΔG stocks were produced by propagation of the virus in 293T cells stably expressing SAD B19 RABV G (also a gift of E. M. Callaway). Once amplified, rRABV ΔG was purified using the same protocol as for recombinant VSV. Titer was estimated by infecting noncomplementing 293T cells with serial dilutions of purified rRABV ΔG and counting eGFP-expressing infected cells at 30 hours postinfection (hpi) by flow cytometry. rVSV eGFP, rVSV RABV G eGFP (rVSV RABV G) [144], and a recombinant VSV expressing the Ebola virus glycoprotein, rVSV EboV GP eGFP (rVSV EboV GP) [166], were amplified, purified, and maintained as previously described [37]. rVSV eGFP was generated by amplification of the eGFP open reading frame (ORF) and insertion into the Xho and MscI sites of pVSV1(+)41 [167]. The resulting virus was recovered as described previously [168].

Protein composition of purified virions. To separate the viral proteins, we subjected purified virions to SDS-PAGE using 10% polyacrylamide (wt/vol) and 0.13% (wt/vol) bis-acrylamide and visualized them by staining with Coomassie blue. Relative amounts of N or G protein were established using ImageJ (U.S. National Institutes of Health, Bethesda, Maryland; http://rsb.info.nih.gov.ezp-prod1.hul.harvard.edu/ij/).

Inhibitors. The following chemicals were administered at the listed concentrations: 0.1 μM bafilomycin A1 (BAF A1; Calbiochem, Millipore); 100 μM dynasore; and 25 μM 5-(N-ethyl-N-

isopropyl)amiloride (EIPA; Sigma-Aldrich). Latrunculin B (LatB; Sigma-Aldrich) concentrations ranged from 0.5 to 6 µM, as illustrated (see Figure 7). One micromolar LatB was administered for internalization assays.

Nucleic acid transfection. To visualize clathrin and actin dynamics simultaneously, we cotransfected rat mCherry-LCa (constructed as described for tomato-LCa [169]) with mouse actin-eGFP into 90%-confluent BS-C-1 cells in 6-well plates. Plasmid DNA was introduced into the cells using FuGene HD (Roche Diagnostics, Indianapolis, IN) according to the manufacturer's instructions, using a ratio of 3 µg DNA to 5 µl FuGENE HD in 100 µl Opti-MEM. Following overnight incubation at 37°C, cells were reseeded onto 25-mm coverslips at 25% confluence. Cells were imaged approximately 5 h later, after complete adherence to the coverslips was verified by visual inspection.

Electron microscopy (EM). To visualize viral morphology, we deposited purified rVSV eGFP or rVSV RABV G particles onto carbon-coated copper grids and stained them with 2% phosphotungstic acid (wt/vol) in H2O (pH 7.5). To visualize viral particles in clathrin-coated pits, we inoculated BS-C-1 cells at a multiplicity of infection (MOI) of 1,000 for 15 min at 37°C. Samples were then processed for ultrathin sectioning as previously described [37, 170]. Virus particles and ultrathin sections of cells were viewed using a Tecnai G2 Spirit BioTWIN transmission electron microscope (FEI, Hillsboro, OR).

Dye conjugation to virus particles. Viral particles were labeled with 40 µg ml−1 Alexa Fluor (AF647) succinyl esters (Molecular Probes, Invitrogen, Eugene, OR) as previously described [37]. Titration of virus preparations before and after labeling showed that dye conjugation had a negligible effect on infectivity.

Infectivity studies. Cytofluorimetry experiments were carried out in 24-well plates and epifluorescence microscopy experiments in black, clear-bottomed 96-well microplates (Corning,

Tewksbury, MA). BS-C-1 cells were treated either 15 min prior to infection or at 2 hpi with DMEM plus inhibitors as indicated on the figures and in the figure legends. rRABV ΔG inoculations were incubated for 2 h at 37°C with an estimated MOI of 0.5, whereas rVSV RABV G inoculations were incubated with an MOI of 0.5 for 1 h at 37°C. Following inoculation, cells were washed and media were replaced as indicated. Cells were processed for epifluorescence microscopy or cytofluorimetry at 4 to 6 hpi for VSV-RABV or 25 hpi for rRABV ΔG. LatB was removed at 12 hpi to prevent cytotoxicity. Cells were washed three times with DMEM and media was replaced with DMEM supplemented with 10% FBS. For epifluorescence microscopy, cells were washed twice with phosphate-buffered saline (PBS) and fixed for 15 min with 4% paraformaldehyde (PFA). The fixed cells were washed with PBS and stained with DAPI (4′,6-diamidino-2-phenylindole) in the presence of 0.1% Triton X-100 for 30 min at 37°C. rVSV eGFP-infected cells were imaged using a CellWorX automated microscope (Applied Precision, Issaquah, WA); rRABV SAD B19 ΔG-infected samples were imaged using an ImageXpress Micro automated microscope (Molecular Devices, Sunnyvale, CA). For cytofluorimetry, cells were washed with PBS and harvested using 0.5 mM EDTA in PBS. Mean fluorescence measurements were obtained using a modified FACSCalibur (Cytek Development, Fremont, CA) instrument and analyzed using FlowJo (Tree Star Industries, Ashland, OR).

Uncoating assay. Confluent BS-C-1 cells seeded onto 12-mm coverslips were exposed for 15 min to DMEM containing 5 μg ml^{-1} cycloheximide (CHX) alone or with an entry inhibitor as indicated. Cells were then inoculated with rVSV RABV G at an MOI of 1,000. Following 1 h of incubation at 37°C, unabsorbed virus was removed by washing with fresh media. The treatment media were replaced, and cells were incubated for 2 h at 37°C. Note that CHX and the indicated entry inhibitors were maintained on cells throughout the inoculation as well as during the subsequent 2 h of incubation. Cells were

washed with PBS and fixed with 4% PFA for 15 min. Following permeabilization with 0.1% Triton X-100, cells were exposed to mouse 23H12 anti-M antibody (gift of D. Lyles) [171, 172] and 1:3,000 propidium iodide (PI; Sigma-Aldrich, St. Louis, MO) and an AF488-labeled goat anti-mouse secondary antibody. Coverslips were mounted onto slides using ProLong Gold antifade mounting media (Molecular Probes). z stacks were collected at 0.3-μm intervals. Images were analyzed and processed using ImageJ, maintaining contrast adjustments constant across samples for the AF488-conjugated secondary-antibody signal.

Internalization assay. Twenty-five to fifty percent-confluent BS-C-1 cells seeded onto 12-mm coverslips were treated with chemicals as indicated. AF647-labeled rVSV RABV G was added at an MOI of 100 and incubated for 30 min at 37°C. Cells were washed with PBS, fixed with 4% PFA, and exposed to anti-RABV G antibody (1:500; Millipore, Billerica, MA), which was detected by a secondary goat anti-mouse AF488 (1:500; Molecular Probes). To stain the cell membrane, we also exposed cells to 10 μg ml−1 AF594-labeled wheat germ agglutinin (WGA; Molecular Probes). Coverslips were mounted onto slides using ProLong Gold antifade mounting media (Molecular Probes). Samples were imaged by spinning-disk confocal microscopy with z stacks collected at 0.3-μm intervals. Stacks were processed using ImageJ (National Institutes of Health, Bethesda, MD; http://imagej.nih.gov.ezp-prod1.hul.harvard.edu/ij/). For increased clarity, z-stack maximal projections were processed to exclude coverslip-bound viruses. The WGA signal was used to generate a mask matching the outline of the cell(s). The area outside the border of the cell was replaced with a black background. Exposure and contrast adjustments were kept constant across samples throughout image acquisition and processing; WGA contrast and brightness were optimized to aid visualization of the cell boundaries.

Transferrin uptake. For cytofluorimetry experiments, BS-C-1 cells were seeded onto 24-well plates to be confluent the next day. For fixed confocal microscopy, BS-C-1 cells were seeded onto 12-

mm coverslips to be 50% confluent the next day for ease of imaging. BS-C-1 cells were pretreated with DMEM plus LatB or DMEM alone for 5 to 10 min. AF488-labeled transferrin (Tfn; Molecular Probes) was added to the media at a final concentration of 20 μg ml−1, and the cultures were incubated for 7 min at 37°C. On ice, cells were rapidly washed with acid solution (PBS, 0.5 M NaCl, 0.2 M acetic acid) and 3 times with PBS. Tfn uptake was assessed by spinning-disk confocal cytofluorimetry. Cells intended for analysis by flow cytometry were harvested and analyzed as described above.

Fixed-cell imaging. Slides were imaged using a Marianas system (Intelligent Imaging Innovations) based on a Zeiss observer microscope (Carl Zeiss MicroImaging, Thornwood, NY) outfitted with a CSU-22 spinning-disk confocal unit (Yokogawa Electric Corporation, Tokyo, Japan) and a 40× (Plan-Neofluar, NA 1.3; Carl Zeiss MicroImaging) or 63× (Plan-Apochromat, NA 1.4; Carl Zeiss Microimaging) objective lens. Excitation wavelengths were 491 nm for AF488, 561 nm for AF594, and 660 nm for AF647. For three-dimensional acquisitions, the vertical position was manipulated in 0.3-μm increments using a PZ-2000 automated stage (Applied Scientific Instrumentation, Eugene, OR). Images were collected using a Photometrics Cascade II electron multiplication camera (Photometrics, Tucson, AZ). SlideBook versions 4 and 5 (Intelligent Imaging Innovations, Denver, CO) were used to command the hardware devices and visualize the acquired data.

Live-cell imaging. Live single-particle tracking on AP2-eGFP-expressing BS-C-1 cells was conducted as described previously, collecting images at 3-s intervals over a period of 10 min per cell (11). Slidebook 4.2.13 and 5.0.0.2 (Intelligent Imaging Innovations) were used to command the hardware devices and visualize the acquired data. Prior to imaging, Alexa-labeled virus was centrifuged briefly on a tabletop microcentrifuge to remove aggregates. Cells were inoculated with a volume of virus calibrated to result in attachment and internalization of approximately 100 particles per cell within 20 min (~1 × 109 PFU of rVSV RABV G). Movies were generated by exporting time-lapse TIFF files from

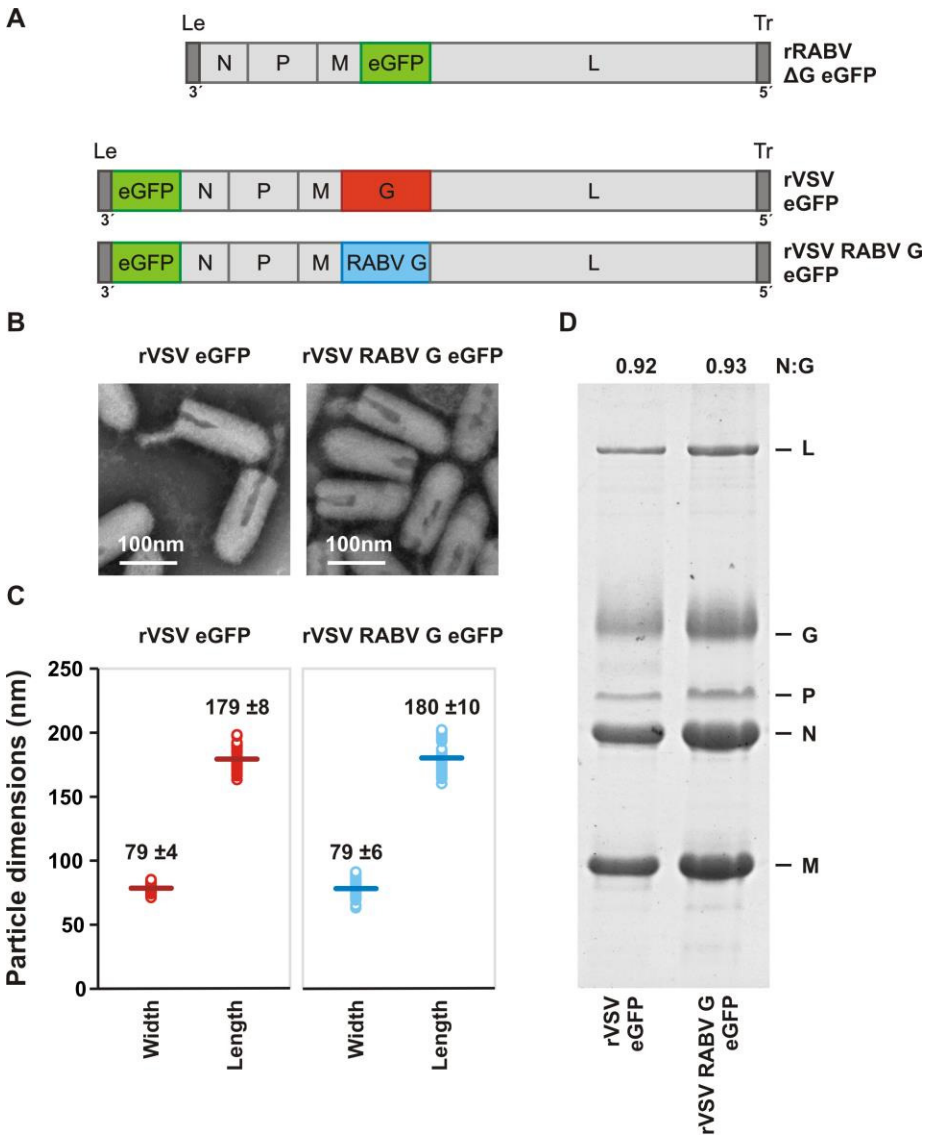

Figure 1.1 Characterization of recombinant VSV expressing RABV G.

A. Genomic structures of rRABV ΔG eGFP, rVSV eGFP, and rVSV RABV G eGFP. The single-stranded, negative-sense RNA genomes are shown in a 3′ to 5′ orientation. N, nucleocapsid gene; P, phosphoprotein gene; M, matrix gene; G, glycoprotein gene; L, large polymerase gene. Noncoding genomic leader (Le) and trailer (Tr) regions serve as promoters for RNA synthesis and genomic RNA encapsidation, respectively. All viruses express the eGFP gene (green) as a marker for infection. The glycoprotein open reading frame of rRABV ΔG eGFP was replaced with that of eGFP. To produce infectious virus, rRABV ΔG was grown in complementing cells expressing SAD B19 G. In rVSV RABV G eGFP, the wild-type VSV G (1,535 nt) was replaced with RABV G (1,574 nt) from the SAD B19 strain. B. Electron micrographs of rVSV eGFP and rVSV RABV G eGFP viral particles demonstrate

Figure 1.1 (continued) morphological homogeneity. Particles were negatively stained with 1% PTA. **C.** Dimensions of individual viral particles measured from micrographs like those shown in panel B. Each open circle represents the measurement for a single virion. A line denotes the mean (± the standard deviation (SD]; n= 50) for each population, the value of which is provided. **D.** SDS-PAGE analysis of purified virions. Viral proteins were stained with Coomassie blue. The ratio of N to G was quantified using ImageJ to estimate the average glycoprotein density in each particle population.

Slidebook and compiling the images into a single AVI file using ImageJ. All contrast editing, cropping, and scaling were performed using ImageJ.

Analysis of time series. Image analysis was performed as previously described [37, 116] with the following modifications. Images were exported from Slidebook 4.2.13 and 5.0.0.2, cropped using ImageJ, and analyzed using a previously described automated image analysis application (IMAB) within MATLAB (MathWorks, Natick, MA) [169]. As previously described [37, 116, 169], only events where single particles docked onto cells and were seen to undergo internalization were included in our analysis. Virus aggregates and predocked particles were excluded from the analysis. Internalization events were confirmed by observation of rapid directional movement of viral particles toward the perinuclear region. For comparison, 50 pits lacking virus particles within the time frame of virus uptake were also analyzed to provide baseline measurements of coat lifetime and intensity.

RESULTS

Recombinant VSV expressing RABV G.

Recombinant VSVs in which the glycoproteins from Ebola, Marburg, and Lassa fever viruses replace the endogenous glycoprotein (G) serve as useful surrogates to study the uptake pathways of these viruses [144, 166, 173] under biosafety level 2 conditions. We adapted such a strategy to permit the study of RABV infection by replacing VSV G with that of RABV SAD B19 (rVSV RABV G) (Figure 1.1A) [144]. As expected, rVSV RABV G retains the morphological features of authentic RABV: rVSV RABV G virions are bullet shaped and measure on average 180 nm in length and 80 nm in width (Figure 1.1B and C). These dimensions are typical for RABV and also match those of the parental VSV strain rVSV eGFP (Figure 1.1B and C) [174, 175]. Purified rVSV RABV G virions incorporate RABV G to an extent comparable to VSV G incorporation into particles (Figure 1.1D). Collectively, these data show that the rVSV RABV G particles are structurally indistinct from those of VSV except that they now contain RABV G on their surfaces and thus appear externally as RABV.

Productive infection of rVSV RABV G occurs through a clathrin-dependent endocytic pathway and requires endosomal acidification.

To determine whether rVSV RABV G serves as a useful surrogate to study RABV entry and define the route of infection, we compared its sensitivity to inhibitors of different endocytic mechanisms with that of a recombinant single-cycle RABV virus, rRABV ΔG. We tested bafilomycin A1 (BAF A1), an inhibitor of the H+ ATPase pump which by blocking endosomal acidification eliminates the trigger of conformational rearrangements in G necessary for membrane fusion; amiloride (EIPA), an inhibitor of macropinocytosis [176]; and dynasore, an inhibitor of dynamin required for the scission step of clathrin-mediated endocytosis [177]. To discriminate between the effect of inhibitors on entry versus postentry

Figure 1.2 Dynamin and endosomal acidification are required for productive RABV G-dependent infection.

A. Schematic of the methods employed for panels B and C. A graphical representation of a cell at each time point indicates the stage of infection. Circles represent viral particles, surface bound (filled) or internalized (hollow). Expression of the reporter gene, eGFP, is shown as a diffuse green in the cytoplasm. BS-C-1 cells were inoculated with virus (MOI = 0.5) and assayed for infection by detection of the eGFP reporter gene either by autoscope microscopy or cytofluorimetry at the collection point (25 hpi for rRABV ΔG; 4 to 6 hpi for rVSV RABV G). The effect of inhibitor on viral infection was assayed by treating cells with drug prior (pre) or following (post) inoculation with virus. Comparison of pretreated and posttreated samples enables determination of the effect of each inhibitor on viral entry. **B.** Fluorescence microscopy of single-cycle rRABV ΔG infection following treatment with inhibitor. The H+ pump inhibitor bafilomycin A1 (BAF A1; 0.1 μM), macropinocytosis inhibitor amiloride (EIPA; 25 μM), and dynamin inhibitor dynasore (100 μM) were tested for their abilities to impact RABV infection. rRABV ΔG infection was detected via expression of the eGFP reporter gene (green). Cell nuclei were labeled with DAPI (blue). **C.** Fluorescence microscopy of rVSV RABV G infection following treatment with inhibitors. rVSV RABV G infection is also detected as expression of the eGFP reporter gene (green). Cell nuclei were labeled with DAPI (blue). Images were collected using the same exposure and processed to the same brightness and contrast settings. Dynasore has a moderate effect on the rate of viral-gene expression; as a result, the brightness and contrast were readjusted in the dynasore insets to highlight lower-intensity infected cells. **D.** Cytofluorimetric analysis of infection. Total eGFP expression following pretreatment with drug was calculated from mean fluorescence intensites using FlowJo software and expressed as percentages relative to that of controls treated following inoculation (% post). rVSV eGFP (VSV) and rVSV EboV GP (EboV) served as prototypical clathrin-dependent and macropinosome-dependent pathogens, respectively. Statistically significant differences are demarcated by asterisks (Student's t test; $P < 0.01$).

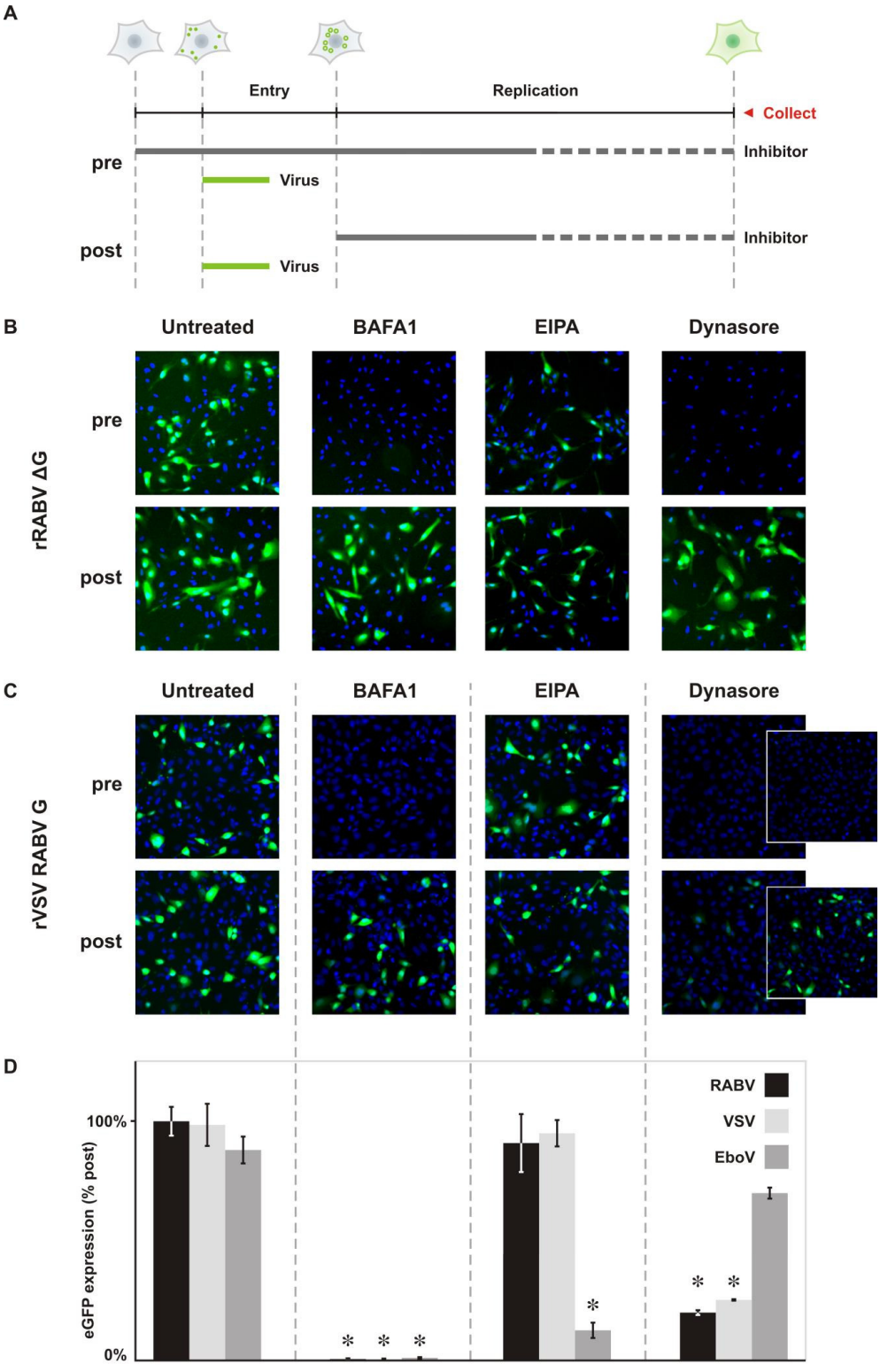

Figure 1.2 (continued)

steps of viral replication, we compared their effects when added prior to or 2 h following inoculation with virus (Figure 1.2A). For controls, we monitored the impact of these inhibitors on infection with rVSV eGFP, a virus that depends upon clathrin-dependent endocytosis and endosome acidification, and a recombinant VSV expressing the Ebola virus glycoprotein (rVSV EboV GP), which requires macropinocytic uptake (Figure. 1.2D). For each virus, infection was measured by the expression of eGFP detected by fluorescence microscopy (Figure 1.2B and C) or cytofluorimetry (Figure 1.2D).

The addition of BAF A1 or dynasore prior to inoculation blocked rRABV ΔG infection, whereas EIPA had no effect. None of the inhibitors had a significant effect following postentry addition. This result indicates that rRABV ΔG entry is dependent on dynamin and is likely clathrin mediated. As expected, productive infection also requires endosome acidification. rVSV RABV G (Figure 1.2C) shared the same sensitivity profile as rRABV ΔG (Figure 1.2B), supporting that this recombinant virus serves as a useful surrogate to study rabies virus entry. To quantitate the reduction in infection, we used cytofluorimetry (Figure 1.2D). Pretreatment of cells with BAF A1 reduced rVSV RABV G infection to 1% of that of postinoculation-treated controls. Pretreatment with dynasore reduced rVSV RABV G infection, like VSV infection, to 20% of that of postinoculation-treated controls, and pretreatment with EIPA had a negligible effect on eGFP expression (Figure 1.2C and D). By contrast, infection of rVSV EboV GP was strongly inhibited by EIPA but not by dynasore (Figure 1.2D). These results support the hypothesis that infection with rVSV RABV G requires dynamin and that macropinocytosis does not play a role in infection. Furthermore, the similarity in sensitivity profiles for rVSV RABV G and VSV is suggestive of a clathrin-dependent route of entry.

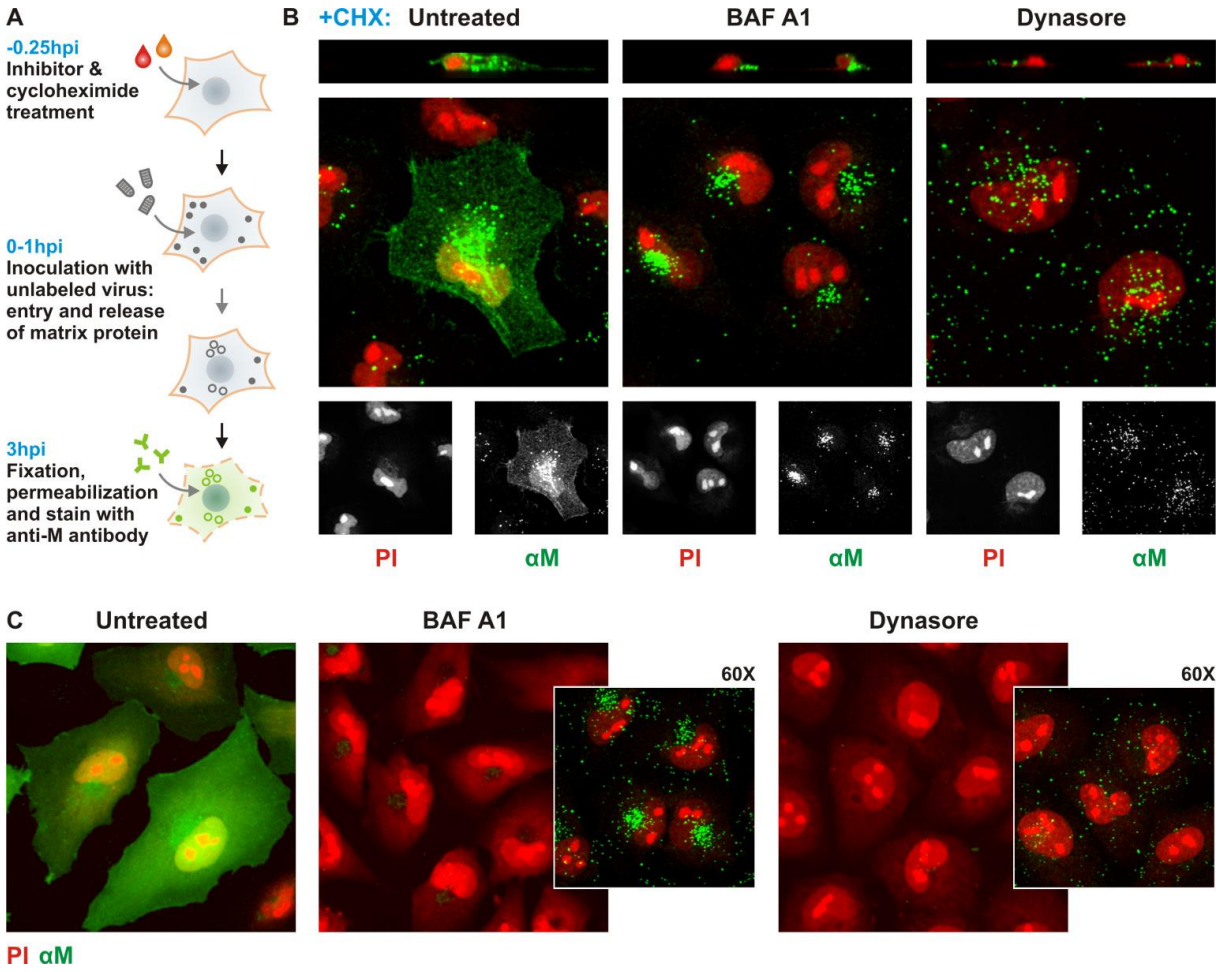

Figure 1.3. Absence of M protein release and expression in cells treated with BAF A1 or dynasore.

A. Schematic of the uncoating assay protocol. Release of M protein is monitored as an indication of viral fusion. Fifteen minutes prior to infection, cells were treated with 5 uM cycloheximide (CHX) to prevent de novo synthesis of viral proteins. CHX was administered alone or in conjuction with entry inhibitor, 0.1 uM BAF A1, or 100 uM dynasore, as indicated. Cells were inoculated with rVSV RABV G virus (MOI = 500) for 1 h. At 3 hpi, cells were fixed, permeabilized (indicated by dashed cell outline), and stained with antibody against VSV M (αM; green) and propidium iodide (PI; red). External, surface-bound virus is shown as filled circles, internalized virus as open circles. Anti-M antibody stained both diffuse M in the cell and tightly packed M in individual particles. **B.** Confocal microscopy of M release in cells treated with entry inhibitors and CHX. Above the merged images are single-plane z-stack cross sections. PI (red) and αM (green) signals are shown separately below the merged images. **C.** Confocal microscopy of M localization in the absence of CHX treatment. Cells were stained with PI (red) and αM (green). Large panels were imaged with a 40× lens objective; insets for BAF A1- and dynasore-treated conditions were imaged with a 60× lens objective, allowing visualization of aggregates of unfused viral particles.

BAF A1 and dynasore block RABV infection at separate steps in internalization.

To identify the steps at which BAF A1 and dynasore block infection, we employed separate assays that directly monitor uncoating (Figure 1.3) and internalization (Figure 1.4) of the virus [178]. For uncoating, we detected the release of internal virion matrix (M) protein following successful membrane fusion. Briefly, cells were infected in the presence of the protein synthesis inhibitor cycloheximide so that only the incoming virion proteins were detected. Successful membrane fusion releases the virion contents into the cytoplasm, a step that is visualized by monitoring the diffuse distribution of the input M protein by immunofluorescence (Figure 1.3A and B), and in the absence of CHX, infection was established in almost every cell (Figure 1.3C). By contrast, intact particles result in high-intensity perinuclear punctate staining, as shown by treatment of cells with BAF A1 in the presence (Figure 1.3B) or absence (Figure 1.3C) of CHX. This is consistent with the fact that inhibition of the vacuolar ATPase prevents the drop in endosomal pH required for RABV G fusion, leading to the accumulation of intracellular particles. In the presence of dynasore, there was no diffuse cytoplasmic M or perinuclear accumulation of intact particles. Intact particles appeared uniformly dispersed over the presumed cell surface and absent from the cell interior (Figure 1.3B and C).

To confirm that dynasore prevents particle internalization at the plasma membrane, we inoculated cells with Alexa Fluor-labeled virions for 30 min and, following fixation, exposed cells to an antibody directed against RABV G in the absence of membrane permeabilization (Figure 1.4A). This approach results in dually labeled surface-bound particles and permits their discrimination from singly labeled internalized particles. Following 30 min of inoculation, approximately half of cell-associated particles were internal and singly labeled, resulting in 42% colocalization of the Alexa Fluor signal with the anti-RABV G stain (Figure 1.4B). Internal particles were distributed between the perinuclear region and the cell periphery. In the presence of BAF A1, rVSV RABV G particles were internalized into

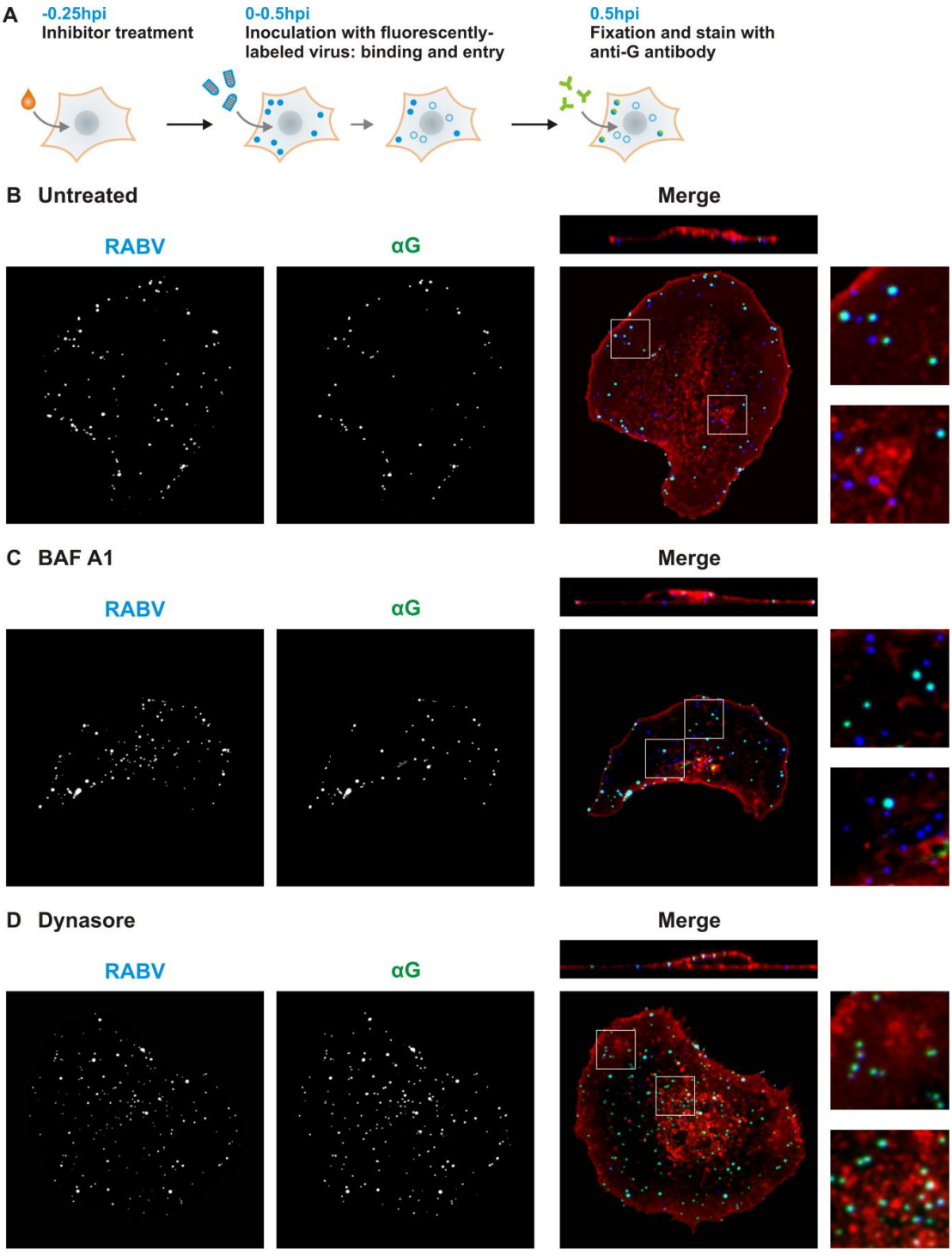

Figure 1.4. Dynasore blocks internalization at the plasma membrane.

A. Schematic of internalization assay. Fifteen minutes prior to infection, cells were treated with DMEM only (B), 0.1 uM BAF A1 (C), or 100 uM dynasore (D). AF647-labeled rVSV RABV G virus

Figure 1.4 (continued) (MOI = 50) was administered to cells for 30 min. During incubation, surface-bound virus (filled blue circles) internalizes and travels to the perinuclear region (open blue circles). Cells were fixed and stained with antibody against RABV G (αG) in the absence of permeabilization, which exclusively dually labels external particles (blue-green filled circles). Internal particles are protected from αG staining and remain singly labeled (open blue circles). WGA staining was used to detect cell surfaces. **B, C,** and **D.** Confocal microscopy of internalization assay in cells treated as listed above. AF647-labeled rVSV RABV G (RABV) and αG signals are shown individually. In the merged panels, the RABV signal is shown in blue, αG in green, and WGA in red. Singly labeled internal particles appear blue and dually labeled external particles appear cyan. Above the merged images are single-plane z-stack cross sections. Smaller panels (right) show magnified portions of the cells corresponding to the white squares in the merged panels.

endocytic compartments, resulting in a percentage of colocalization (44%) similar to that of untreated controls (Figure1. 4C). By contrast, treatment of cells with dynasore resulted in the accumulation of dually labeled particles distributed evenly on the cell surface (Figure 1.4D, 78% colocalization). Those particles remained at the plasma membrane, as detected by WGA staining (Figure 1.4D, z cross-section). We conclude that inhibition of dynamin-dependent processes prevents rVSV RABV G uptake at the cell surface.

Kinetics of rVSV RABV G uptake in clathrin-coated pits.

To further understand the steps of clathrin-mediated uptake of rVSV RABV G particles, we visualized single viral particles undergoing internalization by electron microscopy. Clathrin-coated pits are readily identifiable in electron micrographs as invaginations of the plasma membrane surrounded by an electron-dense coat (Figure 1.5, first row). Vesicles arising from clathrin-mediated endocytosis are largely spherical and have an average interior diameter of 60 nm. As expected for VSV ([37]) and as shown here for rVSV RABV G, viral particles are found within elongated vesicles with electron-dense material visible on the spherical end (Figure 1.5).

Previously we demonstrated that the clathrin-coated structures that internalize VSV take longer to form than pits lacking virus; they also lack the expected content of clathrin and its adaptor molecule,

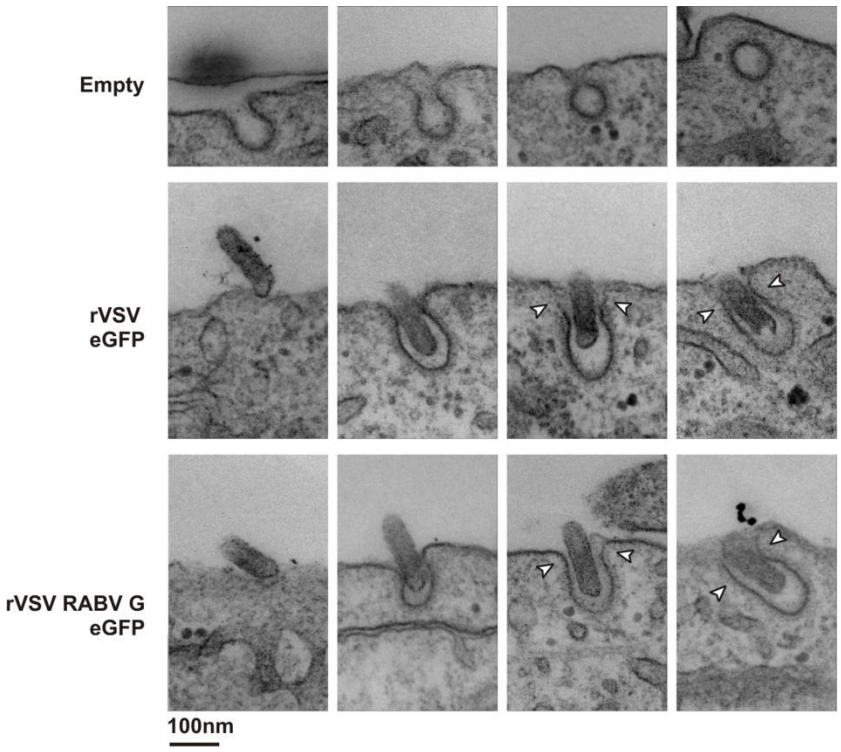

Figure 1.5. Visualization of clathrin-dependent uptake of rVSV RABV G by transmission electron microscopy.

Electron micrographs show the presumed order of internalization for empty, rvSV eGFP, or rVSV RABV G clathrin-coated pits. BS-C-1 cells were exposed to virus at an MOI of 1,000 for 15min prior to fixation and processing as outlined in Materials and Methods. Arrowheads highlight sections of the endocytic vesicle lacking electron dense clathrin.

AP2 [37]. To investigate whether pits internalizing rVSV RABV G share similar properties, we monitored the internalization of single viral particles into BS-C-1 cells stably expressing fluorescently tagged AP2 [37, 116]. We analyzed particles that displayed the following properties: (i) docking of the particle on the cell surface; (ii) a period of surface association with the cell membrane characterized by limited motility and potential association with AP2; and finally, (iii) sustained, rapid, directed movement toward the perinuclear region. A representative internalization event shows docking and a period of short-range, low-speed movement at the cell surface followed by a steady increase in AP2 (Figure 1.6A and C). After reaching peak intensity, the AP2 signal abruptly disappears, and the virus moves rapidly toward the

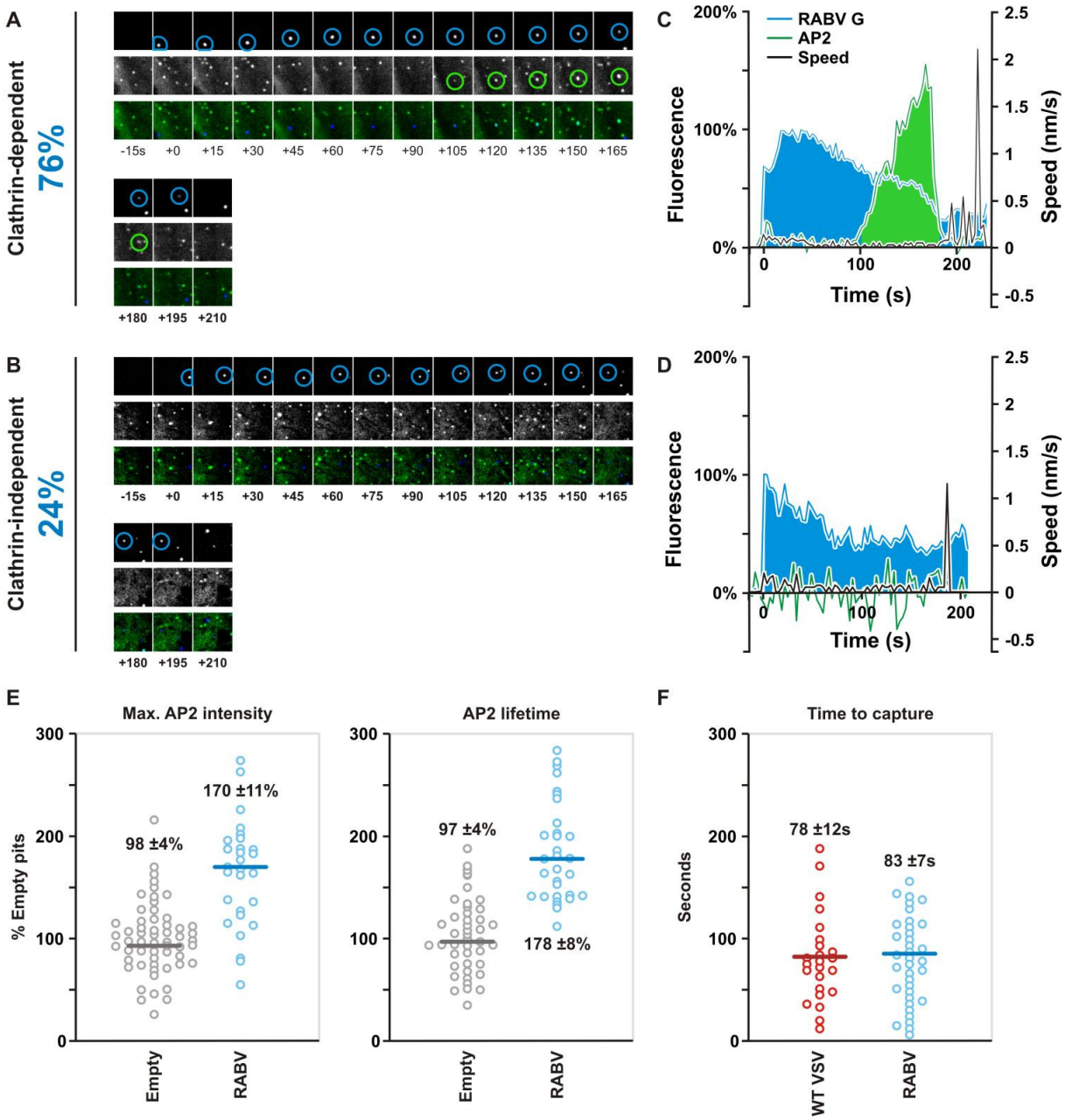

Figure 1.6. Live-cell imaging and kinetics analysis of rVSV RABV G internalization.

A. Tile view of images taken from a 10-min time-lapse movie (see Movie S1 in the supplemental material) of rVSV RABV G labeled with AF647 (top, blue) entering a BS-C-1 cell stably expressing AP2-eGFP (middle, green) via clathrin-mediated endocytosis. Particles were imaged at a rate of 20 images min−1. Circles highlight the presence of detectable virus and AP2, respectively. The percentage (at left) refers to the fraction of recorded events that were clathrin dependent (76%; n = 66). **B.** Tile view of images taken from a 10-min time-lapse movie (Movie S1.2) of AF647-labeled rVSV RABV G (top,

Figure I.6 (continued) blue) entering a BS-C-1 cell stably expressing AP2-eGFP (middle, green) in an AP2-independent manner. The percentage (at left) refers to the fraction of recorded events that were clathrin independent (24%; n = 66). **C.** and **D.** Graphical representations of the particle behaviors illustrated in panels A and B. AF647-labeled rVSV RABV G fluorescence (RABV G) was plotted as a percentage of its maximum. AP2 was plotted as a percentage of the average maximal fluorescence of empty pits. Particle speed is also plotted on the right y axes. **E.** Plots of maximal AP2 intensity and duration during AP2-dependent internalization of rVSV RABV eGFP plotted as a percentage of the average for all measured empty pits. Empty and viral pits are compared. Empty circles refer to individual measurements; bars indicate the median value, which is shown on the plot. For both parameters, the difference between empty and viral pits is statistically significant as determined by Student's t test ($P < 10-12$). **F.** Plot comparing the time between docking and AP2 capture for WT VSV and rVSV RABV G. Empty circles refer to individual measurements; bars indicate the median value, which is shown on the plot. The difference between time to capture of WT VSV and rVSV RABV G is not statistically significant as determined by Student's t test ($P > 0.1$).

perinuclear region (Figure 1.6A and C; see Movie S1.1 in the supplemental material). This loss of the AP2 signal is indicative of the uncoating of clathrin following scission of the coated pit from the plasma membrane [179]. We found that the majority (76%) of rVSV RABV G particles were seen within AP2-containing structures during entry (Figure 1.6A). The remaining particles internalized in the absence of a detectable AP2 signal (Figure 1.6B and D; Movie S1.2).

To compare internalization of rVSV RABV G to that of the related rhabdovirus, VSV, we measured the following parameters: maximum AP2 intensity and duration relative to those of empty pits (Figure 1.6E) and the time from docking to a cell to association with AP2 relative to the time for WT VSV (Figure 1.6F). rVSV RABV G-internalizing pits recruit on average 1.7 times more AP2 than their empty counterparts (median value; n = 66) (Figure 1.6E). In addition, the duration of AP2 recruitment was approximately 1.8 times that of a pit lacking virus. These changes mirror those previously measured for the internalization of WT VSV into pits [37, 116]. We also found that the time to capture of rVSV RABV G particles by coated pits was indistinguishable from that of VSV (Figure 1.6F). Collectively, the fixed and

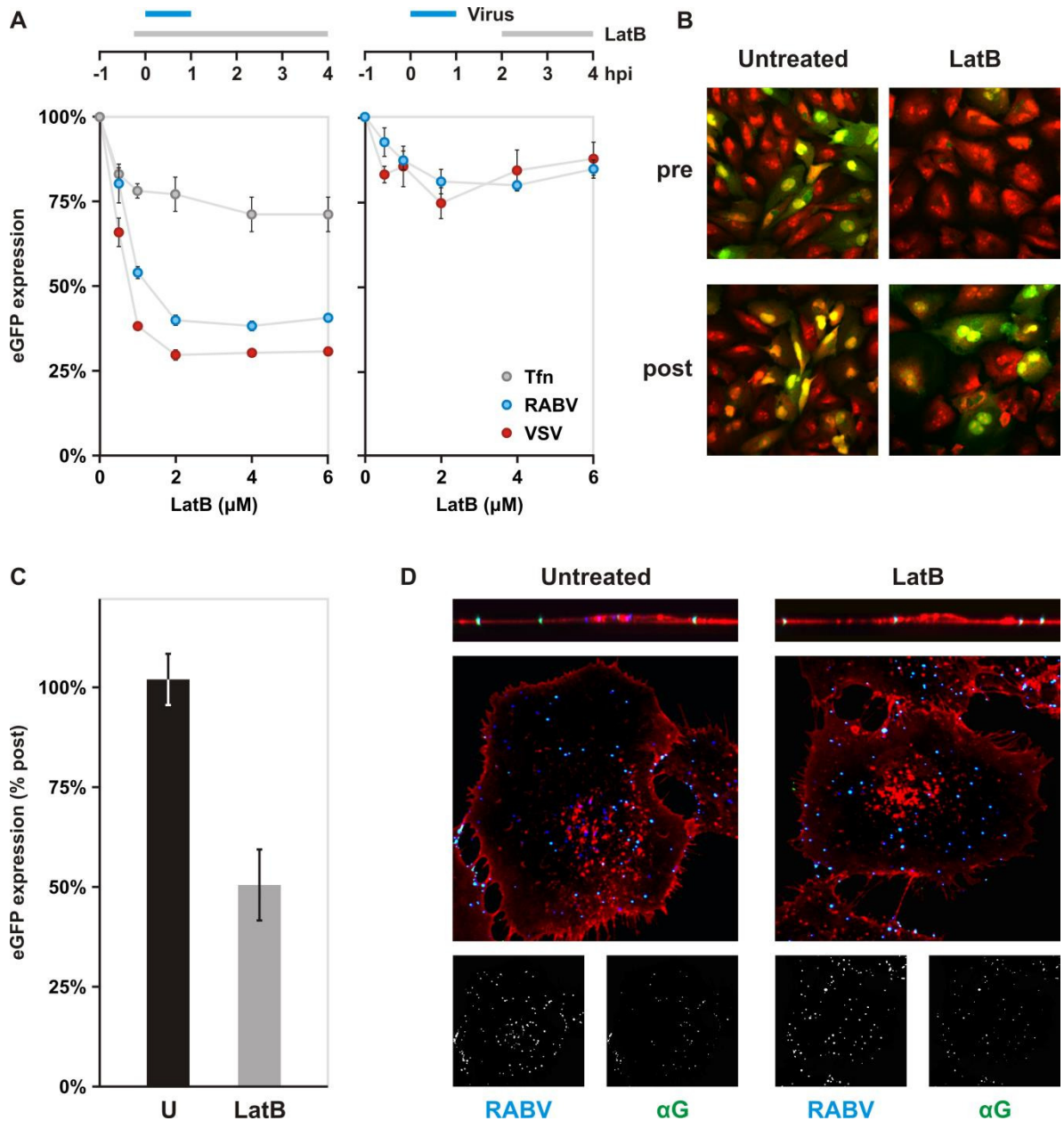

Figure 1.7. Impact of actin depolymerization on rVSV RABV G internalization.

A. Impact of chemical depolymerization of actin on rVSV RABV G (RABV) and rVSV eGFP (VSV) infections. BS-C-1 cells were treated with various concentrations of latrunculin B (LatB) to inhibit polymerization of actin. As shown in the schematic, drug was added either 10 min prior to a 1-h inoculation with virus or at 2 hpi and maintained until analysis. eGFP expression was assayed by cytofluorimetry at 4 hpi. rVSV eGFP is shown in red and rVSV RABV G in blue. Uptake of fluorescent transferrin (Tfn, gray) is included as a control for general disruption of clathrin-dependent endocytosis. Cells were pretreated with LatB 10 min prior to Tfn addition. Cells were incubated with

Figure 1.7 (continued) Tfn for 7 min. Following a wash with acid buffer to remove surface-bound Tfn, intracellular Tfn levels were measured by flow cytometry. **B.** Effect of actin depolymerization on rRABV ΔG infection. BS-C-1 cells were treated with 6 μM LatB prior to inoculation (pre) or at 2 hpi (post). Expression of eGFP (green) from viral genomes was detected by confocal microscopy at 25 hpi. Cells were stained with propidium iodide (red). **C.** Quantification of LatB effect on rRABV ΔG infection. BS-C-1 cells treated as for panel B were collected and analyzed for eGFP expression by flow cytometry. **D.** Confocal microscopy of internalization assay in cells. Above the merged images are single-plane z-stack cross sections. Cells pretreated as indicated were inoculated with AF647-labeled rVSV RABV G (RABV), fixed, and stained with antibody against RABV G in the absence of permeabilization. The LatB concentration used was 1 μM. RABV (blue) and αG (green) signals are shown separately in inlays below the merged images. WGA is shown in red. Singly labeled, internalized particles appear blue; dually labeled, surface-bound particles appear cyan.

live-cell-imaging data support that RABV particles internalize into incompletely clathrin-coated pits with structures and a lifetime similar to those that internalize VSV.

Actin dependence of RABV entry.

We found previously that VSV also internalizes through partially coated clathrin pits which depend on actin to complete uptake [37]. We therefore examined whether RABV entry is also actin dependent. Using the actin-depolymerizing drug latrunculin B (LatB), we disrupted formation of actin structures and monitored the effect on rVSV RABV G infection by cytofluorimetry (Figure 1.7A). Inhibition of actin polymerization prior to the addition of virus resulted in a 62% reduction in rVSV RABV G infection, similar to that observed for VSV (Figure 1.7A). Treatment of cells with LatB at 2 h postinoculation had a marginal effect on infection of both viruses, confirming that the requirement for actin is specific to entry (Figure 1.7A). Inhibition of uptake was also observed for the single-cycle rabies virus, rRABV ΔG (Figure 1.7B and C). Consistent with an entry block, viral particles fail to internalize and remain surface bound on cells pretreated with LatB (Figure 1.7D). Previous work demonstrated that disruption of actin polymerization does not block coated-pit formation or alter the kinetics of internalization in BS-C-1 cells [37, 180]. Accordingly, depolymerization of actin had a negligible effect on

transferrin accumulation as detected by cytofluorimetry (Figure 1.7A) and confocal microscopy (data not shown). Live-cell imaging of clathrin pits also confirmed that the formation and kinetics of coated pits are largely unchanged in the presence of LatB (see Movie S1.3 in the supplemental material). These data demonstrate a requirement for actin polymerization during the internalization of VSV and RABV that is not shared by pits that lack virus particles.

We next visualized the association of actin with clathrin-coated pits during rVSV RABV G entry by live confocal microscopy in BS-C-1 cells transiently expressing fluorescently labeled clathrin light chain and actin (see Movie S1.4 in the supplemental material). No detectable recruitment of actin was observed for pits lacking viral particles. In contrast, when the clathrin machinery was engaged in uptake of rVSV RABV G particles, we observed an accumulation of actin shortly following assembly of the clathrin coat. These results demonstrate that actin recruitment is integral to clathrin-mediated internalization of RABV particles. These data extend our findings on the clathrin-dependent uptake of VSV to another member of the family Rhabdoviridae, RABV, providing further support for the model that the particles are internalized through partially coated pits that require actin for internalization.

DISCUSSION

In this study, we used a combination of infectivity-based and single-particle-tracking approaches to examine how RABV productively enters epithelial cells. We employed a single-cycle rabies virus, rRABV ΔG, and a recombinant VSV in which the endogenous glycoprotein was replaced with that of RABV. We showed that uptake of rVSV RABV G mimics uptake of rRABV ΔG, demonstrating its usefulness as a surrogate for studying RABV entry. We present evidence that RABV internalization into BS-C-1 fibroblasts is primarily clathrin-mediated. Furthermore, RABV uptake proceeds through partially coated clathrin pits which require actin for completion of envelopment, a mechanism shared for internalization of the related rhabdovirus VSV. Live-microscopy approaches revealed that the kinetics of internalization of RABV and VSV are indistinguishable. The presence of RABV G on the surfaces of the particles does not impact the kinetics of internalization of particles by clathrin-coated pits or their time to association with clathrin. This work therefore characterizes the clathrin-dependent process of RABV uptake at the plasma membrane and reveals commonalities with the internalization of VSV into epithelial cells. These results also further support our prior finding that the length of a rhabdovirus particle correlates with the lifetime of the coated pit and the involvement of the actin machinery for coated-pit internalization.

rVSV RABV G as a surrogate to study RABV entry.

Particle morphology as well as the identity, number, and abundance of viral surface proteins that bind cell surface attachment factors at the plasma membrane influences viral entry. The rVSV RABV G particle faithfully replicates the surface characteristics of authentic RABV. It incorporates the single glycoprotein efficiently and retains the characteristic bullet shape. Furthermore, its biological behavior during the entry stages of infection is identical to that of a “single-cycle” RABV. Therefore, rVSV RABV G

is functionally indistinguishable from an authentic RABV particle and can be used as a surrogate to study viral uptake.

Viral factors that impact the mechanism and actin dependence of envelopment in a clathrin-coated pit.

We show that clathrin-coated pits internalizing rVSV RABV G particles have an altered morphology compared to those lacking virus. The amounts of clathrin and adaptors recruited and the duration of the coating process observed by live confocal imaging as well as the appearance of the nascent coated pit by EM support rVSV RABV G uptake through partially coated pits. In addition, uptake of, and infection with, rVSV RABV G or rRABV ΔG are inhibited by chemicals that block actin polymerization. The related rhabdovirus VSV also internalizes via partially coated clathrin pits and requires actin polymerization[37, 116]. The pits are indistinct in their appearance by EM and live-cell imaging, and the uptakes of the viruses follow similar kinetics. These studies also showed that the partially coated pit and the requirement for actin during viral internalization depend upon the size of the particle, as truncated VSV particles enter through fully coated pits and do not require actin polymerization [116]. While we did not examine whether truncated RABV particles are taken up through fully clathrin-coated pits and bypass the need for actin polymerization, we predict this to be the case. The fact that both VSV and RABV particles of similar dimensions internalize through similar coated pits lends further support to this prediction.

Recent studies show that the structural adaptability of clathrin-coated pits is an intrinsic property of the host machinery. Supporting this view, the actin dependence of clathrin-mediated endocytosis is induced by artificially tensing the plasma membrane either by exposing cells to hypoosmotic media or by mechanical stretching of the plasma membrane [117]. Under conditions of

elevated membrane tension, actin is required to provide sufficient force to counteract membrane resistance and constrict the neck of nascent coated pits prior to the final recruitment of dynamin. The incoming viral particle, which represents a physical obstacle to pit constriction, may lead to the recruitment of actin by inducing membrane tension [37, 116, 117]. Therefore, the presence of VSV or RABV G on the surface of the viral particle does not impact the formation of the clathrin-coated pit.

Commonalities in the uptake of two distinct rhabdoviruses.

Despite employing the same endocytic pathway, viruses internalized by clathrin-mediated endocytosis display different behaviors when associating with coated pits. Lateral diffusion into preformed pits has been reported for parvovirus and dengue virus entry [161, 163]. In contrast, VSV and influenza A virus do not exhibit such properties and are internalized by pits that form at or in close proximity to viral particles [37, 162]. The kinetics of uptake also vary, as parvovirus capture is very rapid (<20 s) [161] whereas dengue virus remains surface bound for several minutes prior to capture [163]. For VSV and influenza A virus, the interval between binding and detection of a virus-associated clathrin signal is in the range of minutes [37, 162].

Like those of VSV, RABV particles rarely associate with preexisting pits and show no detectable lateral movement prior to the appearance of the AP2 signal. The interval between rVSV RABV G particle docking and clathrin appearance was indistinguishable from that observed with VSV. These similarities suggest that the clathrin uptake mechanisms for VSV and rVSV RABV G converge upon a common pathway. The rVSV RABV G glycoprotein is derived from the SAD B19 vaccine strain of RABV. Vaccine strains which have been extensively passaged in cell culture are believed to use ubiquitous molecules for cell attachment and entry. Although a recent report suggests that the low density lipoprotein receptor (LDLR) family serves as a VSV receptor, direct interaction of VSV G and LDLR has not been demonstrated

and cells lacking LDLR are susceptible to VSV infection [181]. Additional evidence supports a relatively nonspecific electrostatic interaction of VSV with the host cell surface [182]. Although RABV and VSV engage the clathrin machinery with similar kinetics, we do not think it likely that this reflects the use of a shared cell surface attachment molecule. Whether the engagement of distinct receptor molecules can impact the kinetics with which a given particle associates with the clathrin machinery remains to be determined.

Implications for RABV internalization into different cell types.

RABV infects epithelial cells in the final stages of disease, when virus spreads from the CNS to a variety of extraneural tissues through innervation routes. Epithelial-cell infection is also a primary and necessary step in intranasal or oral infections in animals and in accidental exposures of laboratory workers to RABV [30-33]. The BS-C-1 cells used in this study do not express the putative RABV receptors p75 neurotrophin receptor ($p75^{NTR}$) and neural cell adhesion molecule (NCAM), as both were undetectable by reverse transcription (RT)-PCR (data not shown). Cells were not tested for the presence of the nicotinic acetylcholine receptor (nAChR) because it is known to be expressed only on the postsynaptic membrane of neuromuscular junctions and in the CNS [183]. Infection was also unaffected by ganglioside depletion by neuraminidase treatment (data not shown). Consequently, the means by which RABV attaches to these cells is uncertain. Nevertheless, our observation of a primarily clathrin-mediated entry mechanism for RABV is consistent with previous EM studies with nonneuronal fibroblasts [108]. We also observed, however, the AP2-independent uptake of a minor proportion (24%) of RABV particles. We do not know the entry route for these internalization event(s), but our pharmacological studies show that such events are unlikely to reflect a macropinocytic uptake.

Pathogenic strains of RABV which have not been passaged in culture show a narrow and specific neurotropism. Although our studies were conducted with epithelial cells, RABV infection of neurons and RABV receptor biology support internalization by clathrin-mediated processes. For example, RABV particles are visible in clathrin-coated pits by electron microscopy of cultured hippocampal neurons [160]. Furthermore, $p75^{NTR}$ and NCAM both internalize via clathrin-mediated endocytosis when bound to their endogenous ligands or when cross-linked with antibody [28, 110, 111]. These observations suggest that clathrin-coated pits likely play a central role in RABV uptake in neuronal cells as well as in epithelial cells. Our ongoing studies are aimed at elucidating the internalization mechanism of RABV into primary neuronal cells and evaluating how engagement of specific receptors by RABV G can influence the mechanism and kinetics of particle internalization.

ACKNOWLEDGMENTS

We thank D. Cureton and S. Boulant for discussions and R. Massol for support using the IMAB analysis software. This work was funded by NIH grant AI081842 and NERCE grant U54AI057159. S.P.J.W. is a recipient of the Burroughs Wellcome Investigators in the Pathogenesis of Infectious Disease Award, and S.P. is a recipient of the Giovanni Armenise-Harvard Ph.D. Award.

AUTHOR CONTRIBUTIONS

Silvia Piccinotti performed all experiments and analysis, and co-wrote the manuscript.

Thomas Kirchhausen provided scientific expertise and co-wrote the manuscript.

Sean P. Whelan supervised collection of data and analysis, and co-wrote the manuscript.

CHAPTER 2:

CLATHRIN-MEDIATED UPTAKE AND LONG RANGE AXOPLASMIC TRANSPORT OF VIRIONS INCORPORATING RABIES GLYCOPROTEIN

Silvia Piccinotti, Constance L. Cepko and Sean P. Whelan

[1]Department of Microbiology and Immunobiology, [2]Program in Virology,

and [3]Department of Genetics, Harvard Medical School Boston, Boston, MA, USA ;

Department of Ophthalmology, Howard Hughes Medical Institute, Harvard Medical School, Boston, MA

ABSTRACT

Rabies virus (RABV) is a pathogen of the nervous system with a narrow neurotropism during the early establishing stages of disease. The first critical step to fatal disease progression is invasion of peripheral neurons which serve as a conduit to the brain. The single RABV glycoprotein (G) dictates all steps from receptor engagement to fusion leading to viral genome release. Using a recombinant vesicular stomatitis virus (VSV) incorporating G of the neurotropic CVS-11 strain (rVSV CVS G) and microfluidic compartmentalized culture, we studied uptake of virions into the termini of primary neurons of the dorsal root ganglion and ventral spinal cord. By pharmacologically disrupting endocytosis at the distal neurites, we demonstrate that rVSV CVS G uptake and infection are dependent on dynamin. Imaging of single virion co-uptake with fluorescent endocytic markers further pinpoints endocytosis via clathrin-coated pits as the predominant internalization mechanism. Transmission electron micrographs reveal the presence of viral particles in vesicular structures consistent with incompletely coated clathrin pits first described in the uptake of the related rhabdovirus VSV into epithelial cells. This work extends our previous findings of clathrin-mediated uptake of RABV into epithelial cells to two neuronal subtypes involved in rabies infection in vivo. Infectivity experiments with targeted chemical perturbation of endosomal acidification at the neurites or cell bodies demonstrate that establishment of infection requires pH-dependent fusion of virions at the cell body. These findings correlate infectivity to existing single particle evidence of long-range endosomal transport of RABV.

INTRODUCTION

Rabies virus (RABV), a member of the *Rhabdoviridae* family, is a neurotropic pathogen that causes fatal encephalitis in animals and humans. RABV pathology is strictly neurological; as a result, a critical requirement for pathogenesis is invasion of the central nervous system (CNS). RABV neurotropism is conferred by its single glycoprotein [93], G, which mediates all internalization steps from cell binding to membrane fusion. The ectodomain or receptor-binding regions of RABV G alone can be used as neurotracers [41, 43, 184] and are sufficient to target other biologically active molecules to the CNS [43, 185, 186]. Among other factors, the virulence of specific RABV strains also correlates with the neuroinvasiveness of their G variants [187].

Peripheral neurons, which innervate tissue damaged by the bite of a rabid animal, serve as conduits to the CNS. Although, both sensory and motor neurons at the bite site can be infected [26, 40, 41, 89, 188], retrograde transmission of RABV dictates that motor neurons serve as the primary gateway for CNS invasion and transmission to the brain [43]. RABV overcomes the extremely polarized morphologies of neurons by exploiting host microtubule transport networks that link distal termini to the cell body. Single particle studies suggest, furthermore, that RABV subverts the same long-range endosomal transport networks that mediate neuronal uptake of tetanus toxins and one putative RABV receptor, the low affinity neurotrophin receptor, $p75^{NTR}$ [36, 189]. Evidence from studies of $p75^{NTR}$ signaling, suggest that association with a receptor ectodomain can suffice to trigger sorting into the appropriate axoplasmic transport stream: mere association of $p75^{NTR}$ with its cognate ligand, nerve growth factor, shunts motor neuron $p75^{NTR}$ from a clathrin-independent, recycling endosomal pathway into a clathrin-dependent long-range axoplasmic transport [28]. Defining how RABV G mediates uptake into neurons is therefore critical for understanding how the virus gains access both to the cellular interior and to transport networks critical for delivery of the viral payload to productive sites of infection.

Past studies in non-neuronal cells and hippocampal neurons implicate clathrin-mediated endocytosis (CME) in the uptake of RABV [108, 160, 190, 191]. Importantly, however, the only studies relating route of entry to eventual infection were carried out in non-neuronal cells [191]. Due to the highly specialized and polarized nature of neuronal cells, generalization of results in non-neuronal cells to neurons cannot be presumed. Although several studies report single particle evidence of processive endosomal transport of intact RABV viruses these studies do not yet relate their findings to establishment of infection [7, 8, 36]. Furthermore, current studies utilize vaccine RABV strains and attenuated glycoproteins which may behave differently than their neurotropic counterparts.

We have previously demonstrated that recombinant vesicular stomatitis virus (rVSV) genetically incorporating RABV G faithfully recapitulates RABV entry behavior [191]. We employ this strategy to determine the endocytic route exploited by G of the neurotropic RABV strain, Challenge Virus Strain (CVS), for uptake into peripheral neurons. To model natural RABV infection at neuronal termini, we adapt a polydimethylsiloxane microfluidic culturing platform [155, 156] to physically separate neuronal cell bodies from their neurites. Compartmentalization of neuronal cultures has been previously used to demonstrate bidirectional transport of RABV in sensory neurons [8, 36, 146]. Early studies used Teflon chambers and classical virology techniques to measure viral outputs in somal and dendritic compartments [146]. Adoption of photolithographic and microfluidic techniques in the biological sciences has led to a resurgence of the use of compartmentalized cultures in studies of RABV biology [8, 36]. These recent studies have corroborated and extended early observations of retrograde and anterograde RABV transport in complex with putative receptors by single particle live imaging [8, 36]. We combine infectivity and single particle imaging approaches to study internalization and fusion from the nerve termini of neurons of the dorsal root ganglion (DRG) and motor neuron-rich ventral spinal cords (V SC). We demonstrate that CVS G-mediated uptake is reliant on dynamin-dependent uptake processes and that

the predominant endocytic route is clathrin-mediated. We further provide biochemical evidence that productive infection requires viral fusion at the somatodendritic compartment following long-range transport from the neuronal termini. This work extends previous findings from epithelial cells providing evidence that infection of neuronal cells by rabies virus occurs through a clathrin dependent entry pathway with subsequent membrane fusion occurring at the cell body.

MATERIAL AND METHODS

Fabrication of microfluidic devices. Device masters were manufactured by two-layer soft photolithography onto 3 inch mechanical grade silicon wafers for spin coating (UW3MEC, University Wafers) utilizing established methods [154]. Two negative photoresists were used: SU-8 2002.5 (MicroChem) for the 3 µm microchannel layer followed by SU-8 2050 (MicroChem) for the 100 µm culturing compartment layer. Photoresist was patterned by UV-crosslinking through 20,000 dpi transparency masks (CAD/Art Services), processed and cured according to supplier's instructions. Following a final hard cure at 150°C for 15 min, masters were treated with (tridecafluoro-1,1,2,2-tetrahydrooctyl)trichlorosilane for 45 min to facilitate removal of cured polydimethylsiloxane (PDMS) following moulding. Devices were cast by applying a 10:1 prepolymer:curing agent mixture of Sylgard 184 (Dow Corning) to the master and curing at 65°C for a minimum of 1 h. After curing and release from the master, PDMS devices were cut, and wells punched out with round biopsy punches. We irreversibly bonded devices to cleaned glass coverslips by oxygen plasma bonding in a 500-II Plasma Etcher (Technics). Bonded devices were sterilized under UV in a biosafety cabinet for 10 minutes prior to consecutive overnight coatings with 300 µg mL^{-1} poly-D-lysine (P7886, Sigma-Aldrich) dissolved in 2X borate buffer solution (28341, Thermo Scientific) and 10 µg mL^{-1} laminin (L2020, Sigma-Aldrich) in sterile water.

Neuronal culture. Neuronal tissues were dissected from E14.5-E15.5 embryonic Sprague-Dawley rats. Dorsal root ganglia (DRG) were dissected, dissociated by trypsinization and cultured in Neurobasal media (Gibco) supplemented with B27 (1:50; 17504-044, Gibco), β-nerve growth factor (100 ng mL^{-1}; 450-01, Peprotech), 5% fetal bovine serum (FBS, Tissue Culture Biologicals), 2mM glutamine (101806, MP Biochemicals), 25mM HEPES (0511, AMRESCO) pH 7.4 and 25 µg mL^{-1} β-D-arabinofuranoside (AraC; C1768, Sigma-Aldrich) [192]. Ventral spinal cord neurons were dissected by adapting the strategy outlined

for the harvest and culture of dorsal spinal cord commissural neurons [193]. Instead of harvesting the dorsal portion of the spinal cord, we retained the ventral portion for our cultures. Dissociation of the neurons was also carried out as detailed with the exclusion of the Opti-Prep purification step. V SC neurons were cultured in Neurobasal media (Gibco) supplemented as in [194]. AraC treatment for selective kill-off of dividing non-neuronal cells was included and maintained in DRG media from first plating. For V SC culture AraC was applied after 48h in culture.

For preparation of compartmentalized cultures, we seeded neurons into the S compartment (Figure 1C): 1.5×10^5 DRG or 1×10^5 V SC neurons were dispensed per device. A half-media swap was performed for both DRG and V SC culture following 2-3 days in culture; at this point, 25 µg mL^{-1} AraC (Sigma-Aldrich) was administered to the V SC cultures and maintained. Subsequently, media was periodically supplemented to counteract evaporation in culture. Experimental infections were carried out once adequate neurite outgrowth was observed in the N compartment: typically, by day 7 in culture for DRG and day 10 for V SC neurons. Devices were discarded following 12 days in culture.

Cells and viruses. Neurons, mouse neuroblastoma Neuro-2a cells (N2a; ATCC CCL-131), baby hamster kidney BSR-T7 cells, and African green monkey kidney BS-C-1 cells (ATCC CCL-26; American Type Culture Collection, Manassas, VA) were maintained at 37°C and 5% CO_2. Non-neuronal cells were cultured in Dulbecco's modified Eagle medium (DMEM; Corning) supplemented 10% fetal bovine serum (Tissue Culture Biologicals). N2a media was further supplemented with 2mM glutamine (Sigma) and 25mM HEPES pH 7.4. rVSV eGFP and rVSV eGFP SAD B19 G were amplified, purified and maintained as previously described [37, 116]. rVSV eGFP CVS G (rVSV CVS G) was generated by insertion of the CVS-11 glycoprotein coding region into MluI and NotI restriction sites in a modified rVSV eGFP ΔG backbone. A pUC57 plasmid containing the cDNA of CVS-11 G (Genbank: GQ918139.1) with flanking MluI and NotI sites was commercially synthesized by GenScript. A P0 stock of the virus was recovered by standard

methods in BSR-T7 monolayers [37]. Individual viral clones from the P0 stock were isolated by fluorescent focus assay in N2a culture. These were picked and further amplified in N2a's to generate working stocks of the virus.

Purification of virus from Neuro2a cells. rVSV CVS G stocks were passaged and expanded in Neuro2a (N2a) monolayers. Infections were carried out according to standard technique [37]. At 24hpi supernatant and infected N2a cells were collected and subjected to 2 min sonication in a Branson 1510 ultrasonic cleaner (Branson, Richmond, VA) followed by 30 s vortex to release cell bound viruses. Cell debris was pelleted by centrifugation and the resultant virus supernatant purified by ultracentrifugation. Virus pellets were resuspended overnight in phosphate buffered saline (PBS) + 25 mM HEPES pH 7.4 + 50 mM EDTA. We sonicated the virus resuspension for an additional 2 min, followed by 30s vortex, immediately prior to a final gradient purification over a 15%-45% (wt/vol) sucrose gradient in PBS as previously described [37]. Viral titers were determined by fluorescent focus assay in N2a monolayers.

Dye conjugation to virus particles. We used established methods to label gradient-purified viral particles with 40 μg ml^{-1} Alexa Fluor (AF)-conjugated succinyl esters (Molecular Probes, Invitrogen) [37]. Titration of mock- or AF647-labeled virus preparations showed that dye conjugation had a negligible effect on infectivity.

Protein composition of purified virions. Viral proteins of gradient purified virions were separated by SDS-PAGE in a 10% polyacrylamide (wt/vol) and 0.13% (wt/vol) bis-acrylamide gel. Protein bands were visualized with SimplyBlue SafeStain according to manufacturer's instructions. Viral protein amounts relative to N protein were determined using ImageJ (U.S. National Institutes of Health, Bethesda, Maryland; http://rsb.info.nih.gov/ij/).

Live staining of neurons in compartmentalized culture. Neuronal cytoplasms in the N and S compartments were stained with calcein (diluted 1:1000; C3099, Molecular Probes) or CellTracker (diluted 1:500; C34552 Molecular Probes), and nuclei with NucBlue Live Cell Stain (diluted 1:50; R37605, Molecular Probes) in Neurobasal for 30 min prior to inoculation with virus. Stains were washed once with Neurobasal following removal, prior to infection or imaging by direct fluorescent microscopy.

Inhibitors. The following chemicals were administered at the listed concentrations: 0.1 µM bafilomycin A1 (BAF A1; 196000, Calbiochem, EMD Chemicals); 150 µM dynasore (Sigma-Aldrich); and 25 µM 5-(*N*-ethyl-*N*-isopropyl)amiloride (EIPA; A3085, Sigma-Aldrich).

Infections in compartmentalized culture. Infections were carried out exclusively in the N compartment. For N-compartment inhibitor treatment, culturing media in the S compartment was supplemented to replace evaporated liquid volume, and maintained throughout the experiment. For BAF A1 experiments where inhibitor treatment was also carried out in the S compartment, S compartment media was replaced with Neurobasal alone or BAF A1 diluted in Neurobasal. Neuronal culturing media in the N compartment was replaced with 30 µL of inoculation media. Inoculation media consisted of Neurobasal media alone or with inhibitor as indicated. 10^9 fluorescent foci forming units of virus were administered to the N compartment in 25 µL of inoculation media. At inoculation, liquid volume in the S compartment exceeded the N compartment volume by 5 µL to counteract diffusion of molecules across the channels. Inoculum was maintained for 2 h and then replaced with 55 µL treated or untreated Neurobasal media. For BAF A1 experiments where inhibitor was administered at 9-12 hpi, and additional media swap was carried out. Expression of eGFP was assessed at 26 hpi either by direct live microscopy for DRG neurons or following fixation and immunofluorescence for V SC neurons..

Co-uptake of RABV with fluorescent transferrin and dextran. For all co-uptake experiments neurons were first prestained with calcein or CellTracker as indicated. Infections were carried out, as

described, in the N compartment with inocula containing Tfn conjugated to AF594 (50 µg mL^{-1}; Molecular Probes) or AF488 Dextran (MW 10 000, 1 µg mL^{-1}; Molecular Probes). For fixed experiments, N compartments were washed twice at 2 or 5hpi with Neurobasal, and fixed with 2% (wt/vol) paraformaldehyde in PBS + 5% (wt/vol) sucrose. For live imaging, uptake experiments were carried out in devices bonded to FluoroDish glass bottomed culture dishes (FD35-100, World Precision Instruments, Inc.) and imaged by high resolution spinning disk confocal microscopy.

Immunofluorescence. Neurons were fixed with 2% (wt/vol) paraformaldehyde in PBS + 5% (wt/vol) sucrose. Cell membranes were permeabilized with 0.2% Triton-X in PBS. Cells were consecutively stained with mouse monoclonal antibody against phosphorylated neurofilament H, SMI-31 (1:1000; NE1022, Calbiochem), and AF-conjugated anti-mouse secondary antibody (Molecular Probes, Invitrogen). When indicated, neuronal cells were detected by staining against Neuronal Nuclei (NeuN) with rabbit polyclonal antibody (1:500; ab104225, Abcam) and AF-conjugated anti-rabbit secondary antibody (Molecular Probes). Nuclei were stained with DAPI (1:10,000; Molecular Probes). Devices processed for immunofluorescence underwent a final wash with PBS and were imaged in solution. Non-compartmentalized neurons, cultured on coverslips, were mounted first with ProLong Diamond (Molecular Probes).

Fluorescence microscopy. Devices were illuminated with a Mercury-100W mercury lamp (Chu Technical Corporation) and imaged using a Nikon Eclipse TE300 inverted microscope, outfitted with 4× Plan Fluor, 10× and 20× Plan Fluor objective lenses (Nikon). Images were collected using a SPOT RT Monochrome camera (Spot Imaging Solutions, Diagnostic Instruments Inc.) and recorded with the manufacturer's Spot 3.5 Advanced software.

Spinning disk confocal microscopy. Devices were imaged using a Marianas system (Intelligent Imaging Innovations) based on a Zeiss observer microscope (Carl Zeiss MicroImaging) outfitted with a

CSU-22 spinning-disk confocal unit (Yokogawa Electric Corporation) and a 63× (Plan-Apochromat, NA 1.4; Carl Zeiss Microimaging) objective lens. Excitation wavelengths were 491 nm for AF488, 561 nm for AF594, and 660 nm for AF647. For three-dimensional acquisitions, the vertical position was manipulated in 0.3 µm increments using a PZ-2000 automated stage (Applied Scientific Instrumentation). Live imaging experiments were carried out on a temperature controlled sample holder (20/20 Technology Inc.; Wilmington, NC) maintained at 37°C and 5% CO2.Images were collected using a Photometrics Cascade II electron multiplication camera (Photometrics). SlideBook 5.0 (Intelligent Imaging Innovations) was used to command the hardware devices, and visualize and export the acquired data. Subsequent image manipulation was conducted using ImageJ (U.S. National Institutes of Health, http://rsb.info.nih.gov/ij/).

Transmission electron microscopy. To visualize viral morphology, we deposited gradient purified rVSV CVS G virions onto carbon-coated copper grids and stained them with 2% phosphotungstic acid (wt/vol) in H_2O (pH 7.5). To visualize viral uptake, we inoculated V SC neurons cultured on Aclar with rVSV CVS G at a multiplicity of infection (MOI) exceeding 1,000 for 2 h at 37°C. rVSV uptake samples were prepared by inoculating BS-C-1 cells with rVSV at an MOI of 1,000 for 15 min at 37°C. Samples were fixed and processed for ultrathin sectioning as previously described [37, 170]. Virus particles and ultrathin sections of cells were viewed using a Tecnai G^2 Spirit BioTWIN transmission electron microscope (FEI).

Figure 2.1. Production of a recombinant VSV expressing rabies CVS G.

A. Organization of the negative strand RNA genomes of viruses, rVSV eGFP and rVSV eGFP CVS G. Genomes are shown in a 3' to 5' orientation, including the non-coding genomic leader (Le) and trailer (Tr) regions. Coding regions include the N, nucleocapsid gene; P, phosphoprotein gene; M, matrix gene; G, glycoprotein gene; L, large polymerase gene. Both viruses express an additional eGFP gene (green) as a marker for infection. In rVSV CVS G, the wild-type VSV G (1,535 nt) was replaced with the rabies G (1,575 nt) from the CVS-11 strain. **B.** Transmission electron micrographs of rVSV CVS G virions stained with 1% phosphotungstic acid. Two magnifications are included 30 000X and 68 000X. The rightmost panel is an enlargement of the area indicated and highlights the glycoprotein spikes decorating the viral surface. Scale bars = 50nm. **C.** Protein composition of purified virions by SDS-PAGE. Viral proteins from rVSV eGFP, rVSV SAD B19 G and rVSV CVS G were stained with SimplyBlue SafeStain. Intensity values normalized to N were quantified using ImageJ and are plotted for each viral lane. The calculated numerical ratio of G to N is further reported as a measure of average glycoprotein density for each virus. **D.** Fluorescent focus analysis comparing infectivity of rVSV eGFP (rVSV), rVSV CVS G (CVS), and rVSV SAD B19 G (SAD) in Neuro-2A (N2a) and BSRT7 (BSR) cells. Infections were calibrated to obtain comparable levels of infection in the N2a cells. The same infectious dose was then applied to monolayers of BSR cells for comparison. rVSV foci were evaluated at 24hpi; rVSV CVS G and rVSV SAD B19 G were evaluated at 48hpi due to slower kinetics of infection. **E.** Fluorescence microscopy of N2a and BSR monolayers inoculated with rVSV grown in BSR ($rVSV_{BSR}$), rVSV grown in N2a ($rVSV_{N2a}$), or CVS virus at an MOI_{N2a} of 3. Infection was assessed by eGFP expression (green) at 6hpi. Nuclei are stained with DAPI (blue).

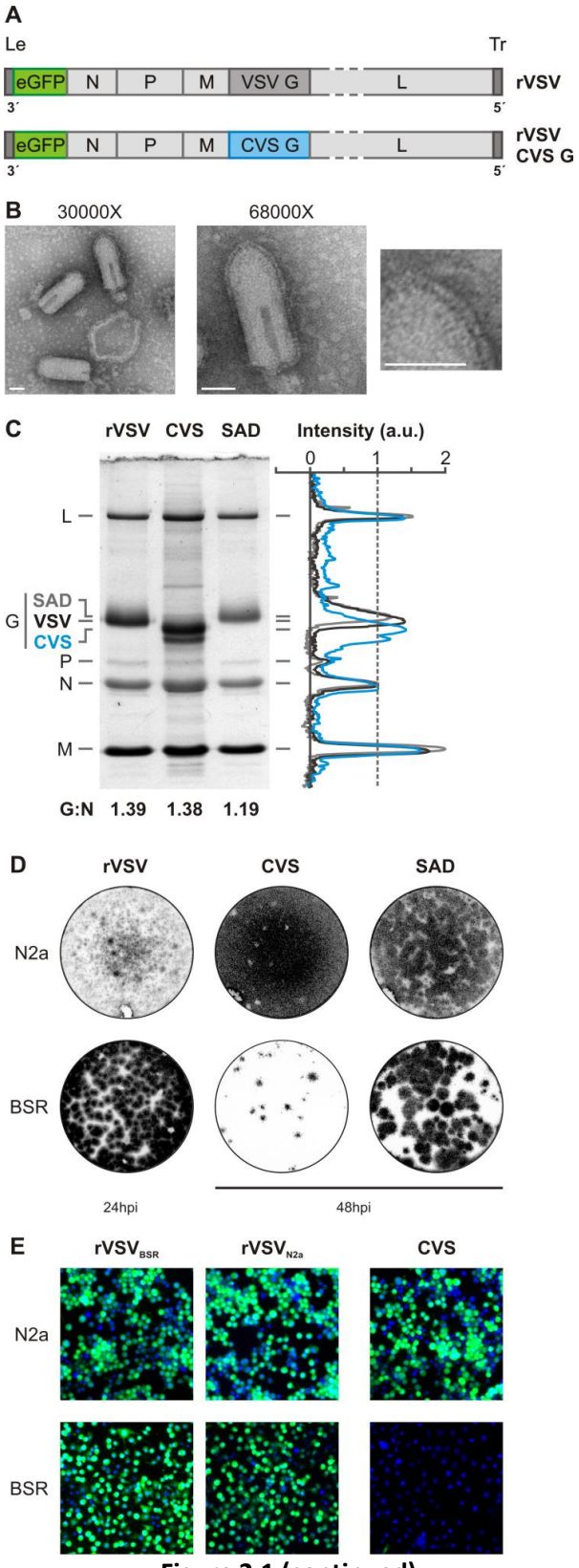

Figure 2.1 (continued)

RESULTS

Restricted tropism of a recombinant VSV expressing the rabies CVS glycoprotein

To study uptake of RABV in neurons, we generated a recombinant VSV (rVSV) in which the glycoprotein (G) gene was replaced with that of the neurotropic rabies strain, CVS (rVSV CVS G; Figure 2.1A). This virus expresses eGFP as a marker of infection. Transmission electron microscopy (TEM) of purified rVSV CVS G showed characteristically bullet-shaped particles with readily discernible glycoprotein spikes (Figure 2.1B) consistent with efficient incorporation of CVS G. SDS-PAGE analysis of the protein composition of purified virions demonstrates comparable incorporation of CVS G into rVSV compared to RABV vaccine strain SAD B19 G or endogenous VSV G (Figure 2.1C).

Neuroinvasiveness is a critical aspect of pathogenic RABV G, and incorporation of CVS G resulted in a correspondent shift in rVSV tropism. BSR-T7 monolayers were less susceptible to rVSV CVS G than its non-neuroinvasive counterparts, rVSV and rVSV SAD B19 G (Figure 2.1D). Inoculation with rVSV CVS G resulted in a pronounced reduction in focus number and a small focus phenotype. The reduced infectivity of rVSV CVS G in BSR-T7 cells was confirmed at 6hpi, pinpointing the defect at an entry step. A viral dose equivalent to MOI = 3 in N2a cells resulted in a calculated effective MOI < 0.05 in BSR-T7 assuming the standard Poisson model of infection (Figure 2.1E). We excluded the possibility that differential lipid composition of virus grown in N2a cells was responsible for the difference in tropism by comparing the infectivity of rVSV grown in BSRT7 ($rVSV_{BSRT7}$) or N2a cells ($rVSV_{N2a}$; Figure 2.1E). Cumulatively, these observations are consistent with a restricted tropism conferred specifically by the CVS strain glycoprotein.

Compartmentalized culture of dorsal root ganglion and ventral spinal cord neurons

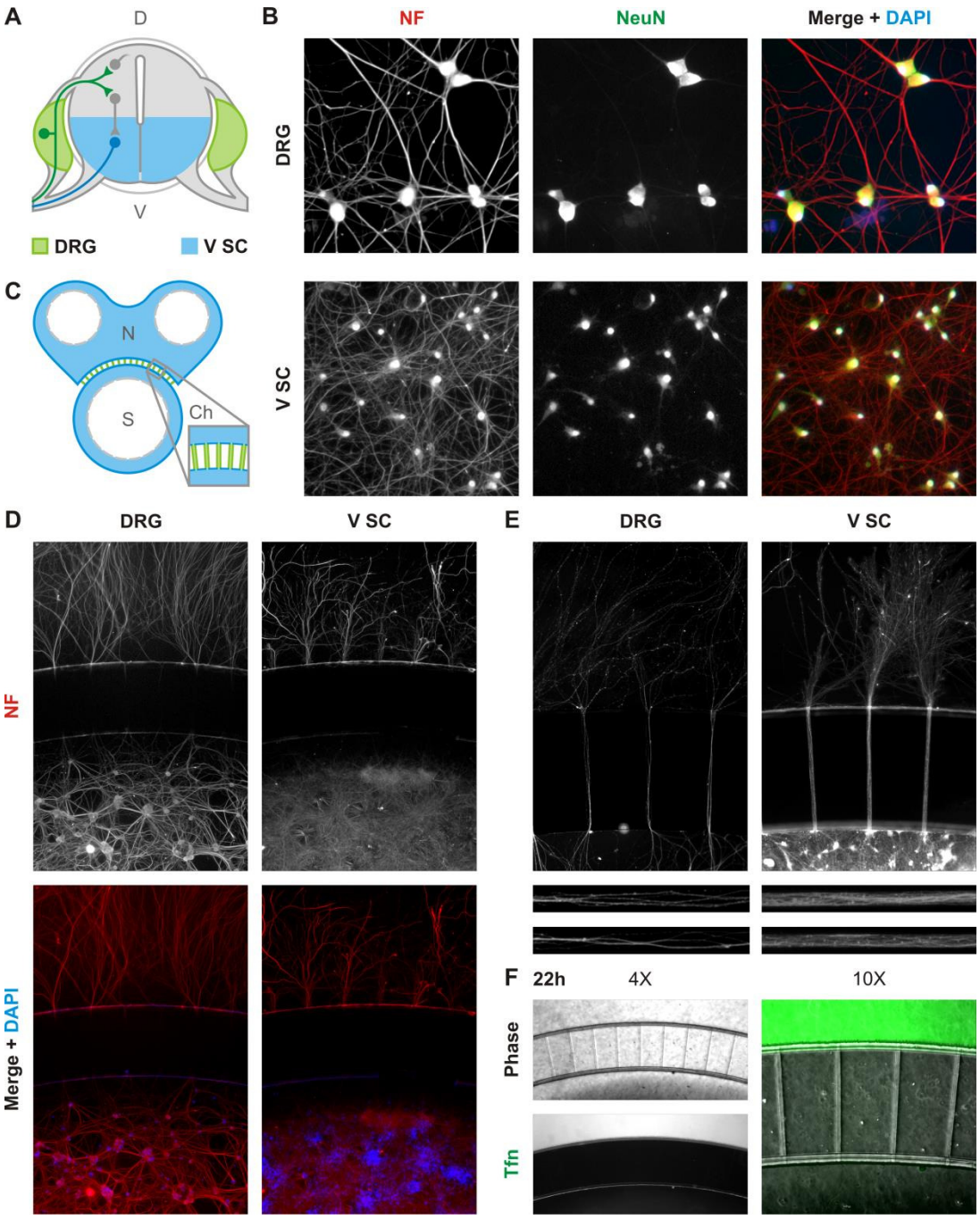

Figure 2.2. Compartmentalized cultures of dorsal root ganglion and ventral spinal cord neurons.

A. Schematic of a cross-section of the spinal cord and dorsal root ganglia including a simplified representation of the connectivity of neurons within those tissues. Shown is a representative motor neuron cell body (blue) projecting out of the ventral (V) spinal cord (SC); a sensory neuron cell body (green) located in the dorsal root ganglion (DRG) innervates into the spinal cord; and interneurons and commissural neurons (grey) are located in the dorsal (D) spinal cord. Tissues dissected and

Figure 2.2 (continued) dissociated to obtain the ventral spinal cord (V SC) and DRG neuronal cultures are indicated in blue and green respectively. Grey tissues were excluded from dissociated culture. **B.** Fluorescence microscopy of DRG and V SC dissociated culture at day 7 stained with DAPI (blue) and antibody against phosphorylated neurofilament H (NF; red) and neuronal nuclei (NeuN; green). **C.** Schematic of the compartmentalized microfluidic culture device. The device includes two compartments, neurite (N) and somal (S), connected by microchannels (Ch). Color-coding indicates the depths of each device region: green = 3µm; blue = 100µm; white corresponds to open wells. **D.** Fluorescence microscopy of dissociated DRG and V SC neurons cultured in compartmentalized devices and stained against NF (red) and with DAPI (blue). Due to limited diffusion of antibodies into microchannels, neurites within these structures appear unlabeled. **E.** Fluorescence microscopy of calcein stained, compartmentalized DRG and V SC neurons demonstrating continuity of neurites through the microchannels. F. Abrogated diffusion of fluorescent transferrin (Tfn, green) across microfluidic channels after 22h in culture.

We investigated RABV uptake in neurons that project into muscle tissue: neurons of the dorsal root ganglia (DRG) and ventral spinal cord (V SC) harvested from embryonic rats (Figure 2.2A). Dissociated DRG and V SC cultures yield neuronal populations with extensive projections as determined by immunofluorescence against the phosphorylated neurofilament H (NF) and the neuronal marker, Neuronal Nuclei (NeuN; Figure 2.2B). Isolation of neuronal termini was achieved by culturing neurons in microfluidic devices (Figure 2.2C). By 10 days in vitro (div) significant neurite outgrowth from cells cultured in the somal (S) compartment was detected in the distal, neurite (N) compartment (Figure 2.2D). Calcein staining demonstrated that neurites are contiguous across the channel (Figure 2.2E). Diffusion of molecules between the N and S compartments was restricted by controlling liquid levels and, therefore, hydrostatic pressure across the microchannels. Indicative of effective fluidic isolation, transferrin (Tfn) tagged with AlexaFluor 488 added unilaterally to the N compartment was retained with no detectable diffusion across the channels for 22h (Figure 2.2F).

Rabies G-mediated infection of neurons is dependent on dynamin

Figure 2.3. Dynasore and EIPA inhibit rVSV CVS G infection in compartmentalized neuronal culture.

Fluorescence microscopy of MF cultures of **A.** DRG neurons or **B.** V SC neurons infected with rVSV CVS G in the N compartment. Neurons were additionally treated with the dynamin inhibitor, dynasore (150µM), or the macropinocytosis inhibitor, EIPA (25µM), as indicated at either 0 or 2hpi and monitored for viral eGFP (green) expression at 26hpi. Cells are further stained against phosphorylated neurofilament H (NF; red) and with DAPI (blue). **C.** Neurites in the N compartment at 26hpi and continuous treatment with the indicated inhibitor, stained against neurofilament H. **D.** Quantitation of percentage eGFP positive neurons in three iterations of the experiment in DRG culture. Error bars indicate the standard deviation for each condition.

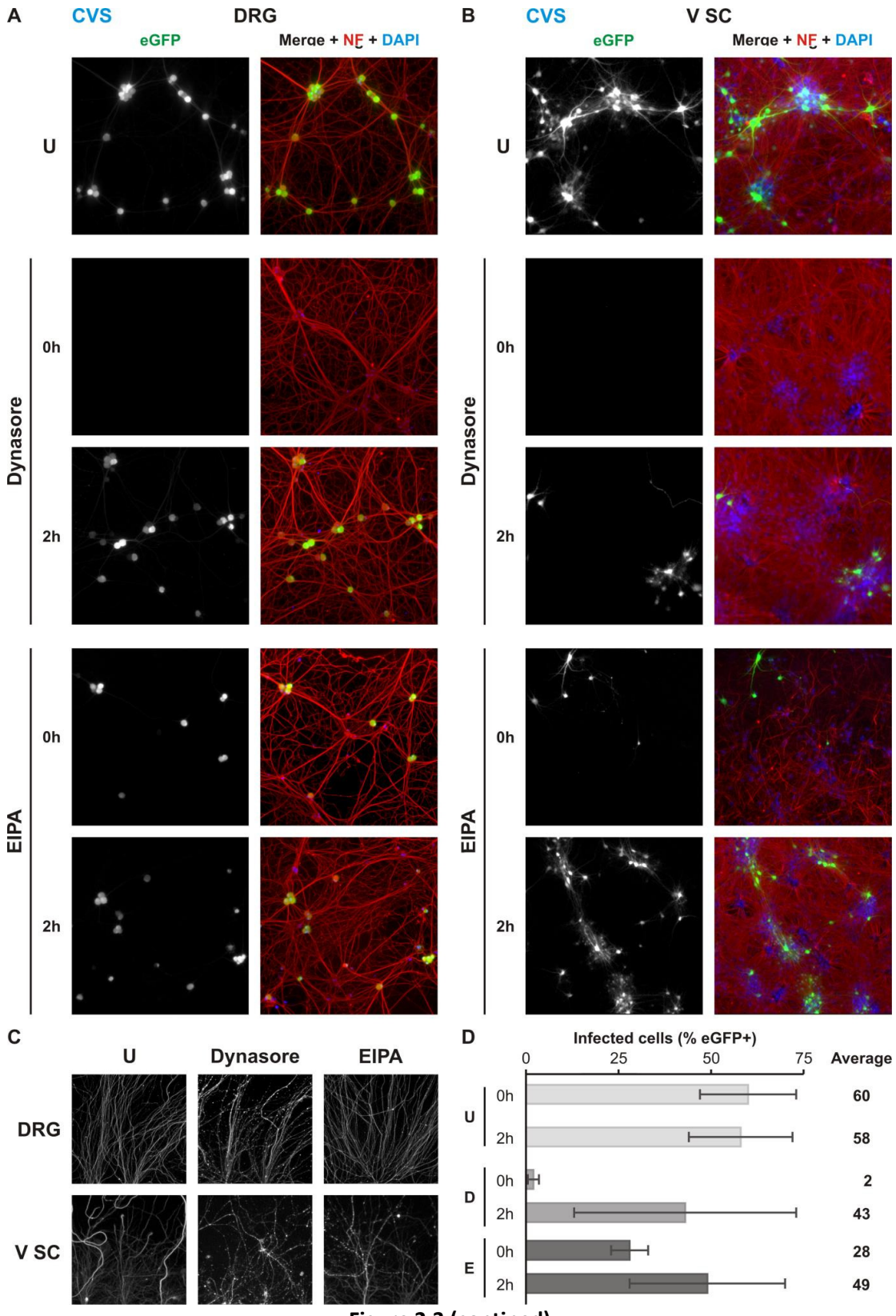

Figure 2.3 (contined)

We evaluated the effect of endocytosis inhibitors on viral infection from the neuronal termini of cultured DRG and V SC neurons (Figure 2.3). We tested dynasore and 5-(N-ethyl-N-isopropyl)amiloride (EIPA) to determine the requirement for dynamin- and macropinosome-mediated uptake respectively. Infection was monitored by the accumulation of virally encoded eGFP. Consistent with dynamin-dependent endocytosis of rVSV CVS G, inoculation in the presence of dynasore caused a near total block of infection in either neuronal population (Figure 2.3A, B). Treatment with EIPA also resulted in a reduction of infection; however, inhibition was not as pronounced as with dynasore.. Because neurite projections cannot be assigned to specific neurons in the somal chamber, the magnitudes of the inhibitory effects of dynasore and EIPA cannot be precisely quantified. This is particularly true for V SC culture which exhibits limited N compartment projection relative to the number of cultured neurons. However, the percentage eGFP positive cells for each condition in DRG culture which displays a greater efficiency of neurite outgrowth was assessed (Figure 2.3C). This analysis confirmed that dynasore decreased the infected neurons from 43% to 2%. In contrast, the effect of EIPA in DRG infection was two-fold. This differed qualitatively from its observed effect in V SC culture, which was significantly more pronounced (Figure 2.3B). Reductions in infection by either inhibitor could not be explained by off-target effects on viral replication since addition of inhibitor at 2hpi had limited effect on infection. Chemical degradation of projecting neurites was also excluded as a contributing factor: intact neurite structures were retained at the experimental endpoint in both treated and untreated cultures (Figure 2.3D).

We previously demonstrated that epithelial uptake of rVSV SAD B19 vaccine strain of rabies (rVSV SAD B19 G) is clathrin-dependent [191]. To identify differences in uptake between epithelial and neuronal cells, we tested the effect of dynasore and EIPA on rVSV SAD B19 G uptake into DRG neurons (Figure 4). Treatment with dynasore resulted in an almost complete block of infection whereas EIPA

Figure 2.4. rVSV SAD B19 G infection of compartmentalized DRG neurons is dynamin-dependent.

A. MF cultures of DRG neurons infected with rVSV SAD B19 G in the N compartment and treated with indicated inhibitor at 0 or 2hpi, also as indicated. Viral eGFP (green) expression was assessed at 26hpi. Cells are further stained against phosphorylated neurofilament H (NF; red) and with DAPI (blue). **B.** Quantitation of percentage eGFP positive neurons in three iterations of the experiment. Error bars indicate the standard deviation for each condition. Abbreviations are as follows: U, untreated; D, dynasore; E, EIPA.

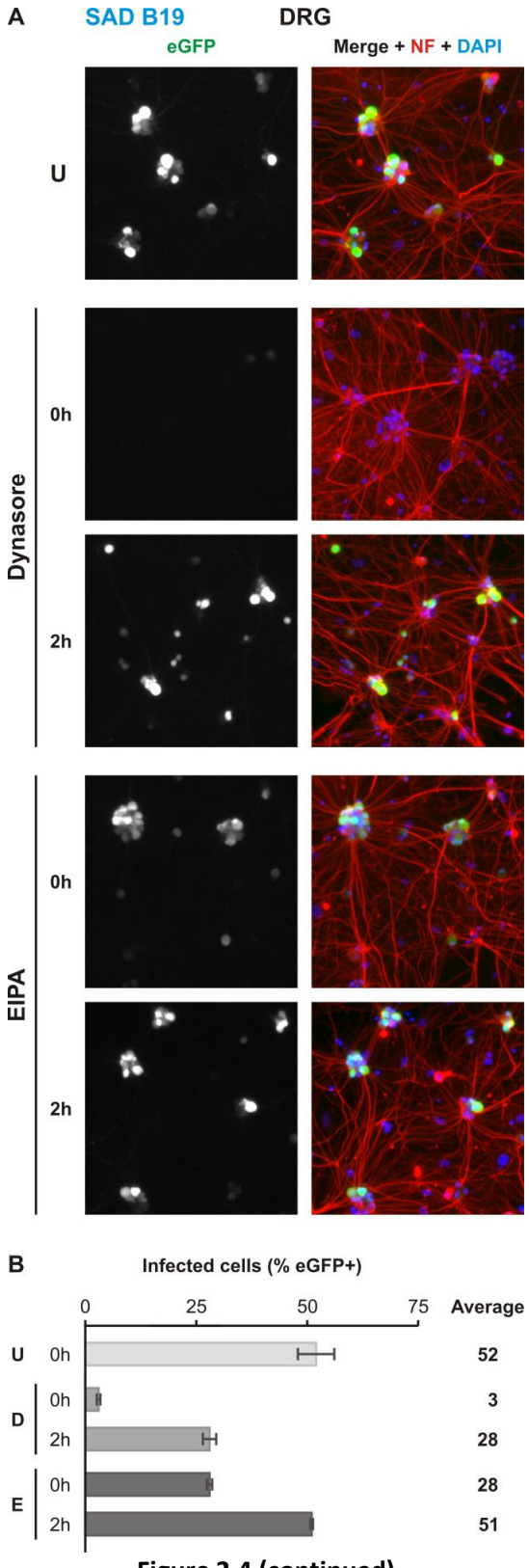

Figure 2.4 (continued)

treatment resulted in a more modest reduction (Figure 2.4B). These results suggest a shared mechanism for SAD B19 G- or CSV G-mediated entry.

Dynamin inhibition blocks virion accumulation in the S compartment and microchannels

Having established that endocytic inhibitors in the N compartment result in a reduction of infected cells in the S compartment, we sought to verify that this was due to a reduction in the number of virions delivered to the soma. The cellular distribution of rVSV CVS G virions labeled with AF647 (rVSV CVS G AF647) was examined by confocal microscopy (Figure 2.5). We first analyzed infected neurons at 26hpi following expression of viral eGFP (Figure 2.5A, B). In untreated controls, efficient uptake and transport of virus was evidenced by detectable cell-associated particles in all compartments and including the cell bodies of some uninfected cells. In contrast, dynasore treatment restricted viral localization to the N compartment (Figure 2.5A). Unlike dynasore, EIPA treatment had a limited effect on virus transport to the soma: viral particles were detectable in both eGFP-positive and -negative neurons (Figure 2.5B). Irrespective of the inhibitor used, viruses were detected in association with N compartment neurites indicating that binding was unaffected.

At 26hpi, persisting intact viral particles represent a population that did not contribute to infection. We, therefore, also assessed rVSV CVS G AF647 uptake disruption at an earlier timepoint, 6hpi (Figure 2.5C, D). Here, we observed no chemical disruption of viral association with the neuronal membrane (Figure 2.5C). In contrast, differential viral accumulation was detected within microchannel neurites. Since extracellular diffusion into the microchannels is restricted, viruses access this compartment only via axoplasmic transport. All observed microchannel viruses are, therefore, assumed to be intracellular. Both dynasore and EIPA administered at the time of inoculation abrogated viral accumulation in the microchannels (Figure 2.5D). Dynasore impacted viral accumulation also when

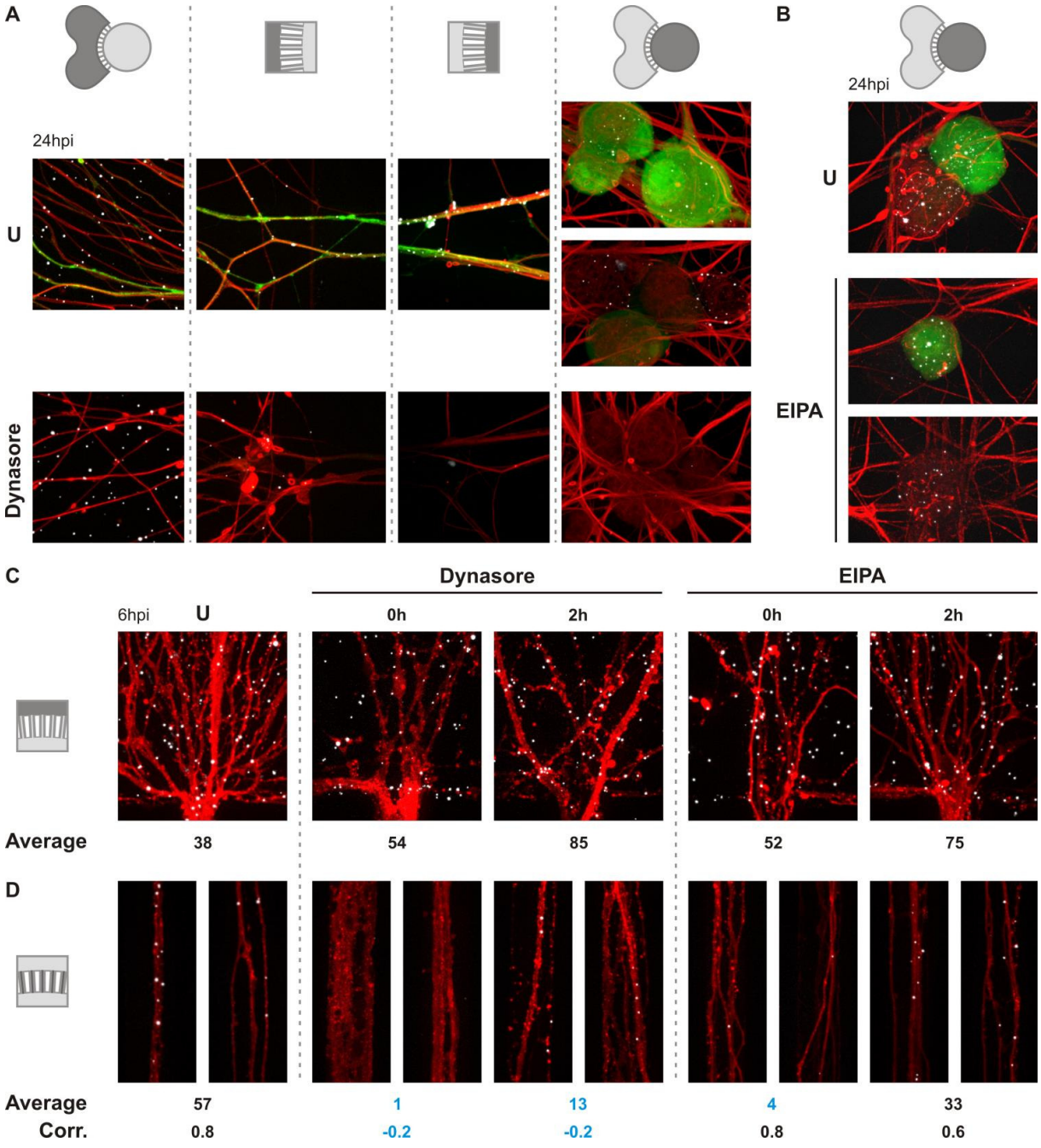

Figure 2.5. Disruption of dynamin blocks viral accumulation in microchannel neurites and cell bodies of DRG neurons in compartmentalized culture.

A. Confocal microscopy of the localization of fluorescently-labeled rVSV CVS G particles in neurons infected in the absence (U) or presence of 150µM dynasore at inoculation. Virus was administered to the N compartment, and the distribution of virions was assessed following reporter eGFP gene expression (green) at 24hpi. Virus particle localization was monitored in the following structures

Figure 2.5 (continued) from left to right: distal neurites, N compartment microchannel opening, S compartment microchannel opening, and S compartment cell bodies. The order of the panels from left to right reflects the direction of transport undergone by the virus. Neurites were stained against phosphorylated neurofilament (red). rVSV CVS G AF647 particles detected by direct fluorescence are displayed in white for ease of viewing. B. Confocal microscopy of rVSV CVS G AF647 (white) accumulation in the cell bodies of DRG neurons infected in the absence (U) or presence of 25μM EIPA at inoculation. Here, infection was carried out in the N compartment and viral distribution assessed at 24hpi in the somal compartment only. Neurons were stained against phosphorylated neurofilament (red); eGFP (green) and rVSV CVS G AF647 (white) were detected by direct fluorescence. C. and D. Localization of incoming rVSV CVS G AF647 particles C. along neurites at the N compartment outlet and D. within microchannels as detected by confocal microscopy at 6hpi. Neurites were stained against phosphorylated neurofilament (red) and rVSV CVS G AF647 particles (white) were detected by direct fluorescence. N compartments of DRGs neuronal devices were inoculated with virus concomitantly (0hpi) or 2h prior to treatment with inhibitor as shown. U indicates untreated controls. Average number of particles per equivalent field of view is reported beneath each panel. The calculated correlation (Corr.) between particle number at the outlet and within individual microchannels is also reported for each condition. Averages and correlations that differ substantially from untreated controls are in blue for emphasis.

added at 2hpi, although the effect was less pronounced. Importantly, we noted a strong positive correlation between the number of cell-associated viruses at the opening to and the number within individual microchannels in untreated controls. Dynasore alone decoupled N-compartment and microchannel accumulation of virus. This non-positive correlation indicates a true block of uptake, consistent with accumulation at the plasma membrane, but loss of uptake and intracellular transport. In contrast, in the presence of EIPA, the correlation between opening and microchannel viruses remained positive. EIPA may, therefore, merely delay, rather than block, endocytosis and transport of virus.

Fluorescently-labeled rVSV CVS G and transferrin are co-packaged for axoplasmic transport

Fluorescent transferrin (Tfn) and dextran (Dex) are commonly used markers of clathrin-mediated and fluid phase endocytosis respectively. To corroborate our inhibitor studies, we asked if rVSV CVS G AF647 is co-packaged with Tfn or Dex during entry (Figure 2.6A, B). In both neuronal populations, we observed limited colocalization of virions with Dex in either the N compartment or

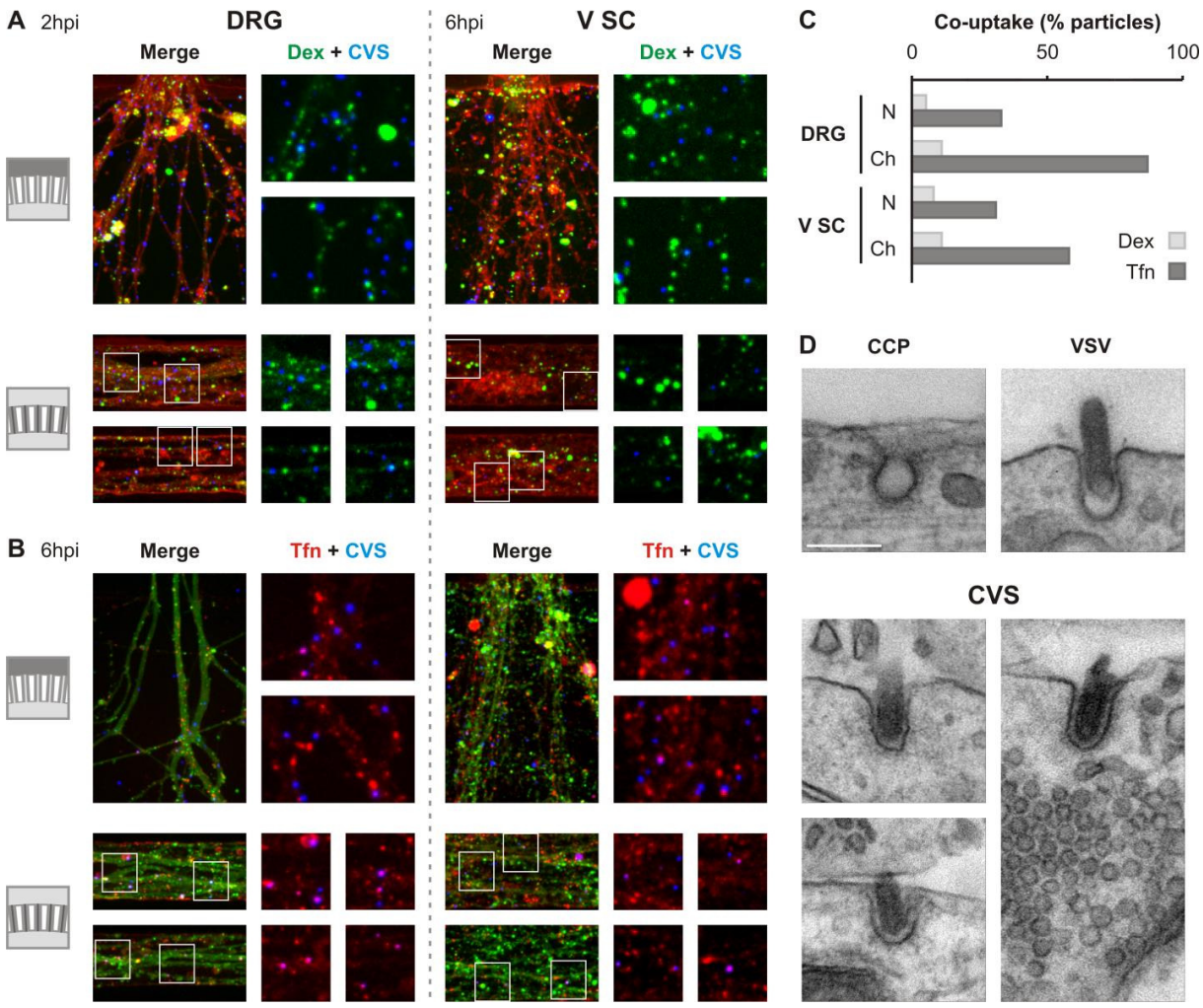

Figure 2.6. rVSV CVS G is co-packaged with transferrin during endocytosis.

A. Confocal imaging displaying limited colocalization between incoming rVSV CVS G AF647 particles and dextran in DRG and V SC neurons. N compartments previously stained with CellTracker (CT, red) were inoculated with rVSV CVS G AF647 (CVS, blue) in the presence of dextran-AF488 (Dex, green), 10,000 MW. Co-localization of virus and dextran was assessed in neurites of the N compartment (top) and microchannels (bottom) at 2 or 6hpi as indicated. Merges combine CT, CVS and Dex signals. Adjacent two-channel panels show only CVS and Dex signals and correspond to enlarged areas of the merged images as shown. B. Confocal imaging of colocalization between incoming rVSV CVS G AF647 particles and transferrin in DRG and V SC neurons. N compartments previously stained with calcein (green) were inoculated with rVSV CVS G AF647 (CVS, blue) in the presence of Tfn-AF594 (Tfn, red). Co-localization of virus and Tfn was assessed as in A. Merges combine calcein, CVS and Tfn signals. Two-channel panels correspond to enlarged areas of the merged images. C. Quantitation of co-uptake of virus and the indicated endocytic markers in the N compartment and microchannels. D. Transmission electron micrographs of endocytic structures and rVSV CVS G uptake into V SC at 2hpi.

Figure 2.6 (continued) Top left: a clathrin-coated pit (CCP). Top right: a VSV particle undergoing clathrin-coated pit envelopment in B-SC-1 cells. Bottom (CVS): three representative images of endocytic structures involved in rVSV CVS G uptake into V SC neurites. Scale bar = 100nm, and applies to all panels.

channel neurites (Figure2. 6A-C). In contrast, a third of incoming rVSV CVS G was associated with Tfn in the N compartment (Figure 2.6B). Significantly, rVSV CVS G colocalization with Tfn was enriched in the microchannels suggesting that internalization via clathrin shunts virus into long-range axoplasmic transport (Figure 2.6B, 2.C). This transportation bias for particles originating from clathrin-coated pits was particularly pronounced within DRG neurons: 87% of virions within the channels colocalized with Tfn versus 33% in the N compartment (Figure 2.6C). Fewer viral particles were associated with Tfn in V SC channel neurites (Figure 2.6B, C): enrichment from 31% in N to 58% colocalization was nonetheless observed. This observation is consistent with results showing greater sensitivity of infection to EIPA in the V SC neurons (Figure 2.3B). However, transmission electron micrographs of rVSV CVS G uptake in V SC displayed viruses exclusively associated with endocytic structures suggestive of clathrin mediated endocytosis (Figure 2.6D).

To ascertain that viral particles colocalizing with Tfn in fixed samples were actively being transported, we performed live imaging studies in DRG neurons (Movies 2.1 and 2.2; Figure 2.7). Within the channels, we recorded single viral particles in the process of long-range axoplasmic transport. Many of these were transported concomitantly with fluorescent Tfn (Movie 2.1). Similarly extensive co-transportation with Dextran was not detected (Movie 2.3).

Fusion of rVSV CVS G occurs following transport to the soma

The final step in rhabdoviral uptake is the pH-induced fusion of virus with the endosomal membrane mediated by conformational changes in G. Within highly polarized neurons, fusion can occur locally at the site of uptake or following endosomal transport at the cell body. Our live imaging data corroborates

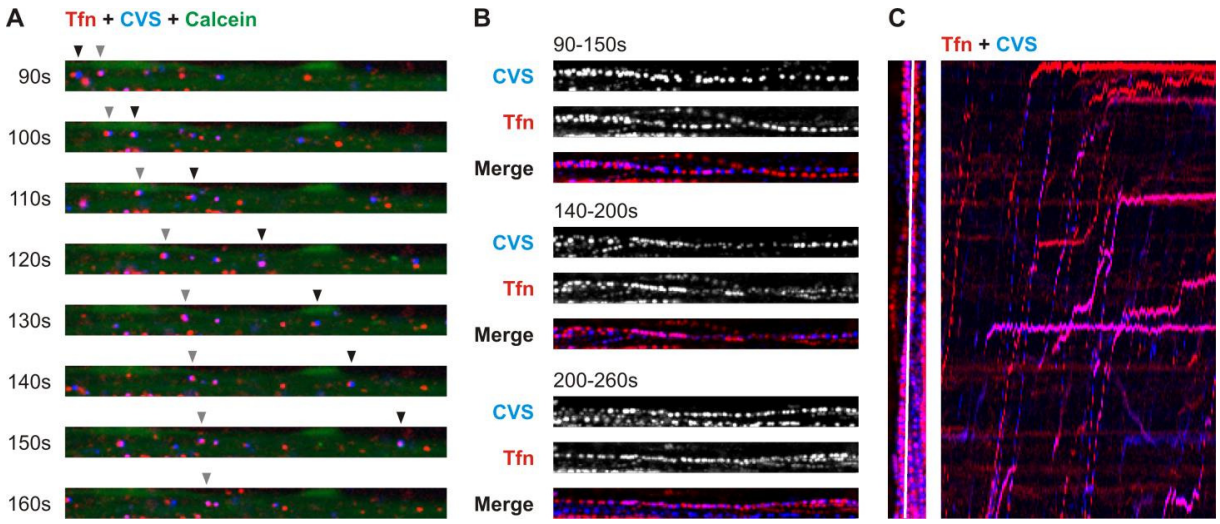

Figure 2.7. Active co-transport of rVSV CVS G and transferrin within DRG neurites.

A. Time-lapse images from confocal live recording of co-transport of rVSV CVS G AF647 (blue) and transferrin-AF594 (Tfn, red) in calcein-stained neurites (green) within a microchannel. Timepoints indicated are matched with timestamps in Movie 1. Arrowheads track two viral particles being co-transported with Tfn. **B.** Thirty timepoints, corresponding to 60s clips from Movie 1, combined into a single image to display tracks of virus (CVS) and Tfn-positive endosomes through a microchannel from cultured DRG neurons. CVS and Tfn tracks are shown individually in greyscale, and merged. Timepoints indicated are matched with timestamps in Movie 1. **C.** Kymograph of Tfn (red) and CVS (blue) particle movement along a single plane from Movie 1. On the left is a projection of all particle and Tfn tracks within the movie and, in white, the plane used to generate the kymograph (right panel).

previously published findings that RABV G directs virions into a long-range vesicular transport route with delayed acidification and release [7, 8, 36]. We sought to extend these single particle observations and investigate the role of delayed fusion on productive infection (Figure 2.8A-C). We administered, Bafilomycin A1 (BAF A1), an inhibitor of vesicular H^+ ion pumps, to the N or S compartment to respectively block localized or delayed fusion and monitored its impact on viral eGFP expression. Cells whose neurites were treated with BAF A1 displayed robust infection in the S compartment despite presence of the inhibitor (Figure 2.8A, B). Under these conditions, viral spread was significantly enhanced relative to untreated counterparts in both DRG and V SC. In contrast, somal treatment with BAF A1 resulted in a robust inhibition of infection (Figure2. 8A-C). Inhibition of infection could be

partially overcome when BAF A1 was administered at 9-12hpi at which point incoming viruses from the N compartment have likely already fused at the cell body. We excluded potential cytotoxicity or off-target effects on the viral life cycle by repeating the experiment in non-compartmentalized culture: post-entry administration of BAF A1 at 2hpi did not interfere with infection (Figure 2.8D). Our results demonstrate that infection cannot be established in the absence of viral fusion at the cell body.

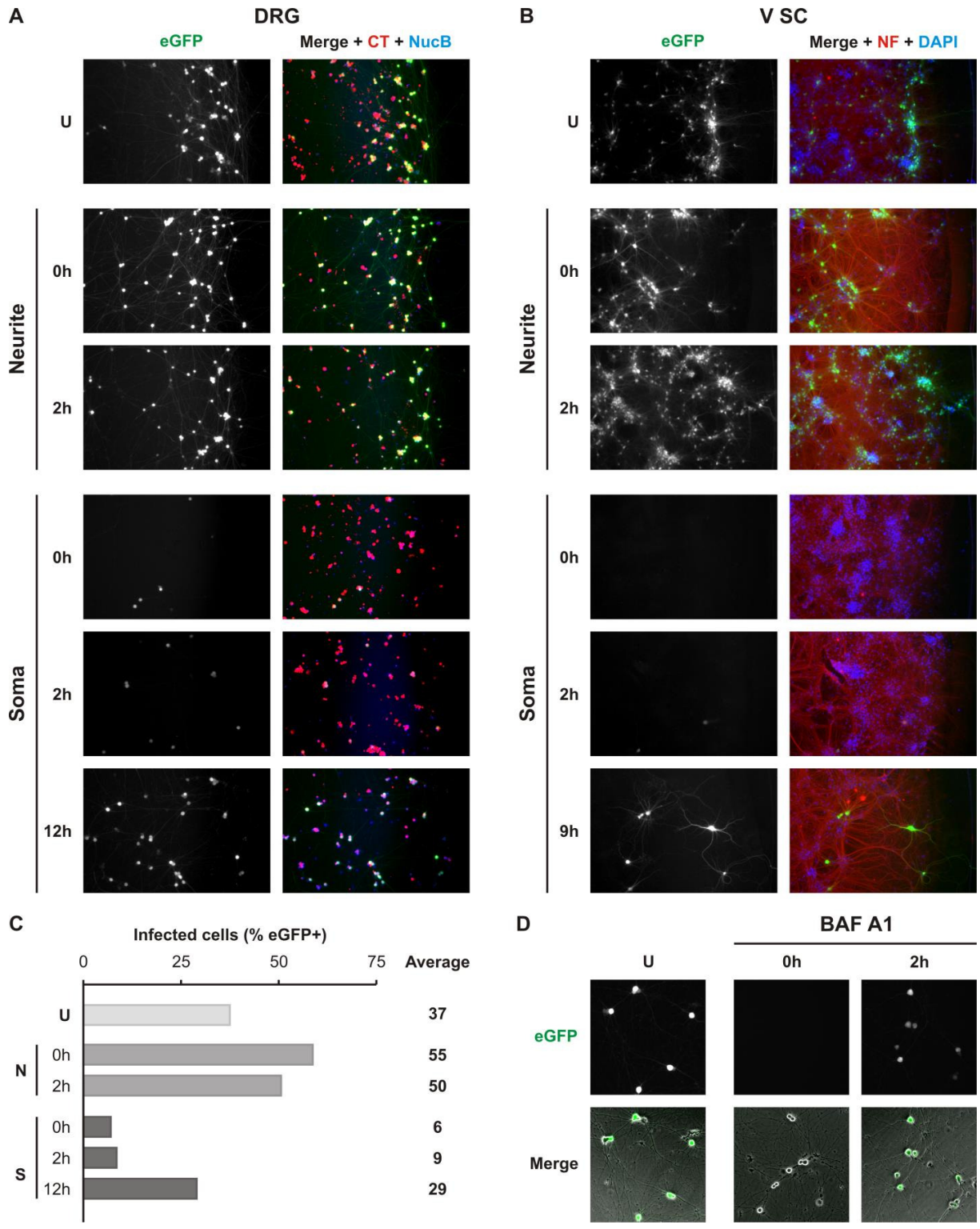

Figure 2.8. Somal endosomal acidification is required for rVSV CVS G infection.

Fluorescence microscopy of compartmentalized cultures of **A.** DRG neurons or **B.** V SC neurons

Figure 2.8 (continued) infected with rVSV CVS G in the N compartment in the presence or absence (U) of 1µM bafilomycin A1 (BAF A1). BAF A1, a block of endosomal acidification, was administered to either the N or S compartment at various timepoints relative to the start of infection. In the N compartment, BAF A1 was added at 0 or 2hpi. In the S compartment, BAF A1 was added at 0, 2, 9 or 12hpi as indicated. Infection was assessed by expression of viral eGFP at 26hpi. DRG neurons in A. were pre-stained with CellTracker (CT, red) and NucBlue (NucB, blue) prior to the start of the experiments. In B., infected V SC neurites were fixed and permeabilized at 26hpi. V SC neurites were detected by immunofluorescence against phosphorylated neurofilament (NF, red) and nuclei were stained with DAPI (blue). **C.** Quantitation of percentage eGFP positive cells following a representative experiment in DRG culture. All conditions, except the untreated control, were tested in duplicate. Averages are provided to the right of the bar graph. D. Fluorescence microscopy of non-compartmentalized DRG cultures infected with rVSV CVS G and treated with BAF A1 at 0 or 2hpi. U indicates untreated controls. Presence of the infection marker, eGFP (green), was assessed at 8hpi. Merged images combine the eGFP signal and phase microscopy of the DRG neurons in culture.

DISCUSSION

Using a neurotropic RABV G protein and compartmentalized peripheral neuron cultures we characterize the viral entry pathway from uptake at the neuronal termini to fusion. We provide evidence for a model of RABV uptake that begins with clathrin- and dynamin-mediated uptake at the plasma membrane. Endocytosed viruses are then transported intact and within endosomes from the distal neurites to the site of fusion at the cell body. Furthermore, we show that somal fusion is required for efficient infection. This work extends the current understanding of RABV uptake by identifying the predominant internalization mechanism at the plasma membrane of two neuronal populations involved in early neuroinvasion *in vivo.* In addition, by combining single particle imaging and infectivity study, we correlate single virion behavior with productive infection.

Evidence for rhabdoviral uptake into partially-coated clathrin pits in neurons

We identify clathrin-mediated endocytosis (CME) as the primary mechanism of productive RABV uptake. Previous studies investigated RABV uptake into non-neuronal [108, 191], neuroblastoma [190] or hippocampal neurons [160]. Our work extends these studies into DRG and V SC neurons that are at the front-line of host neuroinvasion. Furthermore, previous studies in neuron or neuron-like cells were limited to static electron micrographs, which, although informative, cannot be related to infectivity. We base our conclusion on three observations: (i) the susceptibility of infection and single particle uptake to disruption of dynamin; (ii) the co-packaging and -transport of incoming virions with transferrin; and (iii) detection of rhabdoviral particles within coated pits by electron microscopy. Because co-transport with transferrin was visualized following engagement of long-range axoplasmic transport, we cannot exclude that rhabdovirus-containing endosomes fuse or coalesce with Tfn-positive endosomes following internalization at the plasma membrane. However, transmission electron micrographs of uptake into V

SC neurons provide direct evidence for clathrin-dependent uptake: viruses exclusively associated with coated endocytic structures that resemble the rhabdoviral clathrin-coated pits observed in epithelial cells.

Ultrastructural data from transmission electron micrographs reported here suggests that, as in epithelial cells, clathrin-coated RABV endosomes may be only partially coated with clathrin triskelions. Viral pits share the elongated profile characteristic of incompletely coated rhabdoviral endosomes observed in B-SC-1 cells (Figure 2.6D) [37, 116, 191]. Consequently, although this was not explored in this study, it is likely that here too actin polymerization may be a requirement for completion of envelopment and scission from the plasma membrane. There is ample indirect biochemical evidence linking F-actin regulation and CME at both the pre- and post-synaptic membranes [195]. However, studies examining actin polymerization directly during uptake of cargo into neurons are lacking. The morphology of rhabdoviral particles, which exceeds typical internal dimensions of clathrin-coated pits, increases the requirement for actin involvement in CME in non-neuronal cells. If actin involvement extends to neuronal cells, rhabdoviruses may serve as powerful tools for dissecting its role in synaptic CME as well.

Viral fusion occurs following long-range transport to the soma

In this study, we provide evidence of long-range axoplasmic transport of rhabdoviruses incorporating RABV G. Co-transport of virions with Tfn is consistent with trafficking within endosomes. Additionally, exclusive sensitivity of infection to disruption of endosomal acidification in the S compartment demonstrates that viral fusion events leading to productive infection occur at the soma. Previous studies have reported long-range endosomal transport of intact vaccine strain RABV virions within differentiated neuroblastoma cells and DRG neurons [7, 8]. Additionally, lentiviral vectors

pseudotyped with G from the attenuated CVS-B2C strain have been tracked during long-range endosomal transport in compartmentalized motor neuron culture [36]. We extend these observations to the pathogenic CVS-11 G and demonstrate that subsequent establishment of infection is exclusively dependent on pH-dependent fusion at the perikaryon.

A particularly intriguing finding is the robust increase in infection and spread following inhibition of endosomal acidification at the neurites in both DRG and V SC neurons. This observation suggests that some endosomes engaging long-range axoplasmic transport – believed to be characterized by delayed endosomal acidification – undergo acidification before delivery to the soma. In transit acidification causes release of the viral core at a non-productive site for establishment of infection and represents an abortive step in the rVSV CVS G lifecycle. From a molecular standpoint, it suggests that luminal pH within the endosome dictates association and transit along the cytoskeleton. Supporting this view is the observation that luminal pH of long-range endosomal tetanus carriers correlates with motility: endosomes with recorded pHs <6.0 were almost exclusively stationary within axons and soma [189]. In contrast, triggering of the acidification event itself appears to be regulated independently at various sites along the axon. Accordingly, when acidification is blocked in the N compartment, viruses that would otherwise have fused prematurely proceed along the transportation route and are subjected to subsequent acidification event(s). This results in the observed increase in overall infection. We must emphasize that our observations are specific to productive infection from an rVSV core. We do not know whether in-transit acidification occurs *in vivo* or if premature fusion abrogates infection from RABV cores. However, existing evidence of delayed fusion from single particle RABV studies suggests that our observations may be generalizable to full-length RABV infection *in vitro*.

RABV G-mediated uptake of rhabdoviruses into two neuronal populations

Sensory DRG neurons and motor neurons are both susceptible to RABV infection in the host. Due to the morphological and functional differences between these neuronal populations, we explored the possibility of non-identical uptake mechanisms for RABV based on the neuronal subtype. Our infectivity experiments using biochemical perturbation of endocytic processes reveal that productive infection in either neuronal population is dynamin-dependent. Single particle experiments further implicate clathrin-mediated uptake as a major route of RABV endocytosis in both cell types. Accordingly, 90% of particles in DRG microchannel neurites, and 55% in V SC neurites are co-packaged with transferrin.

In addition to the commonalities listed above, we also identified differences in uptake between the two neuronal populations. In V SC culture, a significant fraction of incoming particles was not co-packaged with transferrin. This result, in addition to greater sensitivity of V SC infection to the endocytic inhibitor EIPA, suggests that multiple uptake mechanisms may exist. Consistent with this hypothesis, lentiviral vectors expressing CVS-B2C G undergoing axoplasmic transport in motor neurons were found to colocalize with all three known RABV receptors: p75 neurotrophin receptor, neural cell adhesion molecule, and nicotinic acetylcholine receptor [36]. This raises the possibility that the uptake route could differ depending on the distribution of receptor engagement at the plasma membrane.

The absence of significant colocalization between rVSV CVS G and internalized fluorescent dextran suggests that the alternative uptake route is likely not within macropinosomes, despite the sensitivity of infection to EIPA. Disruption of Na^+/H^+ exchanger (NHE) function is known to underlie the inhibitory action of EIPA on fluid phase endocytosis [196, 197]. NHEs, which regulate intracellular pH homeostasis, have also been shown to modulate neuronal activity [198-200]. The effect of EIPA on viral

infection may, therefore, be an off-target consequence of altered NHE function. Future studies are required to explore this possibility.

Modeling RABV neuroinvasion in vitro

Here we use compartmentalized culture systems to control the site of RABV entry and more closely recapitulate the conditions extant during neuroinvasion at a bite site. However, dissociated monoculture still represents a simplistic model of the primary infection site. Importantly, dissociated ventral spinal cord neurons do not form neuromuscular junctions (NMJs) in the absence of muscle cell innervation, despite generating other synaptic structures. NMJs are highly specialized synapses populated by functionally specific transmembrane proteins. In nerve-muscle cocultures, RABV associates preferentially with NMJs [109]. In the absence of these structures, we observed uniform association of rVSV CVS G with peripheral neuronal membranes by both confocal and transmission electron microscopy. Since association of RABV with synaptic structures is also observed in hippocampal infections [160], we cannot exclude the possibility that viral internalization in our system may represent an atypical pathway unrelated to neuroinvasion in a live host. Importantly, RABV binding to the NMJ is largely mediated by the interaction between G and its receptor, nAChR, as evidenced by its susceptibility to disruption by competition with alpha-bungarotoxin [64]. Curiously, nAChR is expressed exclusively on the post-synaptic membrane of the motor endplate. Due to the high affinity interaction between nAChR and RABV G, RABV particles at the NMJ may be in complex with the receptor during uptake. How this could impact the internalization route or mechanism of RABV at the presynaptic membrane is not known. Further experiments in nerve-muscle coculture within similar compartmentalized devices will be necessary to investigate the role of NMJs and post-synaptic anchoring in the uptake route of RABV.

ACKNOWLEDGMENTS

We thank D. Knipe, S. Reck-Peterson and the members of the Whelan Lab for scientific discussions and suggestions; C. Saenz and the Microfluidics Core Facility at Harvard Medical School for training, equipment and technical assistance throughout the photolithography and device manufacturing process; S. Fenstermacher for providing protocols and practical demonstrations of dorsal root ganglion dissections; and M. Ericsson, E. and L. Trakimas of the Harvard Medical School Electron Microscopy Facility for embedding, sectioning and staining of samples. S.P. would also like to acknowledge the exceptional scientific and emotional support of A. J. Akey, who provided invaluable advice and technical assistance with the photolithographic techniques used in this study, and A. L. Akey who contributed less scientifically, but provided kicks of encouragement. Funding support for this work was provided by NIH/NIAID grant U19AI109740.

AUTHOR CONTRIBUTIONS

Silvia Piccinotti performed all experiments and analysis, and co-wrote the manuscript.

Constance L. Cepko supervised collection of data and analysis.

Sean P. Whelan supervised collection of data and analysis, and co-wrote the manuscript.

DISCUSSION

Here we describe the use of rVSV RABV G surrogate viruses in the study of RABV uptake into epithelial and peripheral neuronal cells. The work of Chapter 1 establishes that rVSV SAD B19 G recapitulates RABV behavior in infectivity-based in vitro entry assays. It further identifies clathrin-mediated endocytosis as the primary mechanism of RABV G-mediated internalization into epithelial cells. By tracking viral envelopment into coated pits in real-time, this work extends to RABV the observation that clathrin-mediated endocytosis of rhabdoviral particles proceeds via endosomes partially coated with clathrin triskelions and dependent on actin for completion of envelopment. Our work adds to existing evidence [116] that particle morphology is the sole viral determinant of partial coating and actin-dependency of clathrin-coated pits. In Chapter 2, we study uptake of neurotropic rVSV CVS G at the termini of primary peripheral neurons cultured in microfluidic compartmentalized devices. We demonstrate that clathrin-mediated uptake of RABV is conserved in dorsal root ganglion and ventral spinal cord neurons, and validate this result with rVSV SAD B19 G. We further provide ultrastructural evidence suggestive of partial coating of clathrin pits engaging virus in neurons of the ventral spinal cord. Finally, we demonstrate that fusion at the cell body is required to establish infection. This work extends existing live imaging studies of RABV G-dependent uptake and axoplasmic transport of intact virions in neurons by characterizing the endocytic process at the plasma membrane and correlating single particle observations with infectivity. As a whole, this work suggests a conserved model of RABV internalization that begins with uptake and envelopment into partially coated clathrin pits at the plasma membrane, followed by passive transport of intact virions within endosomes, and finally fusion and RNP release at the somatodendritic compartment. Our model also suggests that virions fusing prior to delivery to the cell soma fail to establish infection, and that RNP release in the axon therefore represents a non-productive event from the point of view of the virus lifecycle.

This work also establishes rVSV RABV G viruses as useful surrogates for the study of RABV uptake. We propose that rVSV RABV G viruses may facilitate the comparative study of G-dependent uptake of pathogenic and attenuated RABV strains, including street isolates, the full length versions of which cannot easily be cultured in vitro. These, combined with neuronal compartmentalized culture, may serve as a powerful system for answering a broad spectrum of open questions in RABV biology from receptor engagement to transsynaptic spread.

Recombinant vesicular stomatitis virus as a surrogate for the study of enveloped virus entry

To investigate RABV uptake, we relied upon the versatility of the related rhabdovirus, VSV, to produce a surrogate rVSV RABV G which can be studied with increased safety under biosafety level 2 conditions. VSV tolerates genetic replacement of its endogenous glycoprotein with that of foreign enveloped viruses. Such chimeric rVSVs as well as pseudotyped VSVs have been used with great success to identify cellular receptors and entry mechanisms for Ebola [102, 143, 144], Lassa [145], Borna disease [142], Australian bat lyssavirus [201] and viral hemorrhagic fever viruses [202]. However, some important caveats are inherent to the use of rVSV for entry studies: i) the morphology and size of VSV virions is unique to the Rhabdoviridae and can have a mechanistic impact on entry [116]; ii) incorporation of foreign glycoproteins into the VSV membrane may not reflect endogenous densities; iii) membrane lipid composition as well as incorporation of host transmembrane proteins may differ from the physiological particle; iv) virions contain an rVSV core with unique transcriptional and replicative requirements. As a result, rVSV viruses can only serve as effective models up to the point of genome release. In the specific case of rVSV RABV G, many of these considerations do not apply due to the relatedness of the viruses. Here, the only significant limitation is the absence of a RABV core. Our work in epithelial cells has demonstrated that rVSV SAD B19 G and rRABV ΔG infections are indistinguishable from cellular attachment to expression of fluorescent marker proteins (Figure 1.1). Although this is suggestive that

rVSV RABV G may also recapitulate early steps in RABV infection faithfully in neuronal cells, conclusions about infectivity drawn using the rVSV RABV G virus in neuronal cells will have to be validated with full length RABV.

rVSVs display robust growth, particle stability during purification, and a broad range of permissive cell types. They are therefore useful in the study of viruses which lack in vitro culturing systems, grow to low titers, are restricted in common cell culture systems, or lack molecular tools for their study. Street isolates of RABV are of interest in the study of viral uptake. However, they are generally underutilized in basic RABV research due to their poor growth characteristics in tissue culture [203]. As a result, fixed, lab-adapted strains of RABV are widely used to study rabies biology and, indeed, have been invaluable in the determination of RABV virulence factors for vaccine development. Although fixed strains, such as CVS, retain in vivo pathogenicity, adaptation to cell culture in vitro alters viral tropism and receptor usage [204]. As a result, entry studies seeking to replicate native conditions, particularly in neurons, will benefit from the study of street, wild type strains of RABV [68]. Here, incorporation of street isolate Gs into rVSV may produce recombinant viruses with improved growth properties relative to their full length RABV counterparts, reducing the required number of passages for production of high titer stocks for experimentation and limiting or preventing accumulation of adaptive mutations in G. If such a panel of viruses can be generated, it will be invaluable in the study of differences in receptor usage, tropism, and trafficking conferred by specific variants of G.

Shared uptake mechanisms for neurovirulent and vaccine strains of rabies G

The RABV vaccine strain, SAD B19, is nonpathogenic in a variety of carnivorous mammalian species [205, 206] and has been widely used in wildlife oral vaccination campaigns. Despite attenuation of its parental strain in vivo, SAD B19 G, like its pathogenic counterpart CVS G, mediates clathrin-mediated

uptake and successful delivery of virions to the cell body in primary DRG culture. This observation suggests that the attenuation of the SAD B19 strain is likely not related to gross differences in the entry stages of peripheral neuroinvasion relative to CVS. However, in the experiments carried out in this dissertation, MOIs were generally high and viral dose could not be carefully gauged in compartmentalized neuronal culture. Therefore, differences in particle to infectivity ratios resulting from the strain of RABV G may not have been apparent. Comparison of the amino acid sequences and glycosylation patterns of SAD B19 and CVS glycoproteins with those of other RABV strains of differing pathogenicity underscore the need for additional work to dissect differences in neuronal uptake conferred by the two glycoproteins.

Despite attenuation of SAD B19 virus in vivo, residues involved in binding receptors $p75^{NTR}$ [39, 62] and nAChR [69] are conserved in SAD B19 G (Figure D.1). In particular, SAD B19 G retains a lysine and an arginine at positions 330 and 333 (Figure D.1 C,D), which, in addition to mediating binding with $p75^{NTR}$, are required for neuroinvasion of peripheral neurons and strongly correlated with neurovirulence [78]. This suggests that association with these receptors is likely retained in the attenuated G. The binding site of NCAM on RABV G is not currently known, and cannot be assessed. SAD B19 G also retains pathogenic residues which, although not known to affect receptor binding, have nonetheless been shown to confer virulence to the attenuated strain RC-HL (Figure D.2) [94]. In SAD B19, three residues known to correlate with pathogenicity are found to diverge from the virulent Nishigahara comparison strain: serine at residue 182, lysine at 205, and alanine at 242 (Figure D.2 A). The Nishigahara residue at 182 was not conserved among virulent strains, so this residue is not expected to impact virulence. In contrast, K205 and A242 seemed to correlate somewhat with pathogenicity of the aligned strains (Figure D.2 A). Neither of these residues confers pathogenicity in isolation [94]; however, the combined effect of these two specific mutations is not known. Mutation of residue 242 in the avirulent RC-HL strain in

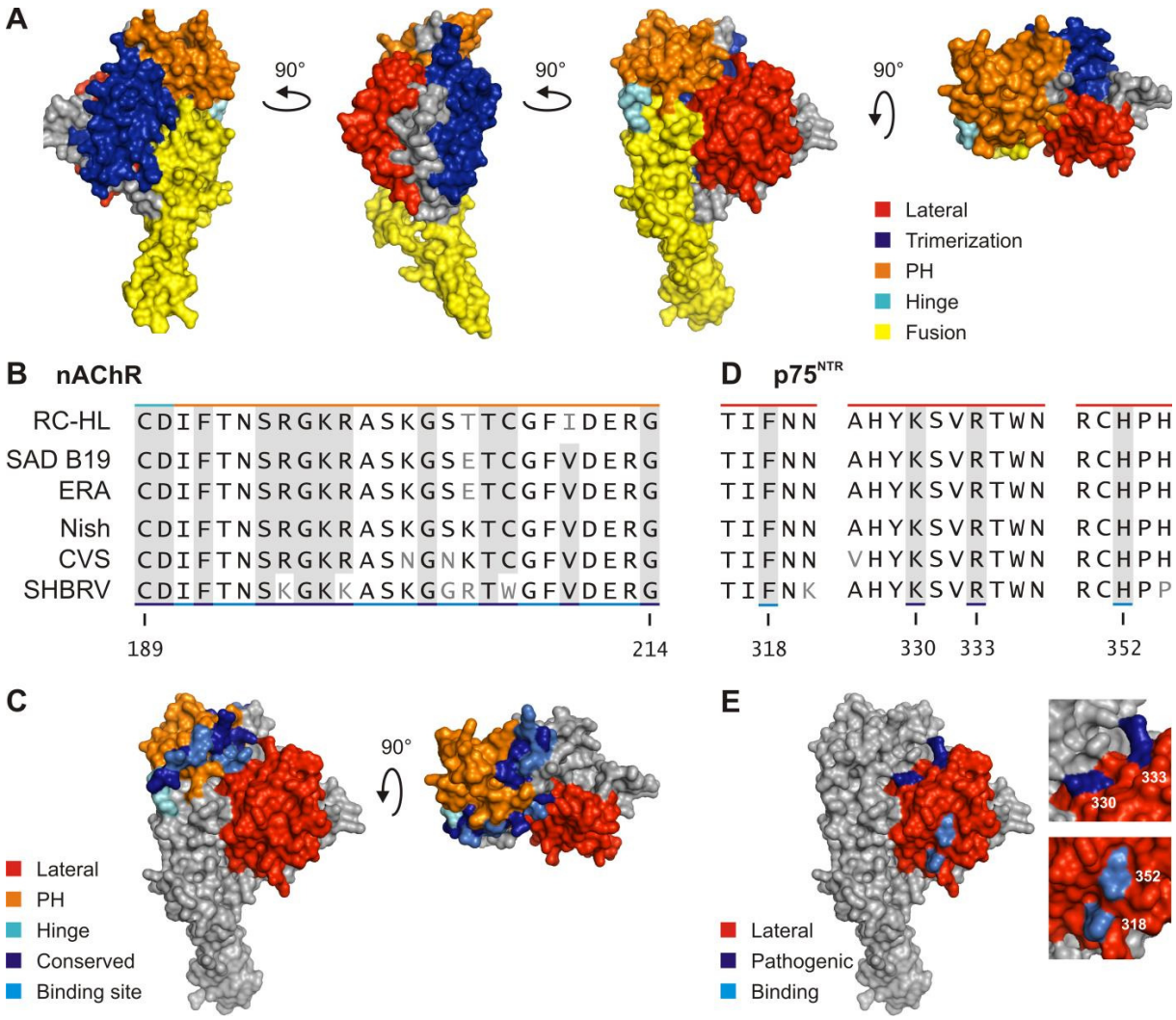

Figure D.1. Phyre2 modeling of the prefusion RABV G ectodomain and receptor binding sites.

A. The CVS G ectodomain sequence was threaded onto the VSV prefusion crystal structure (PDB: 2J6J) using Phyre2 software. Several orientations are provided for reference in which the lateral, trimerization, pleckstrin homology (PH), hinge and fusion domains are color coded as indicated. **B.** Sequence alignment demonstrating conservation of the nAChR binding domain in six fixed RABV strains. Strains are listed in approximate order of pathogenicity from top to bottom with the most pathogenic strains at the bottom. RC-HL is an apathogenic derivative of Nishigahara (Nish). ERA and SAD B19 are derivatives of the SAD parental strain. SHBRV (silver haired bat rabies virus) is a pathogenic fixed strain derived from a bat RABV isolate. Conserved residues are in black and nonconserved residues are shown in grey. Color coding above the sequence indicates the domain of G that each residue maps to (cyan: hinge; orange: PH). Color coding below the sequence highlights conserved residues. Color coding is as in C. **C.** Mapping of the nAChR domain onto the predicted structure of CVS G. The PH, lateral and hinge domains are shown in orange, red and cyan,

Figure D.1 (continued) respectively. Light blue indicates the entire region of homology between RABV G and the toxic loop of curaremimetic toxin, whereas dark blue regions indicate conserved residues. **D.** Sequence alignment showing conservation of residues necessary for p75NTR binding. RABV strains are as in B. Conserved residues are in black and nonconserved residues are shown in grey. Color coding above the sequence indicates the domain of G that each residue maps to (red: lateral). Color coding below the sequence: light blue indicates residues that affect p75NTR binding in vitro, but have not been tested in vivo; dark blue indicates residues that are both required for p75NTR binding and are strongly correlated with pathogenicity and neuroinvasion in vivo. Color coding is as in E. **E.** Mapping of the p75NTR domain onto the predicted structure of CVS G. All residues involved involved in p75NTR binding map to the lateral domain (red). Insets show enlarged annotated regions of the structure.

combination with 255 and 268 to match the Nishigahara strain results in a complete recovery of neurological symptoms and death in adult mice [94]. Therefore, combinatorial effects may play a significant role in defining the contribution to virulence of these residues. Interestingly, although SAD B19 retains the Nishigahara residue at 255, it displays a Q256K mutation at residue 256. The role of this residue has not been studied, but, given its vicinity to D255, it stands to reason that it may represent an attenuating mutation. Intriguingly, the pathogenic ERA strain, whose G sequence differs from SAD B19 at only three residues, displays a glutamine at position 256 and the virulent Nishigahara alanine at position 242. Fitting the sequence of RABV G onto the functionally homologous VSV G, for which the atomic structures of the pre- and post-fusion conformations are known [54, 55], shows that residues 205, 242 and 255 are located within the pleckstrin homology domain (Figure D.2 A,B). This domain does not contribute to the significant conformational states of G: it is not involved in trimerization and undergoes minimal reorganization during pH-driven structural rearrangements in G [54]. However, it may play a role in receptor binding: the nAChR binding site maps to this domain. Residues 205 and 242 are contained within or flank the nAChR binding site in the prefusion state, respectively (Figure D.2 C). Attenuating

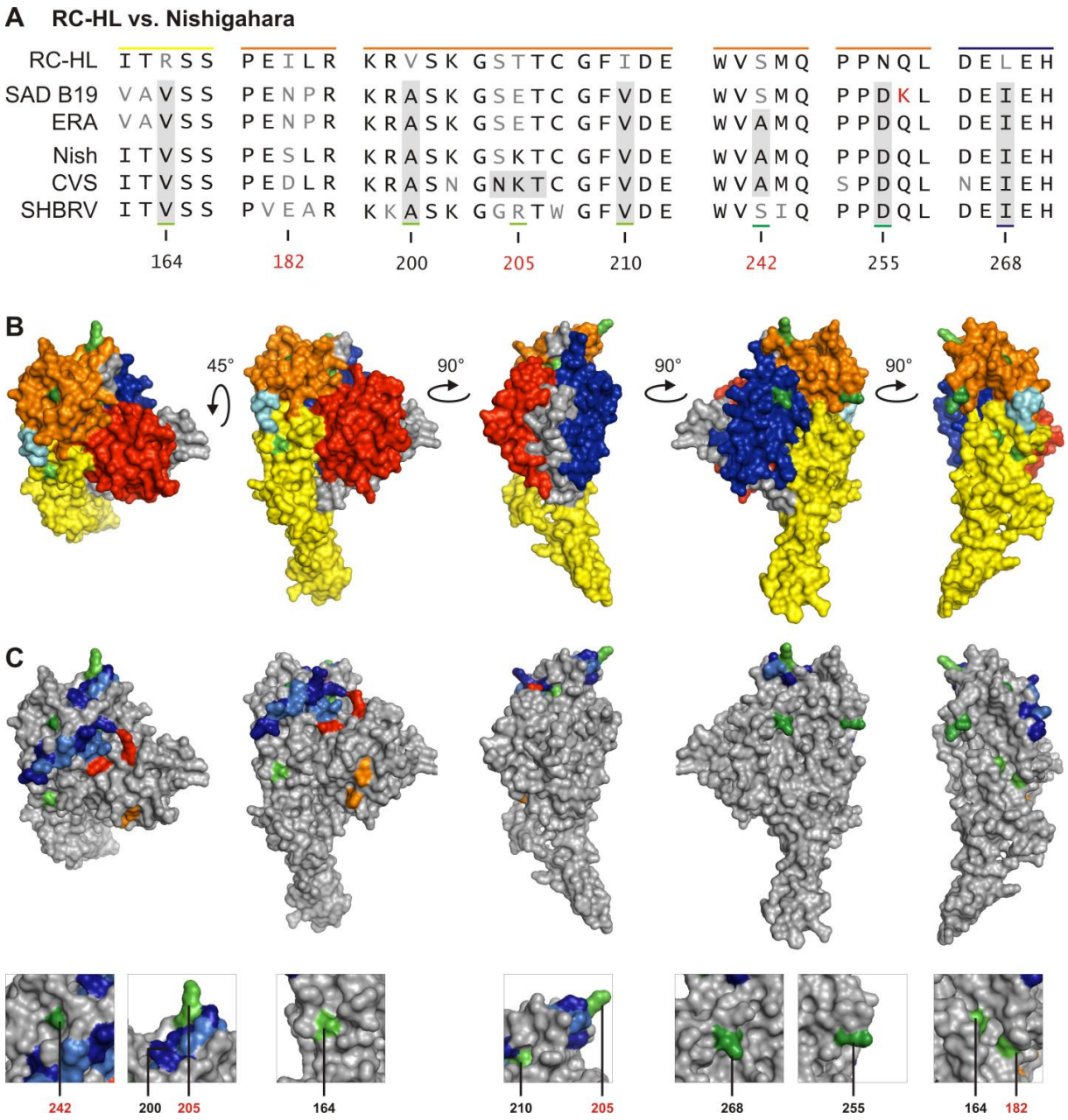

Figure D.2. Map of residues correlated with pathogenicity on the prefusion model of the rabies ectodomain.

A. Residues in G correlated with pathogenicity of the Nishigahara strain RABV were identified by comparison with the apathogenic derivative strain RC-HL. Here, we ask whether these residues are conserved across fixed RABV strains of varying pathogenicity by aligning their G sequences. Strains are as in Figure D.1. Color coding above the sequences shows localization of residues within the domains of G: all residues are located within the pleckstrin homology domain, except for 162-166 located in the fusion domain. Grey shading highlights conservation at the residues of interest.

Figure D.2 (continued) Non-conserved residues are grey font. Non conserved SAD B19 G residue, K256, is highlighted in red. **B.** Individual residues are mapped onto the Phyre2 model of the prefusion structure of RABV G. The structure of G is shown in different orientations to aid viewing of residues of interest, shown in green. Color coding indicates the domains of G: the lateral, trimerization, pleckstrin homology (PH), hinge and fusion domains are in red, blue, orange, cyan and yellow respectively. **C.** Location of residues relative to known binding sites for the nAChR (blue/light blue) and $p75^{NTR}$ (red/orange) receptors. Residues of interest are highlighted in green. nAChR binding site is shown in blue: light blue indicates the binding region, whereas dark blue indicates conserved residues within the region. $p75^{NTR}$ binding site is shown in red and orange: orange indicates residues that affect $p75^{NTR}$ binding in vitro, but have not been tested in vivo; dark blue indicates residues that are both required for $p75^{NTR}$ binding and are strongly correlated with pathogenicity and neuroinvasion in vivo. Insets show enlarged areas of the structure. Insets show enlarged areas of the structure.

residues at these positions could, therefore, theoretically impact receptor binding when combined. This could explain the difference in neurovirulence between the ERA and SAD B19 glycoproteins. However, it must be noted that SAD B19 and CVS G ectodomains differ from that of Nishigahara G by 29 (94% identity) and 42 (90% identity) amino acids, respectively. As a result, studies comparing the Nishigahara and RC-HL Gs to identify residues correlated with pathogenicity may have limited predictive power for identifying pathogenic residues in SAD B19 or CVS G. It remains of interest that, when comparing six strains of RABV, the highest variability was detected in the PH and cytoplasmic tail domains. This may point to these two domains being the greatest contributors to rabies virulence. This is consistent with the view that specific receptor engagement and polarized egress/assembly processes are crucial to retrograde transsynaptic transmission.

In addition to incorporating potentially attenuating mutations, SAD B19 G differs from CVS G in its glycosylation pattern. When resolved by SDS-PAGE analysis, SAD B19 G migrates as a single band, whereas CVS G migrates as a doublet consistent with the reported existence of two glycosylation variants of G [207] (Figures 2.1 C and D.3). Based on their G amino acid sequences, both SAD B19 and CVS G retain the tightly regulated glycosylation Asn-X-Ser site at N37 [97, 208] and Asn-X-Thr site at N319

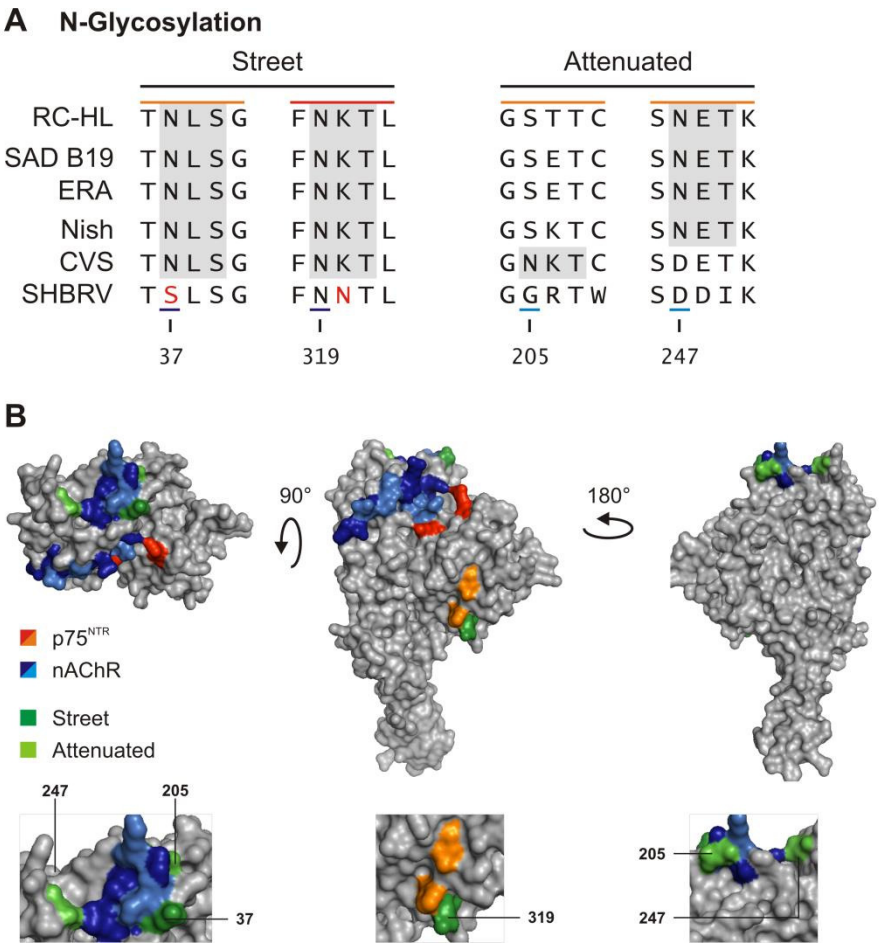

Figure D.3. Location of putative glycosylation sites on the prefusion model of the RABV G ectodomain.

A. Sequence alignment demonstrating conservation of glycosylation sites in six fixed RABV strains. Strains are as in Figures D.1 and D.2. Glycosylation sites at N37 and N319 are commonly found in street isolates, whereas glycosylations at N205 and N247 are associated with attenuation. Color coding shows localization of the sites within the domains of G: N37, N205 and N247 are situated in the pleckstrin homology domain, whereas N319 is in the lateral domain. **B.** Comparison of the glycosylation sites and known receptor sites on G. Glycosylation sites associated with street strains are shown in dark green, whereas glycosylations associated with attenuated phenotypes are shown in light green. nAChR binding site is shown in blue: light blue indicates the binding region, whereas dark blue indicates conserved residues within the region. p75NTR binding site is shown in red and orange: orange indicates residues that affect p75NTR binding in vitro, but have not been tested in vivo; dark blue indicates residues that are both required for p75NTR binding and are strongly correlated with pathogenicity and neuroinvasion in vivo. Insets show enlarged areas of the structure.

associated with street strains [98]. However, they differ in conservation of glycosylation sites typical of fixed strains and correlated with increased G surface expression [209], viral production [98] and attenuation [97, 98, 210]: SAD B19 G retains an Asn-X-Thr site at N247 [98, 209], whereas CVS G is glycosylated at N205 [98, 207]. The glycosylation sites at N37, N247 and N205 all flank the nAChR domain, whereas N319 is in the vicinity of two residues required for $p75^{NTR}$ binding (Figure D.3 B). These observations suggest that differential glycosylation at these sites could disrupt or destabilize interaction putative receptors. Existing evidence suggests that glycosylation primarily impacts post-entry steps of the RABV G life cycle; however the role of glycosylation in neuroinvasion and pathogenicity has not been extensively studied. Interestingly, G from the highly pathogenic bat RABV strain, SHBRV, displays a distinct pattern of glycosylation sites (Figure D.3 A). This suggests that the role of glycosylation in pathogenicity may depend on many factors including RABV strain, host reservoir and tropism. As a result, it is hard to predict the biological consequences of altered glycosylation in SAD B19 G.

As the above analysis attests, many features of G have been shown to impact pathogenicity of RABV strains. However, mechanistic understanding of the role of individual mutations or G modifications in viral entry or egress is lacking. Future experiments addressing this question will benefit from the use of in vitro systems in which receptor association, endocytosis, G synthesis, and egress can be evaluated in isolation. It will also be advantageous to match fixed strains with their attenuated derivatives to obtain the greatest utility in deciphering the role of specific mutations or features of G. Although rVSV RABV G viruses may also be of use to isolate the role of G during entry, post-entry processes will have to be tested or at the least validated with full-length RABV viruses since interaction between the G cytoplasmic domain, RABV M and the RNP cannot be recapitulated within an rVSV system.

Acidification in long-range axoplasmic transport and implications for RABV fitness

Our results in compartmentalized primary neuronal culture demonstrate that a portion of incoming virions fuse prior to arrival at the cell soma. In infections with rVSV CVS G, prevention of acidification at the neurites by administration of the H+ pump inhibitor, BAF A1, increases infectivity and spread. This is consistent with early reports of RABV colocalization with acidified compartments within the synaptic contacts and axons of motor and hippocampal neurons [109, 160]. We conclude, therefore, that release of the rVSV core within the axon interferes with efficient establishment of infection (Figure D.4). We have not tested whether early acidification abrogates infection from RABV cores. However, if virions in vivo are also subject to local or in-transit acidification events, it follows that counteracting strategies would be beneficial to a neurotropic pathogen exploiting this pathway. We speculate that two controversial aspects of RABV biology, namely, primary amplification of RABV in muscle cells [89, 211, 212] and the molecular interaction between RABV phosphoprotein (P) and dynein light chain, LC8 [128, 129], may provide just such a fitness benefit.

In vivo, local replication of RABV in muscle cells is a well-documented, but non-critical step that precedes neuronal infection [89, 211, 212]. The relevance of this step for pathogenesis and CNS invasion remains unclear. If axonal acidification depletes the number of RABV virions that reach the site of replication in the cell body, secondary infection with virions originating from a round of amplification in local muscle tissue may increase the chances of successful neuroinvasion, particularly following inoculation with a low viral dose. Exhaustive investigation of the interactions underlying association of RABV with muscle tissue has provided us with tools to explore the role of muscular amplification in peripheral neuronal infection. Muscular infection is mediated by binding of RABV G with nAChR on the postsynaptic membrane of the neuromuscular junction [42, 109].

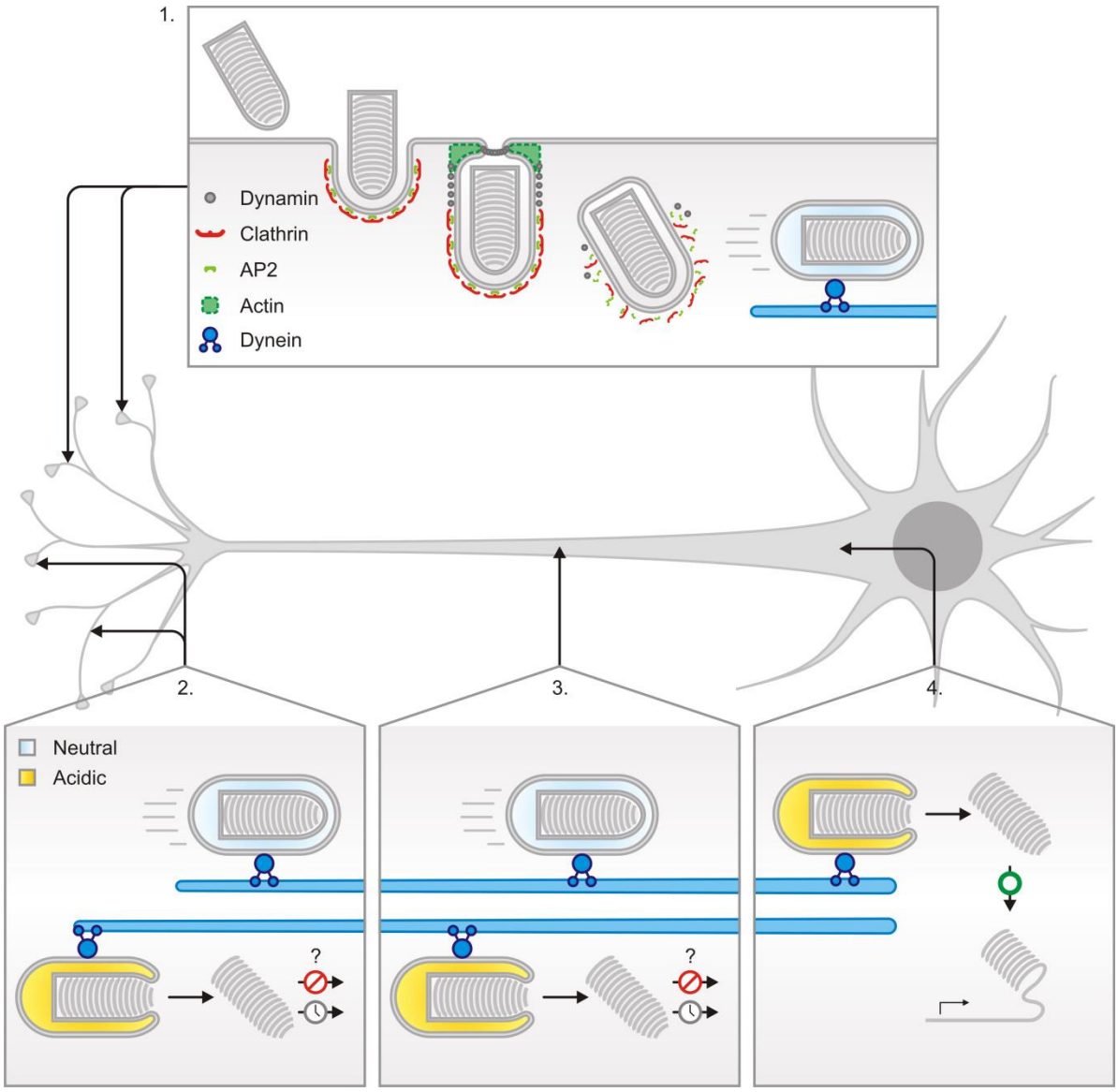

Figure D.4. Model of the predominant RABV G-dependent entry mechanism into neurons of the peripheral nervous system.

Rabies G association with neuronal receptors at the synapse or neurite membrane results in clathrin-mediated endocytosis and transport via microtubules to the somatodendritic compartment. 1. Rhabdoviruses are internalized within endosomes only partially coated with clathrin, which require actin to complete envelopment and scission from the plasma membrane. Following internalization, early endosomes containing virus engage the motors and travel retrogradely through the axon. 2. and 3. Viruses are transported intact within endosomes from the neuronal synapse. However, some endosomes acidify within the neurites either 2. directly at the site of entry or 3. during retrograde axonal transport leading to viral fusion. Ribonucleoprotein release in the neurite either fails to

Figure D.4 (continued) to establish or significantly delays the kinetics of infection. 4. Endosomes acidify upon arrival at the soma releasing RNPs and leading to productive infection.

The binding site of nAChR on G has been mapped to a 13-amino acid region (residues 190-203) which shares homology with the toxic binding loop of curare-mimetic toxins. Binding of RABV G with nAChR can therefore be disrupted by competition with snake venom toxins, most commonly alpha-bungarotoxin, synthetic peptides, or antibodies corresponding to the nAChR binding site on G [64, 70]. Molecular competition or mutation of G could be used to abolish muscular infection in vivo and test the role of an initial viral amplification step in neuroinvasion. A caveat of this approach is that absence of viral concentration at the NMJ or otherwise loss of nAChR binding may independently interfere with direct motor neuron infection. CVS [89], Av01 [89] and CVS-24 [212] strains bypass primary infection of muscles while retaining the nAChR binding site. Thus, an alternative approach could involve comparison of motor neuron infection following low or high dosage intramuscular challenge of these strains with a strain that does initially infect motor neurons. In vivo observations could then be validated in compartmentalized nerve-muscle cocultures in vitro. Within the in vitro model system, MOIs could be carefully controlled, and the viral output kinetics of muscle infection could be independently assessed and used to approximately synchronize infections between muscle-dependent and muscle-independent infections. Furthermore, compartmentalized cocultures of neurons and neuroblastoma cells could serve as a control. If amplification in muscle cells serves as a second source of neuroinvasive viruses, we would expect to see lower infection efficiencies of low dosage inoculation with muscle-restricted RABV strains relative to their wildtype counterparts, but equivalent infection following high dosage inoculation in nerve-muscle cocultures, or across the board in nerve-neuroblastoma cocultures.

The interaction between RABV P and LC8 could similarly provide the virus with a competitive edge to counteract anticipated endosomal acidification in the axon. When the interaction between P

and dynein LC8 was first described, it was hypothesized that P may interface between incoming nucleocapsids and microtubule motors during axoplasmic transport [128, 129]. Subsequent studies challenged this view by demonstrating that a deletion of the LC8 binding region of P neither abrogates CNS invasion in mouse in vivo models of RABV infection [130, 131] nor prevents retrograde transport in compartmentalized cultures of DRG neurons [136]. Identification of a role for the P-LC8 interaction in viral transcription supplanted the originally hypothesized role in transport [131]. We speculate that in addition to its involvement in viral transcription, the P-LC8 interaction may underlie a secondary, redundant transport mechanism for incoming RABV virions subjected to premature fusion. This role could have been overlooked in past studies due to high neuroinvasive dose (either from the initial inoculation or following intramuscular amplification) in vivo, and the use of non-compartmentalized neuronal cultures and high MOIs in vitro [130, 131, 136]. Furthermore, axoplasmic transport was not directly investigated in these studies, which assayed other downstream markers for infection (namely viral genomes, transcripts or proteins). If the interaction between P and LC8 enables a significant recovery of released RNPs from the axon to the somatodendritic complex, we would expect to see less of an inhibitory effect following disruption of endosomal acidification at the somal compartment. This would differ from our rVSV RABV G results. In contrast, a LC8 binding mutant of RABV virus should recapitulate rVSV behavior.

Potential receptor usage in peripheral neurons

Association with the ectodomain of membrane receptors is a defining step in targeting particular endocytic pathways. In the context of RABV neuroinvasion, the question of which receptor provides access to long-range axoplasmic trafficking networks is of particular interest due to the unique cellular distances separating the sites of entry and replication. According to one calculation, viral transport to the somatodendritic compartment by passive diffusion would require hundreds of years per centimeter of cytoplasm [122]. Thus the pivotal event in neuroinvasion is the first specific molecular

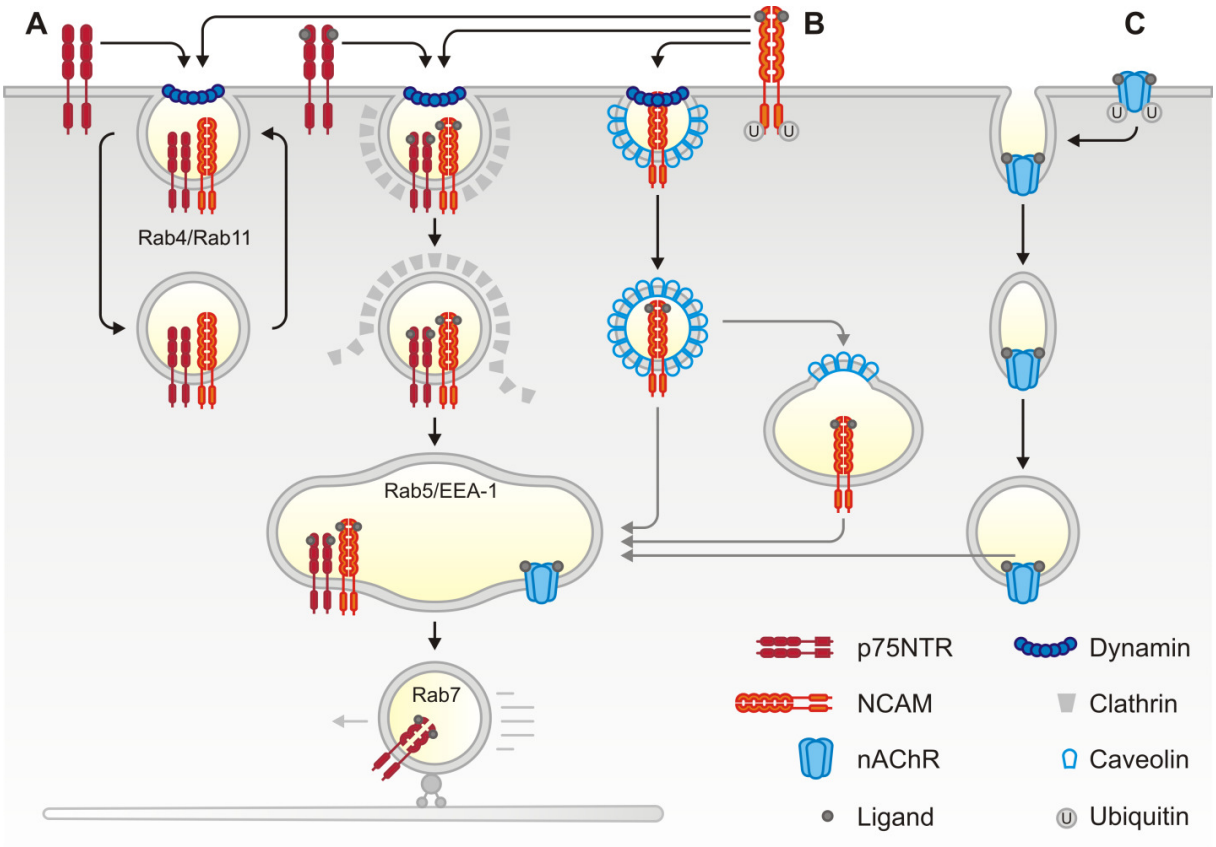

Figure D.5. Entry mechanisms of RABV putative receptors bound to toxins, antibodies or endogenous ligands.

A. Prior to ligand binding, $p75^{NTR}$ (red) is recycled at the plasma membrane by a clathrin- and lysosome-independent mechanism reliant on the GTPases Rab4 and Rab11. Upon administration of its endogenous ligand, nerve growth factor (NGF), $p75^{NTR}$ engages clathrin-dependent endocytic machinery and is shunted into the retrograde axonal transport pathway. This shunting from the recycling endosome to fast axonal transport is reliant on Rab5 and Rab7 GTPases. **B.** NCAM (orange) internalization processes generally resemble those of $p75^{NTR}$; however, evidence drawn from immunofluorescence studies and application of specific inhibitors of clathrin-mediated and caveolar transport indicates that a significant portion of induced NCAM also exploits caveolae for internalization. **C.** Clathrin-independent machinery is also exploited by nAChR (blue), which, unlike $p75^{NTR}$ and NCAM, is internalized via dynamin-independent tubular invaginations following binding of the antagonist α-bungarotoxin (α-BTX). Lack of dynamin involvement excludes clathrin- or caveolin-mediated processes.

interaction between virus and the host cell: receptor-binding. The work presented in this dissertation does not characterize receptor usage during uptake. However, receptor engagement can be inferred

from two lines of evidence: i) reported mechanisms of receptor internalization following binding to endogenous ligands, antibodies or other pathogenic molecules, and ii) studies of axoplasmic transport in DRG and motor neurons that do monitor co-transport of virus with receptor.

We report that clathrin-coated pits mediate internalization of 91% and 55% of rVSV CVS G virions in DRG and V SC neurons respectively. Putative RABV receptors $p75^{NTR}$ and NCAM both can internalize via clathrin-mediated endocytosis following association with or crosslinking of their ectodomains (Figure D.5 A, B). Specifically, binding of nerve growth factor diverts $p75^{NTR}$ dimers from clathrin-independent recycling endosomes into clathrin-coated pits [28]. Clathrin-dependent uptake then shunts ligand-bound $p75^{NTR}$ into Rab7 positive compartments destined for long-range transport to the cell body [28]. Similarly, tetanus toxin, which is internalized within clathrin-coated pits [213], also traffics within $p75^{NTR}$ positive endosomes [214] although no direct binding between TeT and $p75^{NTR}$ has been shown. Uptake of NCAM into primary neuronal cultures is also clathrin-mediated: cross-linking with antibody leads to co-uptake of NCAM with transferrin [110, 111]. Collectively, these observations suggest that RABV binding to either of these receptors could result in clathrin-mediated internalization as a means to gain access to the cell interior and vesicular transport in neuronal cells.

Uptake and axoplasmic co-transport of RABV G virions with $p75^{NTR}$ has been described in compartmentalized cultures of explanted DRG [8] and dissociated motor neurons [36]: virions associated with neurotrophins display rapid, highly processive retrograde transport. In DRG axons, 61% of RABV virions in the retrograde endosomal transport pathway colocalize with $p75^{NTR}$ [8]. In contrast, only 20-30% of particles in motor neurons are co-transported with the receptor [36]. These observations suggest that subversion of the $p75^{NTR}$ internalization pathway may account for as much as 50-66% of clathrin-mediated uptake in DRG and V SC neurons. The remaining percentage of virions found not to colocalize with the neurotrophin receptor may therefore engage an alternate RABV receptor, such as NCAM,

whose uptake is nonetheless mediated by clathrin-coated pits. Supporting this view, in motor neurons 15-30% of RABV G-pseudotyped lentiviruses colocalized with NCAM [36]; this could account for the remaining 50% of particles found to colocalize with Tfn. It must be noted, however, that the possibility of simultaneous co-transport with more than one receptor was not explored in the lentivirus study [36]. Since simultaneous co-transport of RABV virions with $p75^{NTR}$ and another neurotrophin receptor, TrkA, was observed in DRG culture [8], it is a distinct possibility that the percentages of virions engaging specific receptors in the motoneurons may represent overlapping populations.

In both DRG and V SC neurons, a fraction of rVSV CVS G virions is transported independently of Tfn or Dextran. Furthermore, we observed AP2-independent as well as AP2-dependent uptake in BS-C-1 cells. It is unlikely that the binary engagement of RABV G with an individual receptor could result in two distinct uptake mechanisms; it is, therefore, more probable that uptake into these cells is being mediated by multiple receptors. In addition to uptake via clathrin-mediated endocytosis, a secondary mechanism of internalization of NCAM within caveolae has also been reported [110]. RABV binding to NCAM could result therefore in caveolin-dependent uptake. Another possible candidate is nAChR, which colocalizes with 10-20% of in-transit, pseudotyped RABV-G lentiviruses in motor neurons [36]. In support of this view, nAChR internalizes via formation of filamentous invaginations from the plasma membrane in a clathrin-independent manner when bound to the antagonist, alpha bungarotoxin (α-BTX; Figure D.5 C) [112, 113]. Furthermore, nAChR-α-BTX endocytosis is separate from Tfn and Dex uptake despite engagement of Rab5 and Rab7 positive endosomes [113]. However, internalization of nAChR-α-BTX is also dynamin-independent [112]. This conflicts with our inhibitor data that demonstrates total abrogation of infection following treatment with dynasore.

The nAChR-binding site of RABV G has been shown to share antigenic [72], structural [69, 70] and functional [215] homology with α-BTX and other curaremimetic toxins. The approximate reciprocal binding

domain for RABV on the α1 subunit of nAChR has also been mapped[74], and overlaps with the known binding site for α-BTX [216] (Figure D.1 B,C). Although the larger molecular footprint and high surface density of G in comparison to α-BTX could result in different uptake behavior by crosslinking nAChR, it is more likely that α-BTX uptake faithfully models nAChR-dependent internalization of RABV. In contrast, RABV G binds outside of the neurotrophin binding regions of $p75^{NTR}$ (Figure D.1 E) and shares no homology with known ligands of NCAM. Internalization of RABV in complex with these receptors could, therefore, conceivably differ from reported mechanisms of uptake in conjunction with endogenous ligands.

Little is known about the molecular or functional consequences of interaction of RABV G with its individual protein receptors. Extrapolation from studies with endogenous ligands, although interesting, is speculative at best. It is, therefore, of significant interest to determine which receptors are internalized at the plasma membrane in complex with RABV and to relate these interactions to establishment of infection. Because RABV G engagement with its receptors diverges from known ligands, dissecting the outside-in signaling resulting in endocytosis will also be of interest and may reveal new aspects of receptor biology. Because clathrin-mediated uptake of RABV is conserved, studies in more tractable epithelial cells can be combined with neuronal studies broadening the range of feasible experiments. However, tracking the signaling consequences of specific receptor engagement will be of particular interest in compartmentalized neuronal culture where the polarized morphology provides greater spatial and temporal resolution to tease out the signaling pathways.

Broad applicability of neuronal microfluidic platforms to the study of rabies biology

Photolithographic and PDMS replica moulding techniques enable in-house manufacture of fully customized culturing platforms. They represent a significant improvement over traditional

compartmentalization techniques, specifically teflon Campenot chambers, by providing greater reliability, reproducibility, and customizability to the scientific question being addressed [147]. Compartmentalized microfluidic culture platforms are gaining popularity in the study of uptake of pathogenic molecules and egress of viruses from neurons [8, 19, 36, 136, 189]. These studies, including the work described within this dissertation, implement a simple compartmentalized device for separation of neurites and cell bodies. Simple adaptations of the current device design will allow investigation of a range of questions in RABV and viral tracer biology, some of which I will outline here.

From initial neuroinvasion at the neuromuscular junction to retrograde synapse-to-synapse transmission to the brain most entry events critical for RABV infection and pathogenesis *in vivo* occur transsynaptically. Future work, therefore, calls for an expansion from mono- to co-cultures to model these binary contacts. Cocultures of peripheral neurons with muscle cells enable closer recapitulation of the primary site of neuroinvasion in vitro through the spontaneous formation of neuromuscular junctions [217]. In addition, the existing contact between motor neurons of the ventral spinal cord and commissural neurons of the dorsal spinal cord could be artificially recreated by coculture within compartmentalized devices for the study of early RABV transsynaptic transmission events. Whereas the current device design is adequate for cocultures of neuronal cells with non-neuronal substrates, binary neuronal cultures will require a re-engineering of the original basic geometry. Firstly, each neuronal population will require an individual somal chamber into which cell bodies will be cultured. More importantly, however, neuronal outgrowth will need to be directed to avoid formation of non-physiological contacts e.g. axon-axon contacts between motor and commissural spinal neurons. Outgrowth within devices can be controlled. One approach is staggered culturing of each neuronal population and introduction of a physical barrier, such as a methyl cellulose or agarose layer, once the desired axonal population has grown through the microchannels. Alternatively, laminar flow channels

could be introduced to physically or biochemically direct growth along microchannels. With small adjustments, therefore, microfluidic co-culture systems can be adapted to the study of transsynaptic entry of RABV.

Compartmentalized PDMS devices will also be an important tool for the study of directed viral egress from neurons. Viruses have been used with broad success as tracers of neuronal circuitry [43, 185, 186]. Importantly, it has been shown that viral glycoproteins can individually dictate the directionality of spread: for example, rVSV tracers expressing VSV G are transmitted anterogradely, whereas replacement of VSV G with RABV G induces retrograde transmission [184, 185]. Nonetheless, the mechanisms underlying trafficking of progeny viral nucleocapsids and structural proteins to post- or presynaptic membranes for assembly and directional transsynaptic transmission are poorly understood. For example, the exclusivity of RABV retrograde transmission has been brought into question by recent studies demonstrating anterograde transport of progeny RABV in DRG neurons [136]. These results suggest that cell biology of specific neuronal subtypes, in addition to virological determinants, may dictate the directionality of egress. Therefore, the arsenal of viral glycoproteins that can be tested for membrane targeting via the rVSV system may provide a broad toolbox for the discovery of new aspects of neuronal biology and intraneuronal protein trafficking, as well as provide a system for the study of trafficking and membrane targeting of viral glycoproteins. Co-cultures of neuronal and non-neuronal cells within an adapted compartmentalized device can be used for the study of directional viral egress from neurons. Here, neurons would be co-cultured with any broadly susceptible cell type in the N compartment. Infection would be carried out in an intermediate axonal compartment to prevent inoculation of the non-neuronal cells and allow detection of retrograde transport in the somal compartment. Anterograde transmission would result in infection of the epithelial cell monolayer, whereas retrograde transmission

would be identified by spread within the somal compartment. Within this compartmentalized culture, glycoprotein targeting and progeny virion transport could be studied in both live and fixed assays.

Although microfluidic devices are still in their infancy for biological applications, they are a growing field of technical development drawing from the physical and chemical fields which spearheaded the underlying photolithographic techniques. The incorporation of valves, flow regulators and other hydrodynamic assemblies will allow dynamic physiological conditions to be established and tuned in vitro to a degree of temporal and spatial control previously inaccessible. These tools in combination with the growing variety of in vitro neuronal cultures from both primary and stem cell sources will provide an opportunity to recreate connectivity and tissue architecture with unsurpassed fidelity to physiological conditions. Application of these systems to neurovirology, and specifically the biology of rabies, will enable us to study viral pathological mechanisms with unprecedented molecular resolution at both the population and single particle level.

ACKNOWLEDGMENTS

I cannot do justice here to all the people who have helped me along during my PhD, but I am immensely grateful for the family, friends and colleagues who have supported and encouraged me along the way.

In particular, I must thank my advisor Sean Whelan for tirelessly providing for our lab. His gargantuan efforts in addition to his openness to new ideas and techniques have provided me with a freedom to experiment, and indeed, fail and recover as well, that I firmly believe have made me a better experimenter and scientist.

I must also thank my dissertation advisory committee members Connie Cepko, Mike Farzan, David Knipe and Samara Reck-Peterson for their mentorship throughout the years. Their support grounded me during bleak scientific times.

I must also thank Whelan lab members past and present for their friendship and care, as well as their intellectual investment in my work. They have been a wonderful source of scientific expertise and a tremendously tempting source of procrastination at times. I have been privileged to work among such talented scientists.

Finally, I must thank my family. My parents and sister have participated with such ardor to my scientific ups and downs. But most importantly I have an immense debt of gratitude to my husband. He has been through all my worst times and worst rages against dysfunctional or non-cooperative equipment, through all my peaks of excitement and periods of drudgery or despair. His patience has been relentless, and to this day he has never said, “I told you so,” when things have gone predictably awry. I also cannot stress what a phenomenal scientist he is. From him I have learned everything I know about photolithography and more. Last and littlest, I must thank Alexander the Tiny who spurred me through the last two years from within and from without.

REFERENCES

1. He, X.L. & Garcia, K.C. Structure of nerve growth factor complexed with the shared neurotrophin receptor p75. *Science* 304, 870-5 (2004).

2. Diefenbach, R.J., Miranda-Saksena, M., Douglas, M.W. & Cunningham, A.L. Transport and egress of herpes simplex virus in neurons. *Rev Med Virol* 18, 35-51 (2008).

3. Racaniello, V.R. One hundred years of poliovirus pathogenesis. *Virology* 344, 9-16 (2006).

4. Chen, C.S. et al. Retrograde axonal transport: a major transmission route of enterovirus 71 in mice. *J Virol* 81, 8996-9003 (2007).

5. Brahic, M., Bureau, J.F. & Michiels, T. The genetics of the persistent infection and demyelinating disease caused by Theiler's virus. *Annu Rev Microbiol* 59, 279-98 (2005).

6. Martinat, C., Jarousse, N., Prevost, M.C. & Brahic, M. The GDVII strain of Theiler's virus spreads via axonal transport. *J Virol* 73, 6093-8 (1999).

7. Klingen, Y., Conzelmann, K.K. & Finke, S. Double-labeled rabies virus: live tracking of enveloped virus transport. *J Virol* 82, 237-45 (2008).

8. Gluska, S. et al. Rabies Virus Hijacks and accelerates the p75NTR retrograde axonal transport machinery. *PLoS Pathog* 10, e1004348 (2014).

9. Young, V.A. & Rall, G.F. Making it to the synapse: measles virus spread in and among neurons. *Curr Top Microbiol Immunol* 330, 3-30 (2009).

10. Samuel, M.A., Wang, H., Siddharthan, V., Morrey, J.D. & Diamond, M.S. Axonal transport mediates West Nile virus entry into the central nervous system and induces acute flaccid paralysis. *Proc Natl Acad Sci U S A* 104, 17140-5 (2007).

11. Nagata, N. et al. The pathogenesis of 3 neurotropic flaviviruses in a mouse model depends on the route of neuroinvasion after viremia. *J Neuropathol Exp Neurol* 74, 250-60 (2015).

12. Monath, T.P., Cropp, C.B. & Harrison, A.K. Mode of entry of a neurotropic arbovirus into the central nervous system. Reinvestigation of an old controversy. *Lab Invest* 48, 399-410 (1983).

13. de la Torre, J.C. Bornavirus and the brain. *J Infect Dis* 186 Suppl 2, S241-7 (2002).

14. Bajramovic, J.J. et al. Borna disease virus glycoprotein is required for viral dissemination in neurons. *J Virol* 77, 12222-31 (2003).

15. Jang, H. et al. Highly pathogenic H5N1 influenza virus can enter the central nervous system and induce neuroinflammation and neurodegeneration. *Proc Natl Acad Sci U S A* 106, 14063-8 (2009).

16. Salinas, S. et al. CAR-associated vesicular transport of an adenovirus in motor neuron axons. *PLoS Pathog* 5, e1000442 (2009).

17. Antonucci, F., Rossi, C., Gianfranceschi, L., Rossetto, O. & Caleo, M. Long-distance retrograde effects of botulinum neurotoxin A. *J Neurosci* 28, 3689-96 (2008).

18. Caleo, M. & Schiavo, G. Central effects of tetanus and botulinum neurotoxins. *Toxicon* 54, 593-9 (2009).

19. Restani, L. et al. Botulinum neurotoxins A and E undergo retrograde axonal transport in primary motor neurons. *PLoS Pathog* 8, e1003087 (2012).

20. International Committee on Taxonomy of Viruses. ictvonline.org 2015.

21. Lalli, G., Bohnert, S., Deinhardt, K., Verastegui, C. & Schiavo, G. The journey of tetanus and botulinum neurotoxins in neurons. *Trends Microbiol* 11, 431-7 (2003).

22. World Health Organization Expert Consultation on Rabies, TRS 982. World Health Organization. 2013.

23. World Health Organization. Rabies Fact Sheet No. 99. http://www.who.int/mediacentre/factsheets/fs099/en/ (2014).

24. Liepinsh, E., Ilag, L.L., Otting, G. & Ibanez, C.F. NMR structure of the death domain of the p75 neurotrophin receptor. *EMBO J* 16, 4999-5005 (1997).

25. Coulson, E.J. et al. Chopper, a new death domain of the p75 neurotrophin receptor that mediates rapid neuronal cell death. *J Biol Chem* 275, 30537-45 (2000).

26. Hemachudha, T. et al. Human rabies: neuropathogenesis, diagnosis, and management. *Lancet Neurol* 12, 498-513 (2013).

27. Feng, D. et al. Molecular and structural insight into proNGF engagement of p75NTR and sortilin. *J Mol Biol* 396, 967-84 (2010).

28. Deinhardt, K., Reversi, A., Berninghausen, O., Hopkins, C.R. & Schiavo, G. Neurotrophins Redirect p75NTR from a clathrin-independent to a clathrin-dependent endocytic pathway coupled to axonal transport. *Traffic* 8, 1736-49 (2007).

29. Gong, Y., Cao, P., Yu, H.J. & Jiang, T. Crystal structure of the neurotrophin-3 and p75NTR symmetrical complex. *Nature* 454, 789-93 (2008).

30. Winkler, W.G., Baker, E.F., Jr. & Hopkins, C.C. An outbreak of non-bite transmitted rabies in a laboratory animal colony. *Am J Epidemiol* 95, 267-77 (1972).

31. Johnson, N., Phillpotts, R. & Fooks, A.R. Airborne transmission of lyssaviruses. *J Med Microbiol* 55, 785-90 (2006).

32. Winkler, W.G., Fashinell, T.R., Leffingwell, L., Howard, P. & Conomy, P. Airborne rabies transmission in a laboratory worker. *JAMA* 226, 1219-21 (1973).

33. Conomy, J.P., Leibovitz, A., McCombs, W. & Stinson, J. Airborne rabies encephalitis: demonstration of rabies virus in the human central nervous system. *Neurology* 27, 67-9 (1977).

34. Tuffereau, C. et al. The rabies virus glycoprotein receptor p75NTR is not essential for rabies virus infection. *J Virol* 81, 13622-30 (2007).

35. Abul-Hajj, Y.J. The effect of the aromatase inhibitor, 4-(phenylthio)-4-androstene-3,17-dione, on dimethylbenz(A)anthracene-induced rat mammary tumors. *J Steroid Biochem* 34, 439-42 (1989).

36. Hislop, J.N. et al. Rabies virus envelope glycoprotein targets lentiviral vectors to the axonal retrograde pathway in motor neurons. *J Biol Chem* 289, 16148-63 (2014).

37. Cureton, D.K., Massol, R.H., Saffarian, S., Kirchhausen, T.L. & Whelan, S.P. Vesicular stomatitis virus enters cells through vesicles incompletely coated with clathrin that depend upon actin for internalization. *PLoS Pathog* 5, e1000394 (2009).

38. Jackson, A.C. & Park, H. Experimental rabies virus infection of p75 neurotrophin receptor-deficient mice. *Acta Neuropathol* 98, 641-4 (1999).

39. Tuffereau, C., Benejean, J., Blondel, D., Kieffer, B. & Flamand, A. Low-affinity nerve-growth factor receptor (P75NTR) can serve as a receptor for rabies virus. *EMBO J* 17, 7250-9 (1998).

40. Velandia-Romero, M.L., Castellanos, J.E. & Martinez-Gutierrez, M. In vivo differential susceptibility of sensory neurons to rabies virus infection. *J Neurovirol* (2013).

41. Ugolini, G. Use of rabies virus as a transneuronal tracer of neuronal connections: implications for the understanding of rabies pathogenesis. *Dev Biol (Basel)* 131, 493-506 (2008).

42. Watson, H.D., Tignor, G.H. & Smith, A.L. Entry of rabies virus into the peripheral nerves of mice. *J Gen Virol* 56, 372-82 (1981).

43. Ugolini, G. Rabies virus as a transneuronal tracer of neuronal connections. *Adv Virus Res* 79, 165-202 (2011).

44. Ray, N.B., Power, C., Lynch, W.P., Ewalt, L.C. & Lodmell, D.L. Rabies viruses infect primary cultures of murine, feline, and human microglia and astrocytes. *Arch Virol* 142, 1011-9 (1997).

45. Hemachudha, T., Laothamatas, J. & Rupprecht, C.E. Human rabies: a disease of complex neuropathogenetic mechanisms and diagnostic challenges. *Lancet Neurol* 1, 101-9 (2002).

46. Waggoner, J.J., Soda, E.A. & Deresinski, S. Rare and emerging viral infections in transplant recipients. *Clin Infect Dis* 57, 1182-8 (2013).

47. Dietzschold, B. & Koprowski, H. Rabies transmission from organ transplants in the USA. *Lancet* 364, 648-9 (2004).

48. Centers for Disease, C. & Prevention. Investigation of rabies infections in organ donor and transplant recipients--Alabama, Arkansas, Oklahoma, and Texas, 2004. *MMWR Morb Mortal Wkly Rep* 53, 586-9 (2004).

49. Thomas, D. et al. Mass and molecular composition of vesicular stomatitis virus: a scanning transmission electron microscopy analysis. *J Virol* 54, 598-607 (1985).

50. Ge, P. et al. Cryo-EM model of the bullet-shaped vesicular stomatitis virus. *Science* 327, 689-93 (2010).

51. Regan, A.D. & Whittaker, G.R. Entry of rhabdoviruses into animal cells. *Adv Exp Med Biol* 790, 167-77 (2013).

52. Albertini, A.A., Baquero, E., Ferlin, A. & Gaudin, Y. Molecular and cellular aspects of rhabdovirus entry. *Viruses* 4, 117-39 (2012).

53. Gaudin, Y. et al. Rabies virus-induced membrane fusion. *Mol Membr Biol* 16, 21-31 (1999).

54. Roche, S., Rey, F.A., Gaudin, Y. & Bressanelli, S. Structure of the prefusion form of the vesicular stomatitis virus glycoprotein G. *Science* 315, 843-8 (2007).

55. Roche, S., Bressanelli, S., Rey, F.A. & Gaudin, Y. Crystal structure of the low-pH form of the vesicular stomatitis virus glycoprotein G. *Science* 313, 187-91 (2006).

56. Walsh, D. & Mohr, I. Viral subversion of the host protein synthesis machinery. *Nat Rev Microbiol* 9, 860-75 (2011).

57. Baltimore, D., Huang, A.S. & Stampfer, M. Ribonucleic acid synthesis of vesicular stomatitis virus, II. An RNA polymerase in the virion. *Proc Natl Acad Sci U S A* 66, 572-6 (1970).

58. Morin, B., Kranzusch, P.J., Rahmeh, A.A. & Whelan, S.P. The polymerase of negative-stranded RNA viruses. *Curr Opin Virol* 3, 103-10 (2013).

59. Das, S.C., Nayak, D., Zhou, Y. & Pattnaik, A.K. Visualization of intracellular transport of vesicular stomatitis virus nucleocapsids in living cells. *J Virol* 80, 6368-77 (2006).

60. Heinrich, B.S., Cureton, D.K., Rahmeh, A.A. & Whelan, S.P. Protein expression redirects vesicular stomatitis virus RNA synthesis to cytoplasmic inclusions. *PLoS Pathog* 6, e1000958 (2010).

61. Jayakar, H.R., Jeetendra, E. & Whitt, M.A. Rhabdovirus assembly and budding. *Virus Res* 106, 117-32 (2004).

62. Langevin, C. & Tuffereau, C. Mutations conferring resistance to neutralization by a soluble form of the neurotrophin receptor (p75NTR) map outside of the known antigenic sites of the rabies virus glycoprotein. *J Virol* 76, 10756-65 (2002).

63. Thoulouze, M.I. et al. The neural cell adhesion molecule is a receptor for rabies virus. *J Virol* 72, 7181-90 (1998).

64. Lentz, T.L., Burrage, T.G., Smith, A.L., Crick, J. & Tignor, G.H. Is the acetylcholine receptor a rabies virus receptor? *Science* 215, 182-4 (1982).

65. Conti, C., Superti, F. & Tsiang, H. Membrane carbohydrate requirement for rabies virus binding to chicken embryo related cells. *Intervirology* 26, 164-8 (1986).

66. Superti, F. et al. Involvement of gangliosides in rabies virus infection. *J Gen Virol* 67 (Pt 1), 47-56 (1986).

67. Lafon, M. Rabies virus receptors. *J Neurovirol* 11, 82-7 (2005).

68. Schnell, M.J., McGettigan, J.P., Wirblich, C. & Papaneri, A. The cell biology of rabies virus: using stealth to reach the brain. *Nat Rev Microbiol* 8, 51-61 (2010).

69. Lentz, T.L., Wilson, P.T., Hawrot, E. & Speicher, D.W. Amino acid sequence similarity between rabies virus glycoprotein and snake venom curaremimetic neurotoxins. *Science* 226, 847-8 (1984).

70. Lentz, T.L., Hawrot, E. & Wilson, P.T. Synthetic peptides corresponding to sequences of snake venom neurotoxins and rabies virus glycoprotein bind to the nicotinic acetylcholine receptor. *Proteins* 2, 298-307 (1987).

71. Lentz, T.L., Benson, R.J., Klimowicz, D., Wilson, P.T. & Hawrot, E. Binding of rabies virus to purified Torpedo acetylcholine receptor. *Brain Res* 387, 211-9 (1986).

72. Bracci, L. et al. Antipeptide monoclonal antibodies inhibit the binding of rabies virus glycoprotein and alpha-bungarotoxin to the nicotinic acetylcholine receptor. *Mol Immunol* 25, 881-8 (1988).

73. Rustici, M. et al. A monoclonal antibody to a synthetic fragment of rabies virus glycoprotein binds ligands of the nicotinic cholinergic receptor. *J Mol Recognit* 2, 51-5 (1989).

74. Lentz, T.L. Rabies virus binding to an acetylcholine receptor alpha-subunit peptide. *J Mol Recognit* 3, 82-8 (1990).

75. Gastka, M., Horvath, J. & Lentz, T.L. Rabies virus binding to the nicotinic acetylcholine receptor alpha subunit demonstrated by virus overlay protein binding assay. *J Gen Virol* 77 (Pt 10), 2437-40 (1996).

76. Langevin, C., Jaaro, H., Bressanelli, S., Fainzilber, M. & Tuffereau, C. Rabies virus glycoprotein (RVG) is a trimeric ligand for the N-terminal cysteine-rich domain of the mammalian p75 neurotrophin receptor. *J Biol Chem* 277, 37655-62 (2002).

77. Sissoeff, L., Mousli, M., England, P. & Tuffereau, C. Stable trimerization of recombinant rabies virus glycoprotein ectodomain is required for interaction with the p75NTR receptor. *J Gen Virol* 86, 2543-52 (2005).

78. Coulon, P., Ternaux, J.P., Flamand, A. & Tuffereau, C. An avirulent mutant of rabies virus is unable to infect motoneurons in vivo and in vitro. *J Virol* 72, 273-8 (1998).

79. Garcia, N. et al. Localization of brain-derived neurotrophic factor, neurotrophin-4, tropomyosin-related kinase b receptor, and p75 NTR receptor by high-resolution immunohistochemistry on the adult mouse neuromuscular junction. *J Peripher Nerv Syst* 15, 40-9 (2010).

80. Copray, J.C. et al. Expression of the low affinity neurotrophin receptor p75 in spinal motoneurons in a transgenic mouse model for amyotrophic lateral sclerosis. *Neuroscience* 116, 685-94 (2003).

81. Hotta, K. et al. Role of GPI-anchored NCAM-120 in rabies virus infection. *Microbes Infect* 9, 167-74 (2007).

82. Gaudin, Y., Tuffereau, C., Durrer, P., Flamand, A. & Ruigrok, R.W. Biological function of the low-pH, fusion-inactive conformation of rabies virus glycoprotein (G): G is transported in a fusion-inactive state-like conformation. *J Virol* 69, 5528-34 (1995).

83. Doms, R.W., Keller, D.S., Helenius, A. & Balch, W.E. Role for adenosine triphosphate in regulating the assembly and transport of vesicular stomatitis virus G protein trimers. *J Cell Biol* 105, 1957-69 (1987).

84. Gaudin, Y. Reversibility in fusion protein conformational changes. The intriguing case of rhabdovirus-induced membrane fusion. *Subcell Biochem* 34, 379-408 (2000).

85. Gaudin, Y., Ruigrok, R.W., Tuffereau, C., Knossow, M. & Flamand, A. Rabies virus glycoprotein is a trimer. *Virology* 187, 627-32 (1992).

86. Gaudin, Y., Ruigrok, R.W., Knossow, M. & Flamand, A. Low-pH conformational changes of rabies virus glycoprotein and their role in membrane fusion. *J Virol* 67, 1365-72 (1993).

87. Albertini, A.A. et al. Characterization of monomeric intermediates during VSV glycoprotein structural transition. *PLoS Pathog* 8, e1002556 (2012).

88. Stanifer, M.L., Cureton, D.K. & Whelan, S.P. A recombinant vesicular stomatitis virus bearing a lethal mutation in the glycoprotein gene uncovers a second site suppressor that restores fusion. *J Virol* 85, 8105-15 (2011).

89. Coulon, P. et al. Invasion of the peripheral nervous systems of adult mice by the CVS strain of rabies virus and its avirulent derivative AvO1. *J Virol* 63, 3550-4 (1989).

90. Takayama-Ito, M., Ito, N., Yamada, K., Minamoto, N. & Sugiyama, M. Region at amino acids 164 to 303 of the rabies virus glycoprotein plays an important role in pathogenicity for adult mice. *J Neurovirol* 10, 131-5 (2004).

91. Yamada, K., Ito, N., Takayama-Ito, M., Sugiyama, M. & Minamoto, N. Multigenic relation to the attenuation of rabies virus. *Microbiol Immunol* 50, 25-32 (2006).

92. Marston, D.A. et al. Interspecies protein substitution to investigate the role of the lyssavirus glycoprotein. *J Gen Virol* 94, 284-92 (2013).

93. Morimoto, K., Foley, H.D., McGettigan, J.P., Schnell, M.J. & Dietzschold, B. Reinvestigation of the role of the rabies virus glycoprotein in viral pathogenesis using a reverse genetics approach. *J Neurovirol* 6, 373-81 (2000).

94. Takayama-Ito, M., Ito, N., Yamada, K., Sugiyama, M. & Minamoto, N. Multiple amino acids in the glycoprotein of rabies virus are responsible for pathogenicity in adult mice. *Virus Res* 115, 169-75 (2006).

95. Dietzschold, B. et al. Characterization of an antigenic determinant of the glycoprotein that correlates with pathogenicity of rabies virus. *Proc Natl Acad Sci U S A* 80, 70-4 (1983).

96. Ito, Y. et al. Amino acid substitutions at positions 242, 255 and 268 in rabies virus glycoprotein affect spread of viral infection. *Microbiol Immunol* 54, 89-97 (2010).

97. Yamada, K., Noguchi, K. & Nishizono, A. Efficient N-glycosylation at position 37, but not at position 146, in the street rabies virus glycoprotein reduces pathogenicity. *Virus Res* 179, 169-76 (2014).

98. Yamada, K. et al. Addition of a single N-glycan to street rabies virus glycoprotein enhances virus production. *J Gen Virol* 94, 270-5 (2013).

99. Morimoto, K., Hooper, D.C., Spitsin, S., Koprowski, H. & Dietzschold, B. Pathogenicity of different rabies virus variants inversely correlates with apoptosis and rabies virus glycoprotein expression in infected primary neuron cultures. *J Virol* 73, 510-8 (1999).

100. Wirblich, C. & Schnell, M.J. Rabies virus (RV) glycoprotein expression levels are not critical for pathogenicity of RV. *J Virol* 85, 697-704 (2011).

101. Nanbo, A. et al. Ebolavirus is internalized into host cells via macropinocytosis in a viral glycoprotein-dependent manner. *PLoS Pathog* 6, e1001121 (2010).

102. Mulherkar, N., Raaben, M., de la Torre, J.C., Whelan, S.P. & Chandran, K. The Ebola virus glycoprotein mediates entry via a non-classical dynamin-dependent macropinocytic pathway. *Virology* 419, 72-83 (2011).

103. Pelkmans, L. & Helenius, A. Endocytosis via caveolae. *Traffic* 3, 311-20 (2002).

104. Santos, R.I. et al. Oropouche virus entry into HeLa cells involves clathrin and requires endosomal acidification. *Virus Res* 138, 139-43 (2008).

105. Hollidge, B.S. et al. Orthobunyavirus entry into neurons and other mammalian cells occurs via clathrin-mediated endocytosis and requires trafficking into early endosomes. *J Virol* 86, 7988-8001 (2012).

106. Garrison, A.R. et al. Crimean-Congo hemorrhagic fever virus utilizes a clathrin- and early endosome-dependent entry pathway. *Virology* 444, 45-54 (2013).

107. Kunz, S. Receptor binding and cell entry of Old World arenaviruses reveal novel aspects of virus-host interaction. *Virology* 387, 245-9 (2009).

108. Superti, F., Derer, M. & Tsiang, H. Mechanism of rabies virus entry into CER cells. *J Gen Virol* 65 (Pt 4), 781-9 (1984).

109. Lewis, P., Fu, Y. & Lentz, T.L. Rabies virus entry at the neuromuscular junction in nerve-muscle cocultures. *Muscle Nerve* 23, 720-30 (2000).

110. Diestel, S., Schaefer, D., Cremer, H. & Schmitz, B. NCAM is ubiquitylated, endocytosed and recycled in neurons. *J Cell Sci* 120, 4035-49 (2007).

111. Minana, R., Duran, J.M., Tomas, M., Renau-Piqueras, J. & Guerri, C. Neural cell adhesion molecule is endocytosed via a clathrin-dependent pathway. *Eur J Neurosci* 13, 749-56 (2001).

112. Kumari, S. et al. Nicotinic acetylcholine receptor is internalized via a Rac-dependent, dynamin-independent endocytic pathway. *J Cell Biol* 181, 1179-93 (2008).

113. Rudolf, R. et al. Regulation of nicotinic acetylcholine receptor turnover by MuRF1 connects muscle activity to endo/lysosomal and atrophy pathways. *Age (Dordr)* 35, 1663-74 (2013).

114. Johannsdottir, H.K., Mancini, R., Kartenbeck, J., Amato, L. & Helenius, A. Host cell factors and functions involved in vesicular stomatitis virus entry. *J Virol* 83, 440-53 (2009).

115. Schlegel, R., Dickson, R.B., Willingham, M.C. & Pastan, I.H. Amantadine and dansylcadaverine inhibit vesicular stomatitis virus uptake and receptor-mediated endocytosis of alpha 2-macroglobulin. *Proc Natl Acad Sci U S A* 79, 2291-5 (1982).

116. Cureton, D.K., Massol, R.H., Whelan, S.P. & Kirchhausen, T. The length of vesicular stomatitis virus particles dictates a need for actin assembly during clathrin-dependent endocytosis. *PLoS Pathog* 6, e1001127 (2010).

117. Boulant, S., Kural, C., Zeeh, J.C., Ubelmann, F. & Kirchhausen, T. Actin dynamics counteract membrane tension during clathrin-mediated endocytosis. *Nat Cell Biol* 13, 1124-31 (2011).

118. Salinas, S., Schiavo, G. & Kremer, E.J. A hitchhiker's guide to the nervous system: the complex journey of viruses and toxins. *Nat Rev Microbiol* 8, 645-55 (2010).

119. Maday, S., Twelvetrees, A.E., Moughamian, A.J. & Holzbaur, E.L. Axonal transport: cargo-specific mechanisms of motility and regulation. *Neuron* 84, 292-309 (2014).

120. Gumy, L.F., Katrukha, E.A., Kapitein, L.C. & Hoogenraad, C.C. New insights into mRNA trafficking in axons. *Dev Neurobiol* 74, 233-44 (2014).

121. Salinas, S., Bilsland, L.G. & Schiavo, G. Molecular landmarks along the axonal route: axonal transport in health and disease. *Curr Opin Cell Biol* 20, 445-53 (2008).

122. Sodeik, B. Mechanisms of viral transport in the cytoplasm. *Trends Microbiol* 8, 465-72 (2000).

123. Kramer, T. et al. Kinesin-3 mediates axonal sorting and directional transport of alphaherpesvirus particles in neurons. *Cell Host Microbe* 12, 806-14 (2012).

124. Bulenga, G. & Heaney, T. Post-exposure local treatment of mice infected with rabies with two axonal flow inhibitors, colchicine and vinblastine. *J Gen Virol* 39, 381-5 (1978).

125. Baer, G.M. The Natural History of Rabies (New York Academic Press, 1975).

126. Lycke, E. & Tsiang, H. Rabies virus infection of cultured rat sensory neurons. *J Virol* 61, 2733-41 (1987).

127. Tsiang, H. Evidence for an intraaxonal transport of fixed and street rabies virus. *J Neuropathol Exp Neurol* 38, 286-99 (1979).

128. Raux, H., Flamand, A. & Blondel, D. Interaction of the rabies virus P protein with the LC8 dynein light chain. *J Virol* 74, 10212-6 (2000).

129. Jacob, Y., Badrane, H., Ceccaldi, P.E. & Tordo, N. Cytoplasmic dynein LC8 interacts with lyssavirus phosphoprotein. *J Virol* 74, 10217-22 (2000).

130. Rasalingam, P., Rossiter, J.P., Mebatsion, T. & Jackson, A.C. Comparative pathogenesis of the SAD-L16 strain of rabies virus and a mutant modifying the dynein light chain binding site of the rabies virus phosphoprotein in young mice. *Virus Res* 111, 55-60 (2005).

131. Tan, G.S., Preuss, M.A., Williams, J.C. & Schnell, M.J. The dynein light chain 8 binding motif of rabies virus phosphoprotein promotes efficient viral transcription. *Proc Natl Acad Sci U S A* 104, 7229-34 (2007).

132. Cronin, J., Zhang, X.Y. & Reiser, J. Altering the tropism of lentiviral vectors through pseudotyping. *Curr Gene Ther* 5, 387-98 (2005).

133. Kato, S. et al. A lentiviral strategy for highly efficient retrograde gene transfer by pseudotyping with fusion envelope glycoprotein. *Hum Gene Ther* 22, 197-206 (2011).

134. Kato, S. et al. Neuron-specific gene transfer through retrograde transport of lentiviral vector pseudotyped with a novel type of fusion envelope glycoprotein. *Hum Gene Ther* 22, 1511-23 (2011).

135. Kato, S., Kobayashi, K. & Kobayashi, K. Improved transduction efficiency of a lentiviral vector for neuron-specific retrograde gene transfer by optimizing the junction of fusion envelope glycoprotein. *J Neurosci Methods* 227, 151-8 (2014).

136. Bauer, A. et al. Anterograde glycoprotein-dependent transport of newly generated rabies virus in dorsal root ganglion neurons. *J Virol* 88, 14172-83 (2014).

137. Morimoto, K. et al. Characterization of a unique variant of bat rabies virus responsible for newly emerging human cases in North America. *Proc Natl Acad Sci U S A* 93, 5653-8 (1996).

138. Dietzschold, B., Li, J., Faber, M. & Schnell, M. Concepts in the pathogenesis of rabies. *Future Virol* 3, 481-490 (2008).

139. Schnell, M.J., Tan, G.S. & Dietzschold, B. The application of reverse genetics technology in the study of rabies virus (RV) pathogenesis and for the development of novel RV vaccines. *J Neurovirol* 11, 76-81 (2005).

140. Schnell, M.J., Mebatsion, T. & Conzelmann, K.K. Infectious rabies viruses from cloned cDNA. *EMBO J* 13, 4195-203 (1994).

141. Pfaller, C.K., Cattaneo, R. & Schnell, M.J. Reverse genetics of Mononegavirales: How they work, new vaccines, and new cancer therapeutics. *Virology* 479-480, 331-44 (2015).

142. Clemente, R. & de la Torre, J.C. Cell entry of Borna disease virus follows a clathrin-mediated endocytosis pathway that requires Rab5 and microtubules. *J Virol* 83, 10406-16 (2009).

143. Cote, M. et al. Small molecule inhibitors reveal Niemann-Pick C1 is essential for Ebola virus infection. *Nature* 477, 344-8 (2011).

144. Carette, J.E. et al. Ebola virus entry requires the cholesterol transporter Niemann-Pick C1. *Nature* 477, 340-3 (2011).

145. Jae, L.T. et al. Virus entry. Lassa virus entry requires a trigger-induced receptor switch. *Science* 344, 1506-10 (2014).

146. Tsiang, H., Ceccaldi, P.E. & Lycke, E. Rabies virus infection and transport in human sensory dorsal root ganglia neurons. *J Gen Virol* 72 (Pt 5), 1191-4 (1991).

147. Millet, L.J. & Gillette, M.U. Over a century of neuron culture: from the hanging drop to microfluidic devices. *Yale J Biol Med* 85, 501-21 (2012).

148. MacInnis, B.L. & Campenot, R.B. Retrograde support of neuronal survival without retrograde transport of nerve growth factor. *Science* 295, 1536-9 (2002).

149. Campenot, R.B. Local control of neurite development by nerve growth factor. *Proc Natl Acad Sci U S A* 74, 4516-9 (1977).

150. Ch'ng, T.H. & Enquist, L.W. Neuron-to-cell spread of pseudorabies virus in a compartmented neuronal culture system. *J Virol* 79, 10875-89 (2005).

151. Curanovic, D. & Enquist, L.W. Virion-incorporated glycoprotein B mediates transneuronal spread of pseudorabies virus. *J Virol* 83, 7796-804 (2009).

152. Lyman, M.G., Curanovic, D., Brideau, A.D. & Enquist, L.W. Fusion of enhanced green fluorescent protein to the pseudorabies virus axonal sorting protein Us9 blocks anterograde spread of infection in mammalian neurons. *J Virol* 82, 10308-11 (2008).

153. Tsiang, H., Lycke, E., Ceccaldi, P.E., Ermine, A. & Hirardot, X. The anterograde transport of rabies virus in rat sensory dorsal root ganglia neurons. *J Gen Virol* 70 (Pt 8), 2075-85 (1989).

154. Taylor, A.M. et al. A microfluidic culture platform for CNS axonal injury, regeneration and transport. *Nat Methods* 2, 599-605 (2005).

155. Park, J.W., Vahidi, B., Taylor, A.M., Rhee, S.W. & Jeon, N.L. Microfluidic culture platform for neuroscience research. *Nat Protoc* 1, 2128-36 (2006).

156. Park, J.W., Kim, H.J., Byun, J.H., Ryu, H.R. & Jeon, N.L. Novel microfluidic platform for culturing neurons: culturing and biochemical analysis of neuronal components. *Biotechnol J* 4, 1573-7 (2009).

157. Dietzschold, B., Schnell, M. & Koprowski, H. Pathogenesis of rabies. *Curr Top Microbiol Immunol* 292, 45-56 (2005).

158. Gaudin, Y. Rabies virus-induced membrane fusion pathway. *J Cell Biol* 150, 601-12 (2000).

159. Roche, S. & Gaudin, Y. Evidence that rabies virus forms different kinds of fusion machines with different pH thresholds for fusion. *J Virol* 78, 8746-52 (2004).

160. Lewis, P. & Lentz, T.L. Rabies virus entry into cultured rat hippocampal neurons. *J Neurocytol* 27, 559-73 (1998).

161. Cureton, D.K., Harbison, C.E., Cocucci, E., Parrish, C.R. & Kirchhausen, T. Limited transferrin receptor clustering allows rapid diffusion of canine parvovirus into clathrin endocytic structures. *J Virol* 86, 5330-40 (2012).

162. Rust, M.J., Lakadamyali, M., Zhang, F. & Zhuang, X. Assembly of endocytic machinery around individual influenza viruses during viral entry. *Nat Struct Mol Biol* 11, 567-73 (2004).

163. van der Schaar, H.M. et al. Dissecting the cell entry pathway of dengue virus by single-particle tracking in living cells. *PLoS Pathog* 4, e1000244 (2008).

164. Ehrlich, M. et al. Endocytosis by random initiation and stabilization of clathrin-coated pits. *Cell* 118, 591-605 (2004).

165. Wickersham, I.R., Finke, S., Conzelmann, K.K. & Callaway, E.M. Retrograde neuronal tracing with a deletion-mutant rabies virus. *Nat Methods* 4, 47-9 (2007).

166. Wong, A.C., Sandesara, R.G., Mulherkar, N., Whelan, S.P. & Chandran, K. A forward genetic strategy reveals destabilizing mutations in the Ebolavirus glycoprotein that alter its protease dependence during cell entry. *J Virol* 84, 163-75 (2010).

167. Whelan, S.P., Barr, J.N. & Wertz, G.W. Identification of a minimal size requirement for termination of vesicular stomatitis virus mRNA: implications for the mechanism of transcription. *J Virol* 74, 8268-76 (2000).

168. Whelan, S.P., Ball, L.A., Barr, J.N. & Wertz, G.T. Efficient recovery of infectious vesicular stomatitis virus entirely from cDNA clones. *Proc Natl Acad Sci U S A* 92, 8388-92 (1995).

169. Massol, R.H., Boll, W., Griffin, A.M. & Kirchhausen, T. A burst of auxilin recruitment determines the onset of clathrin-coated vesicle uncoating. *Proc Natl Acad Sci U S A* 103, 10265-70 (2006).

170. Maupin, P. & Pollard, T.D. Improved preservation and staining of HeLa cell actin filaments, clathrin-coated membranes, and other cytoplasmic structures by tannic acid-glutaraldehyde-saponin fixation. *J Cell Biol* 96, 51-62 (1983).

171. Lefrancois, L. & Lyles, D.S. The interaction of antibody with the major surface glycoprotein of vesicular stomatitis virus. I. Analysis of neutralizing epitopes with monoclonal antibodies. *Virology* 121, 157-67 (1982).

172. Lefrancois, L. & Lyles, D.S. The interaction of antibody with the major surface glycoprotein of vesicular stomatitis virus. II. Monoclonal antibodies of nonneutralizing and cross-reactive epitopes of Indiana and New Jersey serotypes. *Virology* 121, 168-74 (1982).

173. Garbutt, M. et al. Properties of replication-competent vesicular stomatitis virus vectors expressing glycoproteins of filoviruses and arenaviruses. *J Virol* 78, 5458-65 (2004).

174. Guichard, P. et al. Three dimensional morphology of rabies virus studied by cryo-electron tomography. *J Struct Biol* 176, 32-40 (2011).

175. Mebatsion, T., Konig, M. & Conzelmann, K.K. Budding of rabies virus particles in the absence of the spike glycoprotein. *Cell* 84, 941-51 (1996).

176. Koivusalo, M. et al. Amiloride inhibits macropinocytosis by lowering submembranous pH and preventing Rac1 and Cdc42 signaling. *J Cell Biol* 188, 547-63 (2010).

177. Macia, E. et al. Dynasore, a cell-permeable inhibitor of dynamin. *Dev Cell* 10, 839-50 (2006).

178. Cureton, D.K., Burdeinick-Kerr, R. & Whelan, S.P. Genetic inactivation of COPI coatomer separately inhibits vesicular stomatitis virus entry and gene expression. *J Virol* 86, 655-66 (2012).

179. Kirchhausen, T., Boll, W., van Oijen, A. & Ehrlich, M. Single-molecule live-cell imaging of clathrin-based endocytosis. *Biochem Soc Symp*, 71-6 (2005).

180. Boucrot, E., Saffarian, S., Massol, R., Kirchhausen, T. & Ehrlich, M. Role of lipids and actin in the formation of clathrin-coated pits. *Exp Cell Res* 312, 4036-48 (2006).

181. Finkelshtein, D., Werman, A., Novick, D., Barak, S. & Rubinstein, M. LDL receptor and its family members serve as the cellular receptors for vesicular stomatitis virus. *Proc Natl Acad Sci U S A* 110, 7306-11 (2013).

182. Coil, D.A. & Miller, A.D. Phosphatidylserine is not the cell surface receptor for vesicular stomatitis virus. *J Virol* 78, 10920-6 (2004).

183. Gotti, C., Fornasari, D. & Clementi, F. Human neuronal nicotinic receptors. *Prog Neurobiol* 53, 199-237 (1997).

184. Beier, K.T. et al. Transsynaptic tracing with vesicular stomatitis virus reveals novel retinal circuitry. *J Neurosci* 33, 35-51 (2013).

185. Beier, K.T., Saunders, A.B., Oldenburg, I.A., Sabatini, B.L. & Cepko, C.L. Vesicular stomatitis virus with the rabies virus glycoprotein directs retrograde transsynaptic transport among neurons in vivo. *Front Neural Circuits* 7, 11 (2013).

186. Card, J.P. & Enquist, L.W. Transneuronal circuit analysis with pseudorabies viruses. *Curr Protoc Neurosci* Chapter 1, Unit1 5 (2001).

187. Faber, M. et al. Identification of viral genomic elements responsible for rabies virus neuroinvasiveness. *Proc Natl Acad Sci U S A* 101, 16328-32 (2004).

188. Zampieri, N., Jessell, T.M. & Murray, A.J. Mapping sensory circuits by anterograde transsynaptic transfer of recombinant rabies virus. *Neuron* 81, 766-78 (2014).

189. Bohnert, S. & Schiavo, G. Tetanus toxin is transported in a novel neuronal compartment characterized by a specialized pH regulation. *J Biol Chem* 280, 42336-44 (2005).

190. Lewis, P., Fu, Y. & Lentz, T.L. Rabies virus entry into endosomes in IMR-32 human neuroblastoma cells. *Exp Neurol* 153, 65-73 (1998).

191. Piccinotti, S., Kirchhausen, T. & Whelan, S.P. Uptake of rabies virus into epithelial cells by clathrin-mediated endocytosis depends upon actin. *J Virol* 87, 11637-47 (2013).

192. Pazyra-Murphy, M.F. & Segal, R.A. Preparation and maintenance of dorsal root ganglia neurons in compartmented cultures. *J Vis Exp* (2008).

193. Langlois, S.D., Morin, S., Yam, P.T. & Charron, F. Dissection and culture of commissural neurons from embryonic spinal cord. *J Vis Exp* (2010).

194. Leach, M.K. et al. The culture of primary motor and sensory neurons in defined media on electrospun poly-L-lactide nanofiber scaffolds. *J Vis Exp* (2011).

195. Loebrich, S. The role of F-actin in modulating Clathrin-mediated endocytosis: Lessons from neurons in health and neuropsychiatric disorder. *Commun Integr Biol* 7, e28740 (2014).

196. Masereel, B., Pochet, L. & Laeckmann, D. An overview of inhibitors of Na(+)/H(+) exchanger. *Eur J Med Chem* 38, 547-54 (2003).

197. West, M.A., Bretscher, M.S. & Watts, C. Distinct endocytotic pathways in epidermal growth factor-stimulated human carcinoma A431 cells. *J Cell Biol* 109, 2731-9 (1989).

198. Rocha-Gonzalez, H.I. et al. Identification of the Na+/H+ exchanger 1 in dorsal root ganglion and spinal cord: its possible role in inflammatory nociception. *Neuroscience* 160, 156-64 (2009).

199. Jang, I.S. et al. The Na(+)/H(+) exchanger is a major pH regulator in GABAergic presynaptic nerve terminals synapsing onto rat CA3 pyramidal neurons. *J Neurochem* 99, 1224-36 (2006).

200. Ronicke, R., Schroder, U.H., Bohm, K. & Reymann, K.G. The Na+/H+ exchanger modulates long-term potentiation in rat hippocampal slices. *Naunyn Schmiedebergs Arch Pharmacol* 379, 233-9 (2009).

201. Weir, D.L., Laing, E.D., Smith, I.L., Wang, L.F. & Broder, C.C. Host cell virus entry mediated by Australian bat lyssavirus G envelope glycoprotein occurs through a clathrin-mediated endocytic pathway that requires actin and Rab5. *Virol J* 11, 40 (2014).

202. Tani, H. et al. Analysis of Lujo virus cell entry using pseudotype vesicular stomatitis virus. *J Virol* 88, 7317-30 (2014).

203. Rudd, R.J., Trimarchi, C.V. & Abelseth, M.K. Tissue culture technique for routine isolation of street strain rabies virus. *J Clin Microbiol* 12, 590-3 (1980).

204. Castaneda-Castellanos, D.R., Castellanos, J.E. & Hurtado, H. Differential use of the nicotinic receptor by rabies virus based upon substrate origin. *J Neurovirol* 8, 150-4 (2002).

205. Neubert, A., Schuster, P., Muller, T., Vos, A. & Pommerening, E. Immunogenicity and efficacy of the oral rabies vaccine SAD B19 in foxes. *J Vet Med B Infect Dis Vet Public Health* 48, 179-83 (2001).

206. Vos, A. et al. An update on safety studies of SAD B19 rabies virus vaccine in target and non-target species. *Epidemiol Infect* 123, 165-75 (1999).

207. Wunner, W.H., Dietzschold, B., Smith, C.L., Lafon, M. & Golub, E. Antigenic variants of CVS rabies virus with altered glycosylation sites. *Virology* 140, 1-12 (1985).

208. Kasturi, L., Eshleman, J.R., Wunner, W.H. & Shakin-Eshleman, S.H. The hydroxy amino acid in an Asn-X-Ser/Thr sequon can influence N-linked core glycosylation efficiency and the level of expression of a cell surface glycoprotein. *J Biol Chem* 270, 14756-61 (1995).

209. Shakin-Eshleman, S.H., Remaley, A.T., Eshleman, J.R., Wunner, W.H. & Spitalnik, S.L. N-linked glycosylation of rabies virus glycoprotein. Individual sequons differ in their glycosylation efficiencies and influence on cell surface expression. *J Biol Chem* 267, 10690-8 (1992).

210. Yamada, K. et al. Serial passage of a street rabies virus in mouse neuroblastoma cells resulted in attenuation: potential role of the additional N-glycosylation of a viral glycoprotein in the reduced pathogenicity of street rabies virus. *Virus Res* 165, 34-45 (2012).

211. Murphy, F.A. & Bauer, S.P. Early street rabies virus infection in striated muscle and later progression to the central nervous system. *Intervirology* 3, 256-68 (1974).

212. Shankar, V., Dietzschold, B. & Koprowski, H. Direct entry of rabies virus into the central nervous system without prior local replication. *J Virol* 65, 2736-8 (1991).

213. Deinhardt, K., Berninghausen, O., Willison, H.J., Hopkins, C.R. & Schiavo, G. Tetanus toxin is internalized by a sequential clathrin-dependent mechanism initiated within lipid microdomains and independent of epsin1. *J Cell Biol* 174, 459-71 (2006).

214. Lalli, G. & Schiavo, G. Analysis of retrograde transport in motor neurons reveals common endocytic carriers for tetanus toxin and neurotrophin receptor p75NTR. *J Cell Biol* 156, 233-9 (2002).

215. Donnelly-Roberts, D.L. & Lentz, T.L. Synthetic peptides of neurotoxins and rabies virus glycoprotein behave as antagonists in a functional assay for the acetylcholine receptor. *Pept Res* 2, 221-6 (1989).

216. Dellisanti, C.D., Yao, Y., Stroud, J.C., Wang, Z.Z. & Chen, L. Crystal structure of the extracellular domain of nAChR alpha1 bound to alpha-bungarotoxin at 1.94 A resolution. *Nat Neurosci* 10, 953-62 (2007).

217. Southam, K.A., King, A.E., Blizzard, C.A., McCormack, G.H. & Dickson, T.C. Microfluidic primary culture model of the lower motor neuron-neuromuscular junction circuit. *J Neurosci Methods* 218, 164-9 (2013).

218. Lentz, T.L., Burrage, T.G., Smith, A.L. & Tignor, G.H. The acetylcholine receptor as a cellular receptor for rabies virus. *Yale J Biol Med* 56, 315-22 (1983).

219. Vilar, M. et al. Activation of the p75 neurotrophin receptor through conformational rearrangement of disulphide-linked receptor dimers. *Neuron* 62, 72-83 (2009).

220. Wehrman, T. et al. Structural and mechanistic insights into nerve growth factor interactions with the TrkA and p75 receptors. *Neuron* 53, 25-38 (2007).

APPENDIX

CO-UPTAKE OF RVSV SAD B19 G VIRUS WITH EXOGENOUSLY EXPRESSED RECEPTOR P75^{NTR} INTO BS-C-1 CELLS

INTRODUCTION

Three host cell proteins have been identified as putative receptors of RABV: the low affinity p75 neurotrophin receptor (p75^{NTR}), neural cell adhesion molecule (NCAM), and nicotinic acetylcholine receptor (nAChR) [39, 63, 67, 218]. Internalization and transport to the perinuclear region has been reported for each putative receptor, but considerable heterogeneity exists in the endocytic pathways utilized (Figure D.5). The existence of disparate internalization mechanisms raises the possibility that RABV entry may be mediated by a variety of processes: clathrin-dependent, caveolin-dependent and dynamin- (therefore clathrin- and caveolin-) independent. In addition, convergent internalization pathways may exhibit different uptake rates or recruitment of endocytic machinery resulting from differences in signaling underlying receptor endocytosis. Here, we explored uptake of rVSV SAD B19 G following engagement of the putative receptor p75^{NTR}.

Intracellular signaling domains of p75^{NTR}. P75^{NTR} is a member of the tumor necrosis factor receptor family. The cytoplasmic tail of p75^{NTR} contains a death domain for which the NMR structure has been solved [24]. However, the p75^{NTR} domain diverges significantly from other known domains of that class: it does not associate homotypically or heterotypically with other death domains, and is itself catalytically inactive [25]. Therefore, it is believed to mediate signaling through interactions with cytoplasmic factors rather than active signaling.

The death domain of p75^{NTR} is separated from the transmembrane domain by a juxtamembrane flexible linker. Despite its disordered structure, this region spanning residues 274-303 contains the highest homology across species. Conservation generally suggests great functional relevance of a

particular domain or sequence; correspondingly, studies have shown that deletion of this domain, designated "chopper," abrogates $p75^{NTR}$ pro-apoptotic activities [25]. In addition, several cytoplasmic binding partners have been shown to associate with the Chopper region.

Signaling through $p75^{NTR}$ is triggered by binding of neurotrophins and proneurotrophins to its ectodomain. This domain contains four cystein-rich domains (CRDs) which are engaged by endogenous ligands of $p75^{NTR}$.

Molecular biology of $p75^{NTR}$ signaling following engagement of endogenous ligands. Signaling cascades initiated by $p75^{NTR}$ can lead to apoptosis or, to the contrary, pro-survival neurite outgrowth. Since $p75^{NTR}$ is catalytically inactive, what determines which "command" is issued by $p75^{NTR}$ is primarily the ligand engaging the receptor's ectodomain. Neurotrophin-3 (NT-3), nerve growth factor (NGF) and its unprocessed counterpart, proNGF, are endogenous extracellular ligands of $p75^{NTR}$. Generally, binding of processed neurotrophins to $p75^{NTR}$ induces signaling that is pro-growth; whereas, pro-neurotrophin binding leads to apoptosis. To date, evidence shows that engaging neurotrophins or their unprocessed counterparts leads to dramatically different recruitment of membrane and cytoplasmic factors to the neurotrophin receptor. This is largely due to different conformational outcomes following binding to each class of ligand.

When NGF binds dimeric $p75^{NTR}$, the extracellular domains of the receptor are brought into closer proximity to one another. A transmembrane disulfide bridge in the receptor dimer relays these extracellular conformational rearrangements across the plasma membrane resulting in the opening of the $p75^{NTR}$ cytoplasmic domains. It is therefore presumed that NGF association with $p75^{NTR}$ increases the accessibility of cytoplasmic binding sites to downstream effectors [219]. Consistent with this model, the transmembrane disulfide bridge mediated by C257 of $p75^{NTR}$ is critical for NGF signaling [219]. If this cysteine is mutated, NGF binding fails to result in recruitment of cytoplasmic effectors such as TRAF6 or

NRIF and signaling is blocked. This mutation, however, only affects NGF signaling, and proneutrophin-dependent signaling remains intact. Unlike NGF, proNGF signaling through $p75^{NTR}$ does not require conformational changes propagated to the $p75^{NTR}$ C-terminus. Instead, proNGF recruits sortilin to $p75^{NTR}$ [27]. This interaction is mediated by the pro-domain of proNGF which is cleaved off during processing into NGF. Recruitment of sortilin leads to proteolytic cleavage of $p75^{NTR}$ and release of the cytoplasmic tail of the receptor. Since this mechanism appears to exclude internalization of the ligand-bound $p75^{NTR}$ ectodomain, it is hard to envision how it could contribute to internalization of a viral particle. In contrast, binding of NGF has been shown to cause clathrin-mediated endocytosis of the intact receptor [28]. This observation renders the NGF model of $p75^{NTR}$ signaling and uptake particularly attractive for thinking about a mechanism of RABV internalization mediated by $p75^{NTR}$.

Binding sites of NT-3, proNGF and RABV G on $p75^{NTR}$. To relate what is known about $p75^{NTR}$ signaling to RABV biology, it is relevant to compare what is known about the respective binding sites of RABV G, NT-3, NGF and proNGF. Crystal structures have been solved for dimeric $p75^{NTR}$ engaging a dimer of NT-3. These structures reveal that NT-3 engages the interface between cysteine-rich domains (CRDs) 1 and 2, in addition to CRDs 3 and 4 [29]. These contacts are conserved in both engagement of NT-3, with perhaps lesser engagement of CRD 4, and proNGF [1, 27].

In contrast to the endogenous ligands of $p75^{NTR}$, only CRD1 has been implicated in RABV G binding to $p75^{NTR}$ [76]. Nonetheless, this interaction has been shown to be of high affinity [76]. Although various residues within CRD1 have been tested, a single amino acid has been shown to be indispensable to RABV G binding: Glu33 [76]. Similarly, only a limited number of residues in RABV G have been implicated in association with $p75^{NTR}$: single mutations in H352, F318, L330 and R333 on RABV G either abrogate or decrease $p75^{NTR}$ binding [76].

Given that RABV G binds $p75^{NTR}$ at a different site than the receptor's endogenous ligands, it is difficult to predict what the outcome of such an interaction could be. However, if RABV G uses $p75^{NTR}$ to trigger internalization, it seems most likely that it must recapitulate the conformational and downstream effects of NGF which has been shown to induce internalization of the receptor, in the absence of which RABV cannot infect the cell. In contrast, pro-neurotrophins lead solely to cleavage of the $p75^{NTR}$ intracellular domain which does not intuitively suggest a direct link between internalization and $p75^{NTR}$ engagement for RABV G. However, the unusual binding site of RABV G on $p75^{NTR}$ may also imply that RABV G triggers a novel mechanism for internalization, or alternatively that $p75^{NTR}$ is engaged solely as a factor for attachment and not as a trigger for internalization. In its endogenous role, $p75^{NTR}$ also increases affinity of neurotrophins for their cognate Trk receptors[220], it is therefore possible that engagement of RABV G with $p75^{NTR}$ may similarly increase binding to a secondary co-receptor that has not yet been identified.

The experiments outlined in this section demonstrate detectable real-time engagement and subsequent internalization of rVSV SAD B19 G with $p75^{NTR}$. We further show that internalization does not require the intracellular signaling domains of the receptor, and present evidence that although $p75^{NTR}$ increases association and internalization of rVSV SAD B19 G virus with epithelial cells it does not mediate infection. This, combined with evidence that $p75^{NTR}$ expression fails to render resistant cells susceptible to infection with neurotropic rVSV CVS G, suggests that $p75^{NTR}$ serves primarily as an attachment factor for RABV. This extends existing evidence showing that $p75^{NTR}$ expression does not necessarily correlate with susceptibility to RABV infection [34].

RESULTS

rVSV SAD B19 G binding to the cell surface results in clustering of surface $p75^{NTR}$. BS-C-1 cells exogenously expressing fluorescently tagged NCAM or $p75^{NTR}$ were inoculated with AlexaFluor (AF) 647

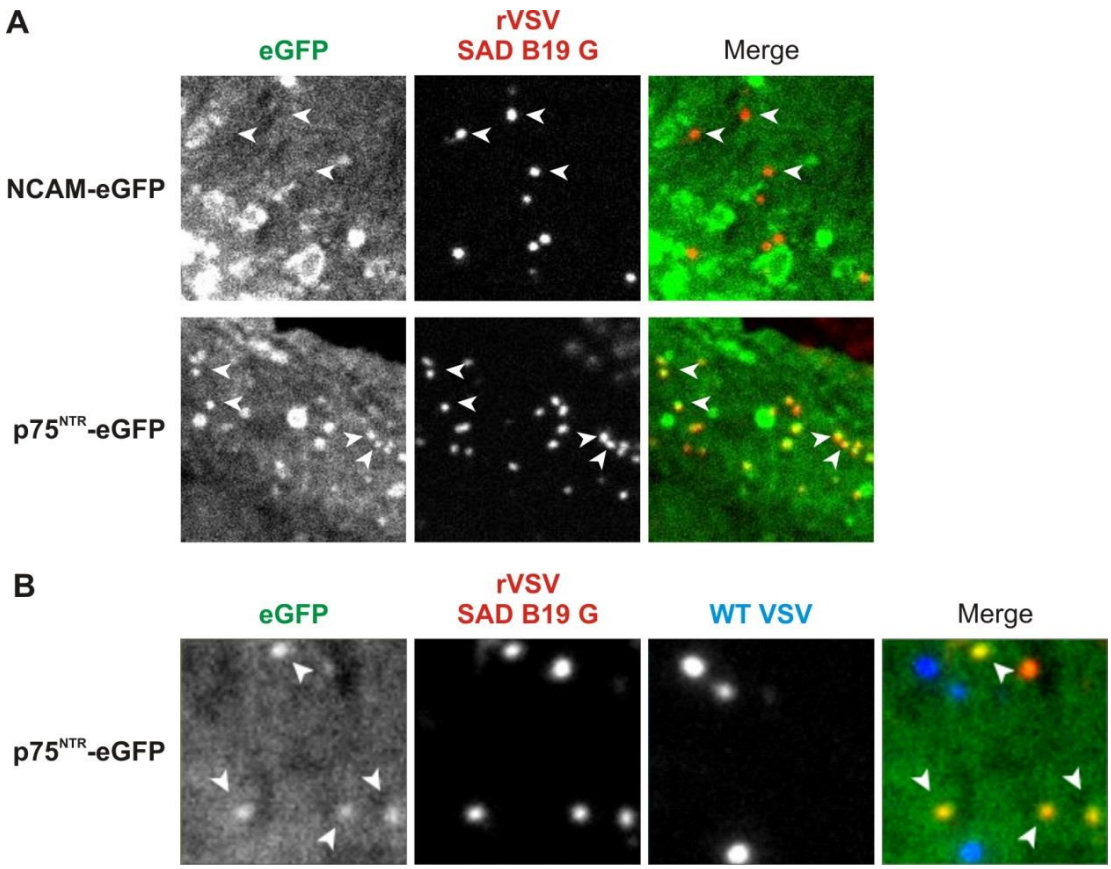

Figure A.1. Binding of rVSV SAD B19 G to the plasma membrane induces G-specific aggregation of the p75^{NTR} receptor.

A. BS-C-1 cells were transfected with NCAM-eGFP or p75^{NTR}-eGFP as indicated with Fugene HD (Roche) according to manufacturer's specifications. On the second day following transfection, cells were inoculated with fluorescently labeled rVSV SAD B19 G virus (MOI = 500) for 30minutes and monitored by live confocal microscopy for colocalization between virus (red) and receptor (green). **B.** BS-C-1 cells transiently expressing p75^{NTR}-eGFP (green) were inoculated with fluorescently tagged rVSV SAD B19 G (red) and WT VSV (blue). Clustering of p75^{NTR}-eGFP was observed for virions incorporating RABV, but not VSV G.

labeled rVSV SAD B19 G virus (Figure A.1 A) and monitored by live imaging for colocalization between virus particles and the receptor. In p75^{NTR}-eGFP expressing cells, recruitment of the receptor was observed in the form of p75^{NTR} clustering in association with incoming rVSV RABV G particles. Clustering presented as eGFP puncta colocalizing with the associated AF647-tagged viral particle (Figure A.1 A), and was found by live imaging to track with the viral particle on the cell surface and during virion

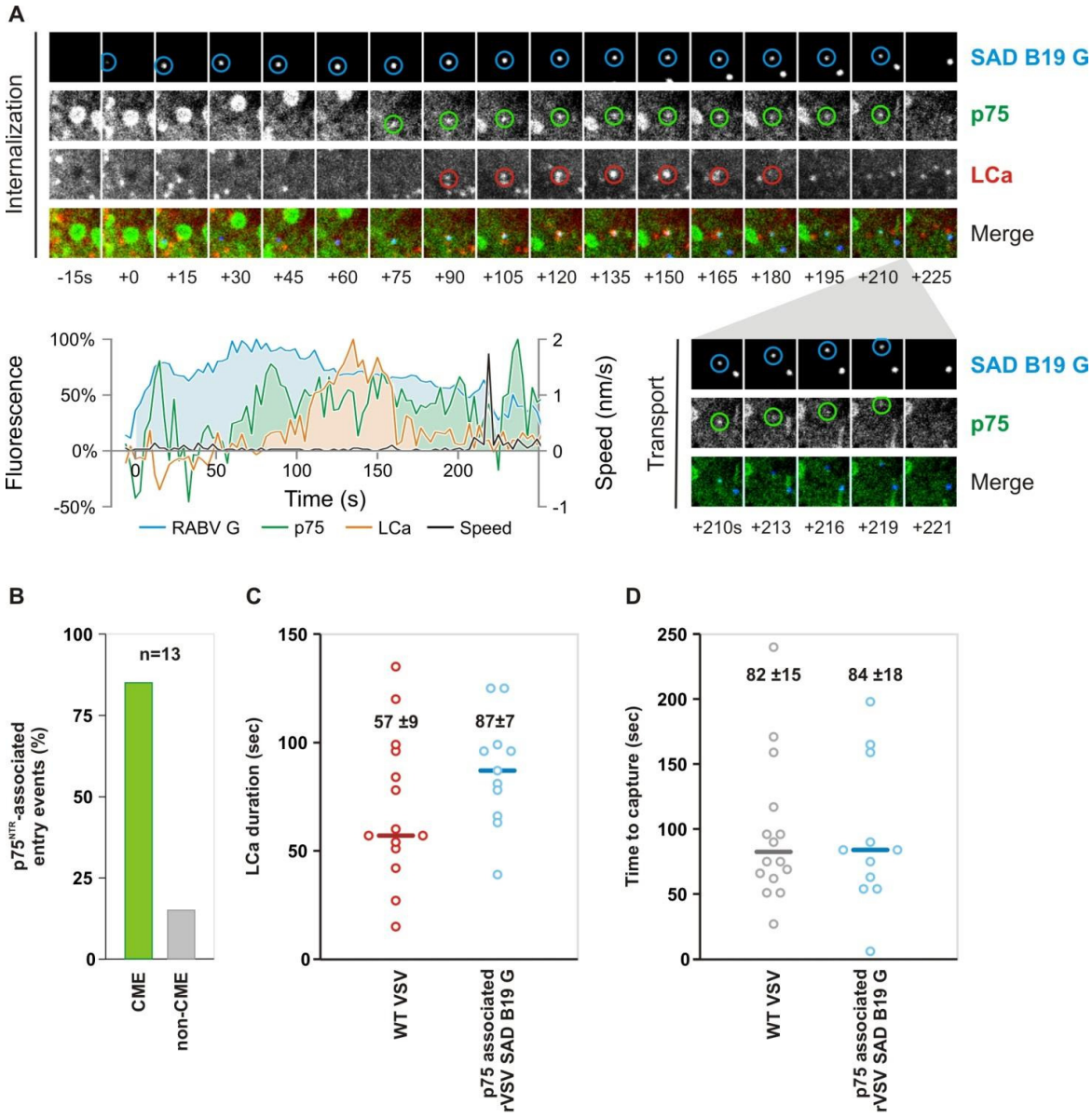

Figure A.2. P75^{NTR}-related entry is clathrin-dependent and exhibits no different in recruitment kinetics than p75^{NTR}-independent entry or WT VSV entry.

A. Tileview of p75^{NTR}-associated entry of AF647 rVSV SAD B19 G particles (blue) in BS-C-1 cells transiently expressing p75^{NTR}-eGFP (green) and pdTomato-conjugated clathrin-light chain (LCa, red). For each channel, target signal is highlighted by a circle corresponding to its color in the merge. P75^{NTR} accumulates over time in a cluster corresponding to and tracking with the viral signal. Association and clustering of p75^{NTR} is maintained throughout engagement of the CCP. In addition, p75^{NTR} remains association during transport following uncoating of the LCa signal consistent with engagement of the receptor. Bottom left corner: Graphical representation of

Figure A.2 (continued) panel A data. Fluorescence values are plotted as % of their maximum. **B.** Percentage of rVSV SAD B19 G virions associated with detectable clusters observed to internalize via clathrin-mediated endocytosis (CME) or via non-CME process as evidenced by colocalization with LCa. **C. and D.** Comparison of distributions of time to LCa C. duration and D. recruitment for WT VSV and $p75^{NTR}$- associated rVSV SAD B19 G entry events. Medians are shown as horizontal bars and reported on the graph; errors are the standard error.

clustering represents a viable indicator of receptor engagement and allows us to monitor the mechanism and kinetics of $p75^{NTR}$-related entry of rVSV RABV G particles. Live imaging of rVSV SAD B19 G co-uptake with receptor was conducted in cells transiently expressing Tomato-tagged clathrin light chain (LCa) and $p75^{NTR}$-eGFP. Binding of nerve growth factor, the endogenous ligand of $p75^{NTR}$, to the receptor shunts $p75^{NTR}$ from a recycling pathway into clathrin-dependent endocytosis leading to internalization and perinuclear transport of the receptor [28]. Although RABV G binds $p75^{NTR}$ at a disparate site from NGF, live imaging data suggests that the majority of rVSV SAD B19 G-bound $p75^{NTR}$ internalizes by clathrin mediated endocytosis (Figure A.2 A, B; Movie SA.1). Clustering of $p75^{NTR}$ was generally detected prior to engagement of CCPs and remained visible throughout the process of internalization and transport indicative of co-uptake of receptor and virion. The kinetics of clathrin coated pit formation at the surface bound virion were further analyzed by live confocal microscopy. Current data suggests that the kinetics of LCa recruitment and LCa lifetime during internalization of rVSV SAD B19 G virions are unaffected by engagement of $p75^{NTR}$ (Figure A.2 C, D). An apparent difference in the duration of clathrin recruitment between p75NTR associated rVSV SAD B19 G and WT VSV likely reflects the small sample number rather than a real effect, since the duration of coated pit envelopment matches previously published data [37]. In addition, these kinetics were comparable to those of AP2 recruitment of WT VSV in untransfected cells.

Truncation of the $p75^{NTR}$ signaling domains does not abrogate rVSV SAD B19 G entry in Bsc1 cells. To determine whether $p75^{NTR}$ signaling is required for internalization of rVSV RABV G, we

Figure A.3. Truncation mutants of p75^{NTR} lacking cytoplasmic signaling domains do not inhibit internalization of rVSV SAD B19 G virions.

A. Schematics of full length p75^{NTR} and its signaling domains, and three truncation mutants fused to mCherry: p75^{NTR}Δdeath, p75^{NTR}-palmΔcyto, and p75NTRΔcyto. **B.** Surface expression of p75NTR truncation mutants. P75^{NTR}-mCherry contains an HA-tag for ease of detection. B-SC-1 cells transiently expressing p75^{NTR} were fixed and stained with anti-HA antibody in the absence of cell membrane permeabilization. Truncation mutants were expressed robustly on the surface of cells displaying mCherry signal. **C.** Truncation of the p75^{NTR} signaling domains does not lead to a defect in viral uptake. B-SC-1 cells transiently transfected with p75^{NTR}-eGFP or truncation mutants tagged with mCherry were infected with AlexaFluor-647 labeled rVSV SAD B19 G for 30min. Non-premeabilized cells were fixed and stained with anti-RABV G antibody to detect surface bound particles. Cells transiently expressing truncations of p75^{NTR} bound and internalized RABV with greater efficiency than the full-length receptor.

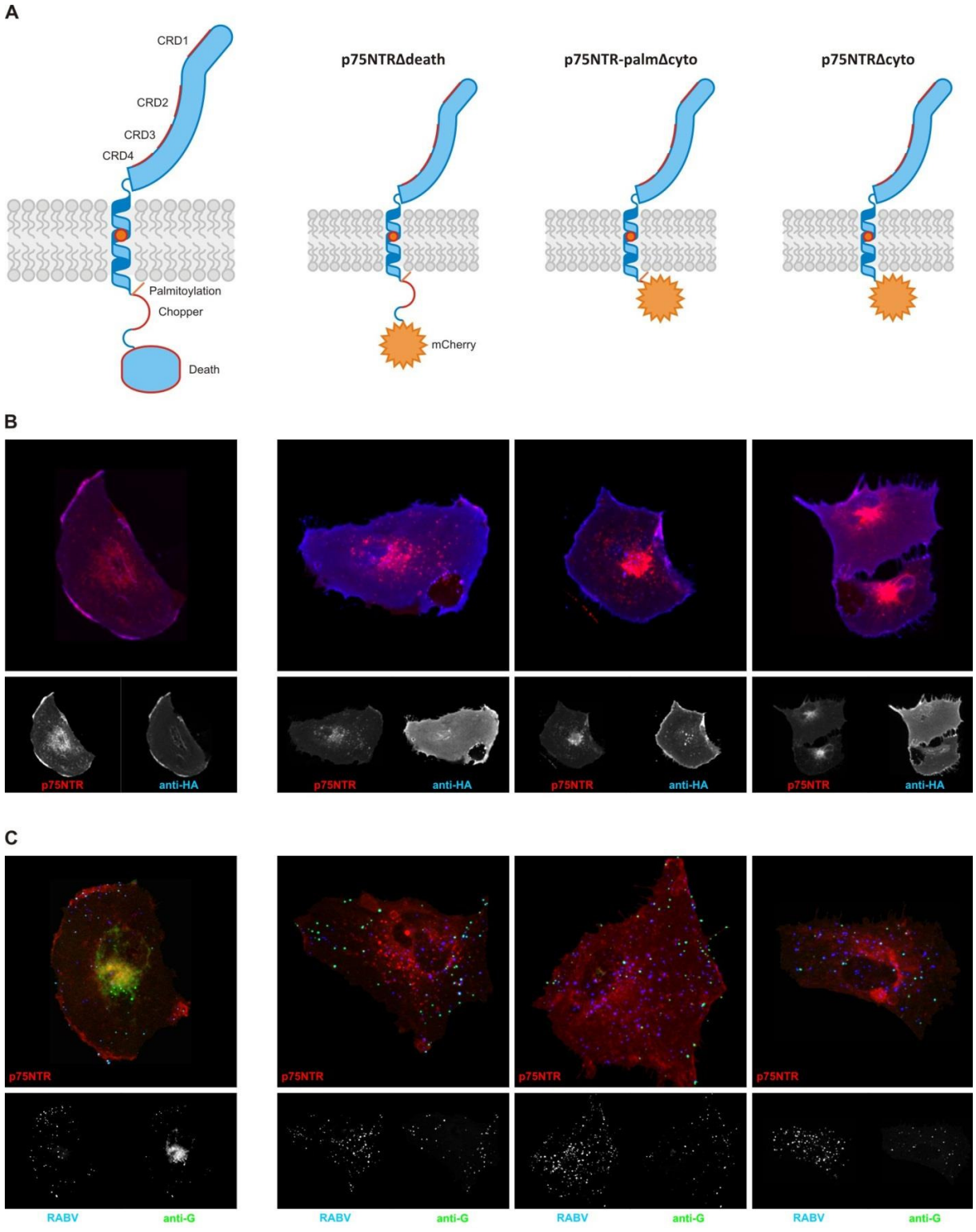

Figure A.3 (Continued)

generated three truncation mutants of $p75^{NTR}$ designed to abrogate some or all of the receptor's cytoplasmic signaling: $p75^{NTR}$Δ274-426 ($p75^{NTR}$Δcyto) and $p75^{NTR}$Δ285-426 ($p75^{NTR}$-palmΔcyto) which lack the entire cytoplasmic tail, and $p75^{NTR}$Δ336-426 ($p75^{NTR}$Δdeath) in which only the death domain was deleted (Figure A.3 A) [25]. $p75^{NTR}$-palmΔcyto retains a palmitoylation site required for efficient trafficking of $p75^{NTR}$ to the plasma membrane. For ease of detection, each mutant was additionally tagged with a C-terminal mCherry fluorophore and hemagglutinin (HA) tag in the extracellular domain. All three $p75^{NTR}$ truncations are robustly expressed and traffic to the cell surface following transient transfection in BS-C-1 cells (Figure A.3 B). Comparison of rVSV SAD B19 G AF647 uptake in cells transfected with full-length or truncated $p75^{NTR}$ receptor revealed that truncation of the cytoplasmic domain of $p75^{NTR}$ does not interfere with virus internalization (Figure A.3 C). In fact, cells expressing truncation mutants appear to have increased susceptibility to rVSV SAD B19 G, displaying greater numbers of internalized particles. Detection of internalized virions colocalizing with $p75^{NTR}$ clusters suggests that internalization is not abrogated despite even high density engagement with the truncated receptor (Figure A.3 D). These results indicate that $p75^{NTR}$ receptors that cannot signal intracellularly do not act as dominant negatives for viral uptake into BS-C-1 cells.

Exogenous expression of $P75^{NTR}$ in cells does not increase the efficiency rVSV RABV G infection in epithelial cells. Live imaging studies have shown that $p75^{NTR}$ engagement has no impact on the route of rVSV SAD B19 G uptake or the kinetics of clathrin recruitment to the virus at the plasma membrane. Bulk entry experiments have further excluded that active signaling from $p75^{NTR}$ is required to induce internalization of the virus. Together, these results challenge a model implicating $p75^{NTR}$ as an active receptor for RABV virus. In contrast they support the view that $p75^{NTR}$ serves primarily as an attachment factor and is dependent on the existence of other unknown factors to mediate infection. To explore this hypothesis, we investigated whether expression of $p75^{NTR}$ in epithelial cells could increase efficiency of

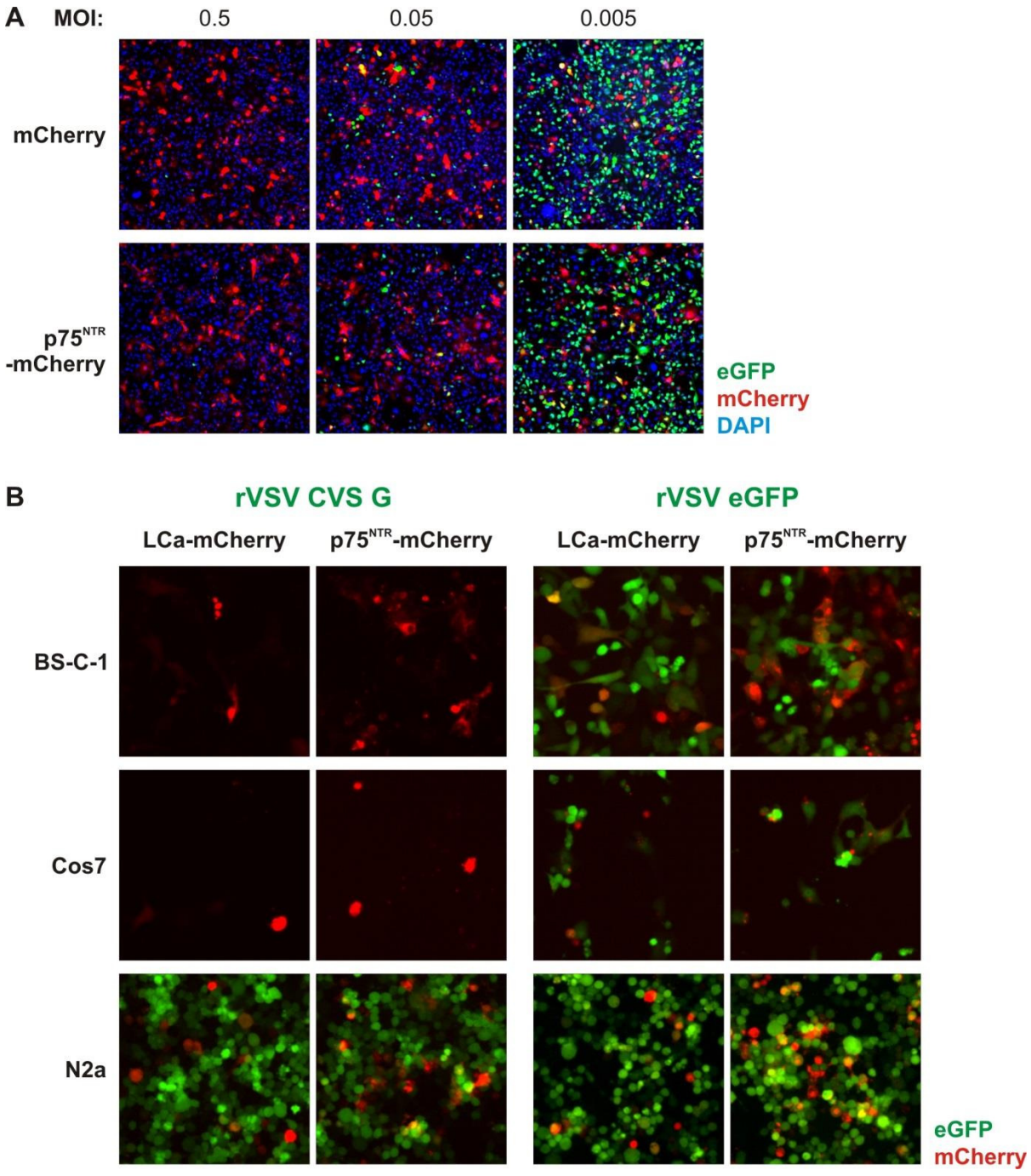

Figure A.4. p75^{NTR} does not increase susceptibility of epithelial cells to infection with rVSV RABV G viruses.

A. Expression of p75^{NTR} does not lead to preferential infection with rVSV SAD B19 G following low MOI inoculation. BS-C-1 cells transiently expressing p75^{NTR}-mCherry or mCherry control plasmid as indicated were inoculated with rVSV SAD B19 G at the indicated MOIs. Preferential infection was assessed by expression of virally encoded eGFP (green). No correlation was observed between

Figure A.4 (continued) expression of mCherry or $p75^{NTR}$-mCherry (red) and viral infection by direct fluorescence microscopy. Cells are further stained with DAPI (blue).**B.** Transient expression $p75^{NTR}$ does not increase susceptibility of resistant cell lines to infection with neurotropic rVSV CVS G virus. BS-C-1, Cos7 and N2a cells transiently expressing a control plasmid (LCa-mCherry) or p75NTR-mCherry (red) were inoculated with neurotropic rVSV CVS G or broadly tropic rVSV eGFP at an MOI_{N2a}=3. Virally encoded eGFP (green) was monitored as a marker for infection by direct fluorescence microscopy .

infection with rVSV SAD B19 G (Figure A.4 A) or the neurotropic rVSV CVS G (Figure A.4 B). In both cases, expression of $p75^{NTR}$ did not result in preferential infection. Importantly, $p75^{NTR}$ was not able to render resistant cell lines susceptible to infection with rVSV CVS G (Figure A.4 B). These results support the hypothesis that $p75^{NTR}$ serves solely as an attachment factor for RABV.

DISCUSSION

Receptor clustering provides evidence of RABV association with the receptor. Here, we report rVSV SAD B19 G-dependent clustering and uptake of the putative RABV receptor $p75^{NTR}$-eGFP. Absence of equivalent aggregation of the receptor under wild type VSV particles indicates that the clustering is specific to RABV G and indicative of active engagement with the receptor. Clustering of receptor molecules – as detected by the formation of high intensity puncta under surface-bound virions – is consistent with the high affinity interaction between RABV G and $p75^{NTR}$ as well as the high density of RABV G trimers studding the viral membrane. This is also in agreement with recent reports of co-uptake and -transport of RABV virions with $p75^{NTR}$ into neurons of the dorsal root ganglion [8] and ventral spinal cord [36], which suggest that high intensity receptor clusters could also form in cells endogenously expressing the receptor.

Similar clustering was not detected in cells transiently expressing fluorescently tagged NCAM. Of the three putative receptors of RABV, NCAM is the least well-studied: the affinity of the interaction between RABV G and NCAM has not been determined, and neither have the reciprocal binding sites on

either protein. The absence of clustering following rVSV RABV G association with NCAM-eGFP expressing cells may suggest a lower affinity between NCAM and RABV G which prevents stable aggregation of the receptor under the viral particle. Alternatively, because surface levels of NCAM expression were not ascertained in transfected cells, it is possible that exogenously expressed NCAM is inefficiently trafficked to the plasma membrane. Lower receptor availability at the cell surface could interfere with the formation of clusters readily detectable by confocal microscopy despite a high affinity interaction. Additional experimentation is required to evaluate these two hypotheses.

Clathrin-mediated co-uptake of rVSV SAD B19 G and p75^{NTR}-eGFP. Live confocal imaging of rVSV SAD B19 G associated with p75^{NTR} clusters reveals that these complexes internalize by clathrin-mediated endocytosis. Analysis of this real time data further shows that the kinetics of clathrin recruitment and accumulation do not differ from those recorded during the uptake of rVSV SAD B19 G in untransfected cells. Although clathrin-mediated uptake of p75^{NTR} clusters in association with RABV G suggests a common uptake mechanism between RABV and NGF, these observations are complicated by a variety of factors. Firstly, BS-C-1 cells are susceptible to SAD B19 G-bearing viruses in the absence of exogenous p75^{NTR} expression. Although p75^{NTR} clustering suggests a high local concentration of this specific receptor under the viral particle, we cannot exclude the possibility that SAD B19 G may be simultaneously interacting with other unspecified receptors. These receptors may actively trigger internalization of rVSV SAD B19 G at the plasma membrane. In this scenario, the p75^{NTR} cluster is a passively taken up along with the viral particle and may serve solely as an attachment factor. Secondly, deletion of the cytoplasmic domain of p75^{NTR} does not interfere with rVSV SAD B19 G uptake into cells. This excludes a hypothesis in which SAD B19 G binding to p75^{NTR} triggers the same conformational changes or downstream signaling as NGF. As a result, although p75^{NTR} is internalized via clathrin-mediated endocytosis following RABV G binding, the molecular mechanism underlying engagement of

this endocytic pathway is likely to differ between $p75^{NTR}$ and NGF even if we assume that $p75^{NTR}$ plays an active role in recruiting clathrin to the site of viral binding. Our results furthermore suggest that the first downstream effector leading to $p75^{NTR}$ endocytosis is likely to be a transmembrane protein, the recruitment of which may be mediated by a mechanism similar to the sortilin recruitment following pro-NGF binding. To investigate further the role of $p75^{NTR}$ in RABV uptake additional experiments are required. To exclude the involvement of unidentified receptors, future experiments would be best carried out in an otherwise restricted cell type whose susceptibility to RABV is restored by exogenous expression of $p75^{NTR}$. Future experiments could include monitoring of downstream signaling partners of $p75^{NTR}$ by Western blot following interaction with RABV G. These experiments could help determine whether RABV G induces any signaling through $p75^{NTR}$ or merely utilizes the receptor to anchor itself onto target membranes.

$p75^{NTR}$ serves as a passive attachment factor in RABV G-mediated infection. The role of $p75^{NTR}$ in RABV infection is controversial. Several lines of evidence suggest an important role for $p75^{NTR}$ during RABV uptake: i) $p75^{NTR}$ can render resistant cell lines susceptible to RABV [39]; ii) RABV G and $p75^{NTR}$ bind with high affinity [76]; and iii) mutations that strongly attenuate RABV pathogenicity in vivo also abrogate association of the virus with $p75^{NTR}$ [34]. However, existing studies also indicate that $p75^{NTR}$ likely does cannot serve as a receptor in the absence of critical co-factors or receptors: importantly, $p75^{NTR}$ expression does not correlate with RABV infectivity or pathogenesis [34, 38]. Our work supports the view that additional factors beyond $p75^{NTR}$ expression are required to mediate RABV entry into cells. $P75^{NTR}$ alone did not increase infection rates in epithelial cells resistant to rVSV CVS G, or following very low MOI infection with rVSV SAD B19 G. Deletion of the $p75^{NTR}$ signaling domains also had no adverse effect on rVSV SAD B19 G co-uptake into BS-C-1 cells. These results combined with previous data supporting a critical role for $p75^{NTR}$ in RABV uptake suggest that $p75^{NTR}$ is likely to serve as a critical attachment factor

for RABV rather than a true receptor for entry. As such the significance of $p75^{NTR}$ may arise by ensuring that the virus interacts with the membranes of cell types important for RABV pathogenesis.

MOVIE CAPTIONS FOR CHAPTER 1

Movie S1.1: **Clathrin-dependent rVSV RABV G internalization.** Time-lapse imaging of particle tracked in Figure 1.5A. BS-C-1 cells stably expressing AP2-eGFP (green) were inoculated with AF647-labeled rVSV RABV G particles (blue), and imaged by high resolution live confocal microscopy at 3s intervals. Particle docks on the bottom left hand corner of the field of view at t=15s.

Movie S1.2: Clathrin-independent uptake of rVSV RABV G. Time-lapse imaging of particle tracked in Figure 1.5B. BS-C-1 cells stably expressing AP2-eGFP (green) were inoculated with AF647-labeled rVSV RABV G particles (blue), and imaged by high resolution live confocal microscopy at 3s intervals. Particle docks on the right edge of the field of view at t=15s. No AP2 recruitment is detected prior to rapid movement outside of the field of view.

Movie S1.3: Clathrin pit dynamics in the presence of LatB. BS-C-1 cell stably expressing AP2-eGFP (green) imaged by high resolution live confocal microscopy prior to (top panel) and following administration of 1μM LatB (bottom panel). Coated pit behavior is compared side by side. Time-lapse images were captured every 3s.

Movie S1.4: **Actin recruitment during uptake of rVSV RABV G.** BS-C-1 cells transiently transfected with actin-GFP (green) and LCa-mCherry (red) were inoculated with AF647-labeled rVSV RABV G particles (blue), and imaged by high resolution live confocal microscopy at 3s intervals. Left-hand panel shows a merge of all three channels, followed from left to right by the AF647, LCa-mCherry and actin-GFP channels. A mask of the AF647 signal (white outlines) is overlayed on the individual channels to indicate the position of the particles relative on the LCa and actin signal.

MOVIE CAPTIONS FOR CHAPTER 2

Movie S2.1: **Retrograde cotransport of rVSV CVS G AF647 with fluorescent transferrin (Tfn)**. Time-lapse imaging of particle tracked in a microchannel of compartmentalized culture of DRG neurons stained with calcein (green). AF647-labeled rVSV RABV G particles (blue) and Tfn-AF594 (red) are imaged by high resolution live confocal microscopy at 2s intervals at 3hpi. Retrograde axoplasmic transport is directed from bottom to top.

Movie S2.2: Time-lapse imaging of particles tracked in Figure 2.7. Compartmentalized culture of DRG neurons stained with calcein was inoculated with AF647-labeled rVSV CVS G particles (blue), and imaged by high resolution live confocal microscopy at 2s intervals at 3 hpi. **Movie S2.3:** Clathrin pit dynamics in the presence of LatB. BS-C-1 cell stably expressing AP2-eGFP (green) imaged by high resolution live confocal microscopy prior to (top panel) and following administration of 1µM LatB (bottom panel). Coated pit behavior is compared side by side. Time-lapse images were captured every 3s.

Movie S2.3: rVSV CVS G AF647 viruses engaging retrograde axoplasmic transport do not colocalize with fluorescent dextran (Dex). Time-lapse imaging of particle tracked in a microchannel of compartmentalized culture of DRG neurons stained with CellTracker(red). AF647-labeled rVSV RABV G particles (blue) and Dex-AF488 (green) are imaged by high resolution live confocal microscopy at 1.2s intervals at 4hpi. Retrograde axoplasmic transport is directed from bottom to top.

MOVIE CAPTIONS FOR APPENDIX

Movie SA.1: **Co-internalization and transport of rVSV SAD B19 G with clustered p75^{NTR}**. BS-C-1 cells transiently transfected with p75^{NTR}-eGFP (green) and clathrin light chain (LCa)-mCherry (red) were inoculated with AF647-labeled rVSV SAD B19 G particles (blue), and imaged by high resolution live confocal microscopy at 3s intervals. A viral particle of interest is highlighted with a cyan outline. p75NTR molecules aggregate in association with incoming rVSV SAD B19 G particles prior to recruitment of LCa and internalization of the particle. Association of virus with clustered receptor is maintained during directed transport of the virus within the endosome.